REPUBLIC OF TURKEY
YILDIZ TECHNICAL UNIVERSITY
GRADUATE SCHOOL OF NATURAL AND APPLIED SCIENCES

COMPARATIVE STUDY OF THE INTERACTION OF BURIED STRUCTURES WITH GROUND AND SUPERSTRUCTURE USING DIFFERENT APPROACHES

Rafet ŞİŞMAN

DOCTOR OF PHILOSOPHY THESIS
Department of Civil Engineering
Structural Engineering Program

Advisor
Prof. Dr. Yusuf AYVAZ

December, 2020

REPUBLIC OF TURKEY
YILDIZ TECHNICAL UNIVERSITY
GRADUATE SCHOOL OF NATURAL AND APPLIED SCIENCES

COMPARATIVE STUDY OF THE INTERACTION OF BURIED STRUCTURES WITH GROUND AND SUPERSTRUCTURE USING DIFFERENT APPROACHES

A thesis submitted by Rafet ŞİŞMAN in partial fulfillment of the requirements for the degree of **DOCTOR OF PHILOSOPHY** is approved by the committee on 28.12.2020 in Department of Civil Engineering, Structural Engineering Program.

Prof. Dr. Yusuf AYVAZ
Yıldız Technical University
Advisor

Approved By the Examining Committee

Prof. Dr. Yusuf AYVAZ, Advisor
Yıldız Technical University _____

Assoc. Prof. Dr. Serkan BEKİROĞLU, Member
Yıldız Technical University _____

Assoc. Prof. Dr. Ufuk YAZGAN, Member
İstanbul Technical University _____

Assoc. Prof. Dr. Murat Serdar KIRÇIL, Member
Yıldız Technical University _____

Asst. Prof. Dr. Ahmet Utku YAZGAN, Member
Maltepe University _____

I hereby declare that I have obtained the required legal permissions during data collection and exploitation procedures, that I have made the in-text citations and cited the references properly, that I haven't falsified and/or fabricated research data and results of the study and that I have abided by the principles of the scientific research and ethics during my Thesis Study under the title of Comparative Study of the Interaction of Buried Structures with Ground and Superstructure using Different Approaches supervised by my supervisor, Prof. Dr. Yusuf AYVAZ. In the case of a discovery of false statement, I am to acknowledge any legal consequence.

Rafet ŞİŞMAN

Signature

Dedicated to my late father

ACKNOWLEDGEMENTS

I am very thankful to my respectful advisor Prof. Dr. Yusuf AYVAZ for his guidance during this thesis. I am grateful to valuable members of the thesis monitoring committee, Assoc. Prof. Dr. Ufuk YAZGAN and Assoc. Prof. Dr. Serkan BEKİROĞLU, for their comments on the study during preparation of the thesis. I also appreciate to members of the thesis defense committee, Assoc. Prof. Dr. Murat Serdar KIRÇIL and Asst. Prof. Dr. Ahmet Utku YAZGAN for their comments on the thesis. Besides, I appreciate to faculty members of Yıldız Technical University Civil Engineering Department.

Beside my efforts, my wife gave me a huge support during this study. Existence of her and my son highly motivated me to complete the thesis. I am very grateful to my family for their patience and support.

During my doctoral education I was supported by scholarship of Scientific and Technological Research Council of Turkey (TUBITAK) Grant: 2211-E Direct Domestic Doctoral Scholarship Program, I appreciate to Scientific and Technological Research Council of Turkey (TUBITAK) for their support.

Rafet ŞİŞMAN

TABLE OF CONTENTS

LIST OF SYMBOLS

V_{S30}	Average of shear wave velocity at upper 30 m soil depth
R^2	Coefficient of determination
α	Complex impedance ratio
k	Complex wave number
C_N	Courant number
ω_d	Damped radial frequency of a SDOF dynamic system
C	Damping constant of a SDOF dynamic system
F_D	Damping force in a SDOF dynamic system
I	Dynamic impedance
F_K	Elastic restoring force in a SDOF dynamic system
g	Earth's gravity, i.e. 9.81 m/s^2
F_E	External force acting on a system
Q	External load acting on a finite element
G_1	First amplitude constant to be determined
F	Force causing shear stresses
f	Frequency
F_f	Frequency dependent transfer function
$\tilde{V}_g$	Global displacement vector
$\tilde{Q}_g$	Global external load vector
$\tilde{K}_g$	Global stiffness matrix
$\ddot{X}_g$	Ground acceleration acting to a SDOF dynamic system
f_{max}	Highest frequency of interest in numerical analyses
U	Internal strain energy

$\tilde{V}$	Local displacement vector
$\tilde{Q}$	Local external load vector
$\tilde{K}$	Local stiffness matrix
ρ	Mass density
M	Mass of a SDOF dynamic system
$C_{N,max}$	Maximum value of Courant number
V_{min}	Minimum propagation velocity
N	Number of stories
C_D	Numerical model dash-pot constant
l_e	Numerical model element size
u	Particle displacement due to shear wave propagation
v	Particle velocity due to shear wave propagation
δ_{base}	Peak displacement at surface structure base level
δ_{roof}	Peak displacement at surface structure roof level
y	Position variable along considered displacement direction
x	Position variable along shear wave propagation
W_p	Potential energy of external loads
ω	Radial frequency of a SDOF dynamic system
A	Representative area of numerical model dash-pot
P	Resultant force acting on mass in SDOF dynamic system
$\ddot{X}$	SDOF system acceleration
X	SDOF system displacement
$\dot{X}$	SDOF system velocity
G_2	Second amplitude constant to be determined
N_1	Shape function with maximum value at nodal point '1'
N_2	Shape function with maximum value at nodal point '2'
N_3	Shape function with maximum value at nodal point '3'
N_m	Shape function with maximum value at nodal point 'm'
γ	Shear deformation

G	Shear modulus
τ	Shear stress
V_S	Shear wave velocity
Z	Soil layer thickness in wave propagation
S_a	Spectral acceleration
S_d	Spectral displacement
S_v	Spectral velocity
K	Stiffness of a SDOF dynamic system
ε	Strain in considered displacement direction
σ	Stress in considered displacement direction
Δ	Surface structure drift ratio in percent
h_{eff}	Surface structure effective height
W_F	Surface structure foundation width
T_B	Surface structure fundamental period
R_L	Surface structure lateral distance ratio
M_{str}	Surface structure mass
$\tilde{a}$	Surface structure peak acceleration
$\tilde{\Delta}$	Surface structure peak drift ratio in percent
h_{sto}	Surface structure storey height
h_{tot}	Surface structure total height
t	Time
Δt	Time step for numerical analyses
Π_p	Total potential energy
R_D	Underground structure depth ratio
H	Underground structure height
t_w	Underground structure wall thickness
W	Underground structure width
V	Vertical displacement along a finite element
V_i	Vertical displacement at nodal point 'i'

V_1	Vertical displacement at nodal point '1'
V_2	Vertical displacement at nodal point '2'
V_3	Vertical displacement at nodal point '3'
V_m	Vertical displacement at nodal point 'm'
ξ	Viscous damping ratio of a SDOF dynamic system
λ	Wave length
E	Young's modulus

LIST OF ABBREVIATIONS

ANN	Artificial Neural Network
BEM	Boundary Element Method
DOF	Degree of Freedom
FAS	Fourier Amplitude
FF	Free Field
PGA	Peak Ground Acceleration
PSA	Pseudo Spectral Acceleration
PSV	Pseudo Spectral Velocity
SDOF	Single Degree of Freedom
SS	Soil Site
SSFF	Surface Structure Free Field
SSI	Soil - Structure Interaction
SSSI	Structure - Soil - Structure Interaction
SSUS	Surface Structure Underground Structure
USFF	Underground Structure Free Field
USSSI	Underground Structure - Soil - Structure Interaction

LIST OF FIGURES

LIST OF TABLES

ABSTRACT

Comparative Study of the Interaction of Buried Structures with Ground and Superstructure using Different Approaches

Rafet ŞİŞMAN

Department of Civil Engineering
Doctor of Philosophy Thesis

Advisor: Prof. Dr. Yusuf AYVAZ

Metro stations and tunnels are some of the crucial infrastructure systems for modern everyday life in big cities. Considering the seismic vulnerability of megacities such as Istanbul, the dynamic interaction effects on surface structures due to existence of these kind of underground structures are not thoroughly investigated. The aim of this thesis is to investigate the above mentioned interaction problem, i.e. the dynamic interaction effects on a surface structure due to existence of an underground structure. For this purpose two dimensional numerical models which utilizes Finite Element Method are generated and dynamic time history analyses are performed. Material non-linearity is only considered for the soil domain and the surface structure and underground structure are modelled as linear-elastic. The surface structure is modelled as a Single Degree of Freedom system with a mat foundation lying on the soil deposit. The underground structure is modelled as a frame structure which is embedded in the soil deposit. A Ricker wavelet with 1 Hz dominant frequency is used as input motion acceleration history for the numerical analyses. There are totally 3528 numerical models which correspond to combinations of seven different case parameters. The case parameters are; input motion amplitude, soil layer properties, underground structure depth ratio, underground structure height, underground structure wall thickness, surface structure lateral distance ratio and surface structure fundamental period. The numerical analyses results include surface structure acceleration and drift responses along with spectral responses of ground surface accelerations. Additionally, importance order for the case parameters are

obtained by an Artificial Neural Network based sensitivity analysis. This thesis reveals that directly including the surface structure in the numerical model yields higher amplifications in the responses due to existence of underground structure. The surface structure responses may amplify or de-amplify depending on the distance between the surface structure and the underground structure.

Keywords: Soil - structure interaction, underground structures, finite element method, Opensees.

ÖZET

Gömülü Yapıların Zemin ve Üstyapı ile Etkileşiminin Farklı Yaklaşımlarla Karşılaştırmalı Olarak İncelenmesi

Rafet ŞİŞMAN

İnşaat Mühendisliği Anabilim Dalı
Doktora Tezi

Danışman: Prof. Dr. Yusuf AYVAZ

Metro istasyonları ve tüneller, büyük şehirlerdeki modern günlük yaşam için çok önemli altyapı sistemlerinden bazılarıdır. İstanbul gibi mega şehirlerin sismik kırılganlığı dikkate alındığında, bu tür yeraltı yapılarının varlığından dolayı yüzey yapıları üzerindeki dinamik etkileşim etkileri tam olarak araştırılmamıştır. Bu tezin amacı, yukarıda bahsedilen etkileşim problemini, yani bir yer altı yapısının varlığından dolayı bir yüzey yapısı üzerindeki dinamik etkileşim etkilerini incelemektir. Bu amaçla Sonlu Elemanlar Yöntemi kullanan iki boyutlu sayısal modeller oluşturulmuş ve dinamik zaman alanı analizleri yapılmıştır. Doğrusal olmayan malzeme davranışı sadece zemin tabakası için dikkate alınmıştır ve yüzey yapısı ve yer altı yapısı doğrusal-elastik olarak modellenmiştir. Yüzey yapısı, zemin tabakasına oturan radye temelli Tek Serbestlik Dereceli bir sistem olarak modellenmiştir. Yeraltı yapısı, zemin tabakasına gömülü bir çerçeve yapı olarak modellenmiştir. 1 Hz hakim frekansa sahip bir Ricker dalgacığı, sayısal analizler için girdi yer hareketi ivme kaydı olarak kullanılmıştır. Yedi farklı senaryo parametresinin kombinasyonuna karşılık gelen toplam 3528 sayısal model vardır. Senaryo parametreleri; girdi yer hareketi genliği, zemin tabakası özellikleri, yer altı yapısı derinlik oranı, yer altı yapısı yüksekliği, yer altı yapısı duvar kalınlığı, yüzey yapısı yanal mesafe oranı ve yüzey yapısı hakim periyodudur. Sayısal analiz sonuçları, yer yüzeyi ivmelerinin spektral tepkilerinin yanı sıra yüzey yapısı ivmelerini ve göreli ötelenmelerini de içerir. Ek olarak, senaryo parametreleri için önem sırası Yapay Sinir Ağı tabanlı duyarlılık analizi ile elde edilir. Bu tez, yüzey yapısının doğrudan sayısal modele dahil edilmesinin, yer altı yapısının varlığından dolayı yanıtlarda daha yüksek büyütmeye sebep olduğunu ortaya

koymaktadır. Yüzey yapısı tepkileri, yüzey yapısı ile yer altı yapısı arasındaki mesafeye bağlı olarak büyüyebilmekte veya küçülebilmektedir.

Anahtar Kelimeler: Zemin - yapı etkileşimi, yer altı yapıları, sonlu elemanlar yöntemi, Opensees.

1
INTRODUCTION

1.1 Motivation for the Study

In this section, necessity of the study will be given based on a formal definition of earthquakes. The theory of global plate tectonics should be understood before defining the earthquakes. The Earth's inner structure composes of three parts, the core, the mantle and the crust. The core also composes of two parts, the inner core which is solid and the outer core which is liquid. The outer part of the mantle is softer and can experience time-dependent plastic deformations. The crust is a rigid and relatively brittle thin layer covering surface of the mantle. Due to the high level of radiation at the inner core, there is a continuous heat transfer from the core to the crust. The heat transfer is known as the convection currents, which results in magnetic field of the Earth, heating of the ground surface and movement of the crustal plates. The first two outcomes are vital for humankind and in case of their absence there would be no life on the Earth. On the other hand, the third outcome brings us the earthquakes.

The crustal plates may diverge from each other or converge to each other during their movement. When two plates converge to each other, they collide and stuck. Since the convection currents are continuous, elastic strain energy accumulates at this boundary. The crust mostly composes of basalt and granite which cannot endure stresses over their strength. Once the accumulated stress exceeds the material strength, the plate ruptures at the most weak zone. The deployed elastic strain energy releases in the form of vibration which is named as earthquake. The earthquakes can be defined as shaking of the ground surface due to sudden release of elastic strain energy at plate boundaries.

The center of the plate rupture is named as hypocenter of the earthquake. The depth of hypocenters varies in a wide range. The earthquakes which occur at depths of 0 to 70 km are named as shallow earthquakes. The earthquakes which occur at depths of 70 to 300 km are named as intermediate earthquakes. And the earthquakes which occur at depths of 300 to 700 km are named as deep earthquakes [1]. When an earthquake

occurs, the vibrating motion propagates in any direction through the Earth's body (i.e. crust, mantle and core). The vibrations are classified as vibrations in the direction of propagation (i.e. P waves or primary waves or pressure waves) and vibrations perpendicular to the direction of propagation (i.e. S waves or secondary waves or shear waves). The P waves have higher propagation velocities and can propagate in solid medium, liquid medium and air medium. On the other hand, the S waves have lower propagation velocities and can propagate in only solid medium.

As stated above, the P and S waves (i.e. body waves or seismic waves) propagate in any direction. However, generally the propagation towards ground surface is considered in earthquake engineering studies. The seismic waves departing from the hypocenter travel through rock and soil stratums to reach the ground surface. During this propagation, seismic waves tend to amplify, especially while passing from soft soil layers. The amplified seismic waves causes more damage on structures located on the ground surface. This process is named as soil site amplification and the response at ground surface is named as soil site response. Soil site amplification is an important phenomenon in earthquake engineering studies.

The level of amplification and the frequency content of the soil site response depend on characteristic properties of the underground structure (i.e. subsurface soil layers). The seismic waves propagates in constant velocities within a subsurface layer. These propagation velocities are characteristic properties of subsurface layers. The mass densities of these two layers are also characteristic properties. A more comprehensive characteristic property can be defined by using these two properties, i.e. the dynamic impedance. As shown in Equation 1, the dynamic impedance (I) is multiplication of the mass density (ρ) and seismic wave propagation velocity (V_S).

$$I = \rho . V_S \tag{1.1}$$

For two adjacent subsurface layers there are two different characteristic propagation velocities and mass densities. Thus, the dynamic impedances of the two layers are not the same. The dynamic impedance ratio between adjacent layers controls the level of transmitted wave amplitude from bottom layer to top layer. Beside transmitted portion of the seismic waves, there also seismic waves that reflect from the subsurface layer boundaries. The reflected seismic waves travel towards the Earth's core and are dissipated due to internal damping. This dissipation process is named as the radiation damping and the level of radiation damping. The dynamic impedance ratio also controls the level of radiation damping.

Metropolitans are home to millions of people and still get growing in terms of population. The urban life in megacities is highly depending on the infrastructure lying under the city. The underground structures such as tunnels, metro stations, underground reservoirs and pipelines are vital parts of the urban life. On the other hand, existence of these kind of underground structures creates anomalies in the subsurface layers. Excavating some portion of the soil layers and/or putting stiffer structures into the soil layers alters the dynamic impedance of the layers. Thus, the soil site response changes due to the variation in the dynamic impedances.

Moreover, the underground structures are expected to survive even after destructive seismic events. The underground structures and the surrounding soil layers exhibit dynamic interaction during the seismic events. The shear strains, which would be experienced by the soil deposit during the seismic event in the case of absence of the underground structure, can be altered in the case of existence of the underground structure due to the dynamic interaction.

Ignoring the dynamic interaction between the underground structures and surrounding soil layers can lead to miscalculation of seismic behavior of the underground structures. On the other hand, ignoring the dynamic impedance alteration in subsurface layers also leads to miscalculation of seismic behavior of the superstructures. This thesis aims to present a comprehensive research on the dynamic interaction between underground structure, surrounding soil and surface structure. Better understanding of seismic behavior of the structures interacting are provided by using the research results.

1.2 Literature Review

In case of a structure to be located on a relatively soft soil deposit, the soil response would deviate from the soil response in case of absence of the structure. Also the structure response would differ from the fixed base structure response. The process, in which the structure effects the soil response and the soil deposit effects the structure response, is named as Soil Structure Interaction [2].

Although, the Soil Structure Interaction (SSI) term is generally used for the process described above, the interaction between an underground structure and surrounding soil can also be considered as SSI. On the other hand, the interaction between neighboring surface structures via the underlying soil deposit is named as Structure Soil Structure Interaction (SSSI). However, there is not a common term for describing the interaction between an underground structure and a surface structure. Thus, in this study, this phenomenon is referred to as Underground Structure Surface Structure

Interaction (USSSI).

The literature survey is grouped under five headings as Classical Soil Structure Interaction, Surrounding Soil Underground Structure Interaction, Structure Soil Structure Interaction, Underground Structure Surface Structure Interaction and Design of Underground Structures. There are a large number of studies which investigated the phenomena mentioned above. A brief summary of each study is given below, under related heading.

1.2.1 Classical Soil Structure Interaction

Zaman et al. [3] developed a simple thin-layer element which can be used for dynamic soil structure interaction problems. The element they developed, which was based on finite element method, considers four modes of deformation, such as no slip, slip, de-bonding and re-bonding. They defined soil structure interface as a medium with normal and shear stiffness. In this study, soil structure interface was modelled as elastic-plastic hardening material. They validated the developed thin-layer element on a nuclear power plant structure model. The authors concluded that the results from dynamic response analyses were satisfying.

Ayvaz et al. [4] applied modified Vlasov model to seismic analysis of plates resting on elastic soil layer. They studied the effects of soil layer thickness, plate dimensions and ratio between plate dimensions on dynamic response. Finite element method was used and Newmark β numerical integration scheme was utilized. In this study, a number of graphs were presented to show the effects of soil layer thickness and plate dimensions on dynamic out-of-plane response of the plate. They concluded that the maximum displacement increases with increasing soil layer thickness, independently from ratio of plate dimensions. They also stated that the maximum displacement is more sensitive to the soil layer thickness than to ratio of plate dimensions.

Ayvaz and Özgan [5] performed free vibration analyses for beams resting on elastic soil layer by utilizing modified Vlasov model. In their study, they aimed to analyze effects of soil layer depth, beam length, ratio of soil layer depth to beam length and vertical deformation parameter on frequency parameters of the beam. For those analyses finite element method based software was used by the authors. They illustrated both frequency parameters and mode shapes for ten modes and six modes respectively. The authors concluded that the effect of soil layer thickness is more significant than the other investigated parameters in their study.

Garip [6] investigated soil-structure interaction for reinforced concrete structures

under seismic load. In this study, a number of numerical models were prepared to perform time domain seismic analyses. SAP2000 [7] finite element software was utilized during this study. Five different building models were analyzed in conjunction with six different soil models. In this study, viscous boundary conditions were defined to prevent reflection of waves from domain boundaries. Lateral displacement histories of top storey were given in the thesis.

El-Ganainy and El-Naggar [8] studied seismic performance of three dimensional frame structures with varying number of underground stories. They considered moment resisting steel frame structures with shallow foundation footings and performed a number of parametric analyses. In this study, only two number of soil classes were considered which corresponds to firm and soft soil sites. They utilized synthetic earthquake records generated in accordance with National Building Code of Canada 2005. As a result of their parametric study, they presented force and deformation demand increases due to soil structure interaction. They concluded that on contrary to what most building codes assume, soil structure interaction can increase both force demand and deformation demand. It was also stated that buildings with no underground stories resting on flexible soil sites are more vulnerable with respect to soil structure interaction.

Mutlu [9] studied the dynamic interaction of a structure resting on a single layer with different stiffness. In this study, effect of SH waves over semicircular foundations lying over stiff or flexible soil were investigated. The author gave displacement results for different cases of stiffness ratio between soil and foundation. It was concluded that the results from this study are in good harmony with the literature. It was also concluded that the displacement amplitude is not depending on the incidence angle of the SH wave.

Kirkit [10] investigated the dynamic interaction of soil, pile and superstructure in clayey soils by using numerical analysis results. Numerical models were prepared by using OpenSees software which is a powerful finite element method code. In this study two dimensional plain strain elements were used in finite element analyses. The author provided verification for the numerical models used in this study by using the analytical solutions available in the literature. Then, a number of parametric analysis were performed to show the effect of some phenomena (i.e. the stiffness ratio between pile and soil, pile slenderness ratio, etc.). The author concluded a number of findings about seismic behavior of piled structures in interaction with surrounding soil. An interesting conclusion made in this study is that the presence of piles in the ground can create a relatively stiffer area below the superstructure and this can lead to amplification of the forces acting on the super structure.

Kiliçer [11] studied the effects of soil structure interaction on design of reinforced concrete structures. The advanced Vlasov model was utilized to define the interaction between soil and structure. The author used a finite element package software in conjunction with his own code. In this study, validation of the analyses results was assured by using a mat foundation example from the literature. The author presented the effects of a number of parameters on dynamic response of reinforced concrete structures. It was concluded that the effect is seen to be non-negligible.

1.2.2 Surrounding Soil Underground Structure Interaction

Crhichlow [12] studied the effect of underground structure on seismic motions of ground surface. In this study, underground geology in shallow depths were investigated which were subjected to damped, vertically propagating SH waves. The author utilized finite element method to build two dimensional numerical models for the study. The author used spectral methods (i.e. power spectral ratio plots) to determine effect of position, shape, depth and size of underground anomaly. The author used the gathered information to estimate underground structure by using ground motions.

Dravinski [13] studied the amplification effect of elastic inclusions in a half-space on seismic ground motions. The author considered scattering of P, SH, SV and Rayleigh waves by elastic inclusions buried in elastic half-space. Linear elastic material was adopted for soil and inclusions. Displacement results were determined using numerical analyses and given. It was concluded that presence of underground inclusion may lead to large amplifications of surface ground motion. The author also concluded that angle of incidence, frequency of excitation, burial depth have significant effect on peak values of ground surface.

Yiouta-Mitra et al. [14] presented the effect of underground structures in earthquake resistant design of surface structures. In this study, soil medium was modelled as visco-elastic and circular underground structures were considered to put forward preliminary criteria for design of surface structures. This study is an alternative for the analytical studies in the literature, a large number of parametric analysis were conducted using a commercial finite difference method software, FLAC [15]. A number of diagrams were given to represent the effect of underground structure on ground surface motion amplification.

Smerzini et al. [16] studied the effect of underground cavities on surface earthquake ground motion under SH wave propagation. Soil medium was modelled as linear elastic domain and underground structures were modelled as elastic inclusions, tunnel

with ring shaped linings and cavities. The investigated SH waves are antiplane waves which causes out of plane motions. Parametric analyses were performed to represent the effect of a number of phenomenon on ground surface motion. It was concluded that ground surface response was dominated by the fundamental vibration mode of the portion of soil between the cavity and ground surface itself. A simple relation was also given to estimate fundamental frequency as a function of embedment depth. Amplification factors for response spectra were also obtained.

Hao et al. [17] derived analytical solution for diffraction of anti-plane waves caused by an underground semicircular cavity. In this study a novel de-coupling technique was employed which is named as "improved cosine half-range expansion". They presented derivation and analysis procedures in detail. They aimed to establish an analytical solution which can be used as a benchmark for future numerical analyses for wave propagation problems.

Abuhajar et al. [18] studied the effect of underground structures on amplification of seismic ground motion for sands with varying densities. Sands with different densities were investigated in this study. The authors adopted three different load cases for the study. In this study three different earthquake time histories were used. The authors concluded that existence of box culverts can cause 50

Sgarlato et al. [19] presented a case study about the effect of underground cavities on seismic site response, based on recordings from Catania area in Italy. In this study, both natural cavities and artificial tunnels (i.e. engineering structures) were investigated. The authors considered a comparatively shallow depth to take geological properties into account. They assessed some earthquake recordings and ambient noise records by using spectral ratio techniques. It was stated that 70 earthquake recordings and 30 ambient recordings were used in this study. It was concluded that spectral ratio plots have peaks in the frequency range 3 Hz to 7 Hz nearby the cavity and those peaks tend to disappear with increasing distance from the cavity. The authors also concluded that the height of cavity plays an important role on local site amplifications, for instance heights over 4 m show significant H/V amplification.

Besharat et al. [20] studied the effect of underground structures on free field ground motion during earthquakes. In this study, finite difference package software was used. Three different cases were considered: before excavation free filed seismic analysis, seismic analysis after tunnel construction and seismic analysis after construction with weak soil conditions. The authors defined the weak soil properties as 50% reduction in stiffness. Damping effect of tunnel linings and surrounding soil was neglected in this study. It was concluded that in case of presence of a buried tunnel, amplitudes in

acceleration time histories tend to increase.

Liang et al. [21] investigated the amplification effect of underground cavities on seismic ground motions. They utilized the time domain indirect boundary element method by frequency transform. Two main properties of the system were studied, distance between cavities and spectrum of incident waves. Two earthquake recordings were used in this study, Taft earthquake and El Centro earthquake. It was concluded that the effect of underground cavities should be considered during seismic design of surface structures.

Sica et al. [22] investigated the amplification effect of shallow cavities in nonlinear soils. In this study nonlinear properties of soils were accounted. The numerical model used in this study was analogous to a real case. Two dimensional nonlinear site response analyses were performed using QUAD4-M [23] finite element code. To investigate the effect of cavities on ground surface motion, a free field model, a single cavity model and a multiple cavity model were created using the finite element code. The authors concluded that the effect of cavities should be properly considered during seismic analyses.

Baziar et al. [24] studied the effect of underground tunnels on the ground surface acceleration. Both centrifuge tests and numerical simulations were performed in this study. The authors utilized FLAC 2D software [15] in the simulations which is based on finite difference method. Centrifuge tests were used to calibrate numerical models and parametric studies were carried out using those numerical models to investigate effect of buried structures on ground surface acceleration. Kobe and Northridge earthquakes were used as input motions and the Hardin–Drnevich model was used to consider stiffness reduction. It was concluded that the results yield that presence of an underground structure amplifies motions with long periods and deamplifies motions with short periods.

Alielahi et al. [25] investigated the seismic ground amplification effect of unlined tunnels subjected to vertically propagating SV and P waves. The soil medium was modelled as a linear elastic medium in this study. The authors utilized a time domain boundary element method based algorithm to perform analyses. They concluded that the amplification of ground surface motion due to presence of a tunnel is increased in long periods. They also illustrated the variation of the amplification factor and fundamental period of the soil medium versus the buried depth of the tunnel. Some simple relations were given for preliminary seismic design of structures located near underground structures.

Wang and Cai [26] studied the effects of wavelength to excavation span ratio on

ground motion around deep underground excavations (i.e. mine excavations). It was stated that ground motion around deep excavations is significant over rock support structures. The authors calculated amplification factor by using peak particle velocities in excavation field and free field. They utilized SPECFEM2D [27] software in this study which is a two dimensional spectral element method software. It was concluded that the wave field becomes more complex as the wavelength to excavation span ratio decreases.

Alielahi and Adampira [28] effect of twin parallel tunnels on seismic ground response due to vertically propagating in-plane waves. Time domain Boundary Element Method was used by assuming linear elastic soil medium in this study. SV waves and P waves were investigated which causes in-plane motions. Fortran 90 code was developed to perform numerical analyses. A number of tables and spectra were given as a preliminary study for seismic design code development. It was concluded that tunnel structures amplifies long period components of incident waves and deamplifies short period components of incident waves. The authors also concluded that twin tunnels with a close spacing can cause more amplification in comparison with a single tunnel.

Alielahi et al. [29] investigated the effect of underground cavities on the seismic response of canyons by utilizing Boundary Element Method. They examined the seismic response of semi-sine shaped canyons above an underground cavity with varying dimensions, cover depths and locations. They modelled the soil medium as linear elastic and analyzed the system by using direct boundary element technique in the time domain. The authors concluded that different cavity geometries results in different interaction between cavity and ground surface. At the end, they gave spectral amplification coefficients for the canyon surface for different cases of canyon-cavity interaction.

Alielahi and Adampira [30] presented site specific response spectra for seismic motions in soil deposits with shallow cavities. In this study two dimensional site effects due to presence of buried structures and cavities were investigated. Time domain Boundary Element Method was utilized and soil site assumed to have a linear elastic behavior. Vertically propagating SV waves were considered, which means only in-plane motion was taken into account. The authors aimed to obtain seismic amplification functions for the ground surface motion in case of presence of underground cavity. Secondly they tried to obtain seismic ground response spectra above various types of underground structures. They concluded that the seismic amplification of soil site is increased in long periods in case of underground cavity.

Baziar et al. [31] studied the effect of ratio of tunnel lining flexibility to surrounding

soil flexibility on the ground surface acceleration response. They modelled a box shaped subway tunnel resting on bedrock by using a numerical model verified by using centrifuge test results. The authors concluded that tunnels different flexibility ratios have different effects on ground surface motions. They also concluded that the effect of flexibility ratio is more prominent in higher frequencies. They also stated that as the flexibility ratio increases the acceleration response moves away from the free field response, thus this effect must be taken into account in highly seismic regions.

Rostami et al. [32] investigated the effects of interaction between soil and tunnel on ground surface acceleration histories. They utilized ABAQUS [33] finite element method software to create numerical models. They used three different earthquake recordings as input motion for their numerical models. At the end of the study they illustrated the ground surface velocity history, structural response spectrums and frequency content of ground motions in case of presence of circular underground structure. The authors concluded that presence of a circular tunnel may cause changes in ground surface motion.

1.2.3 Structure Soil Structure Interaction

Qian and Beskos [34] investigated the dynamic interaction between rigid surface foundations in 3D. They modelled the foundations as massless, rigid and perfectly bonded to the soil medium. The utilized frequency domain Boundary Element Method. The whole study includes theoretical background of the dynamic interaction investigation. The effects of distance and frequency on the interaction between adjacent surface foundations were investigated through parametric analyses. The authors concluded that ATC-3 [35] regulations which omits the coupling effect between foundations does not always leads to conservative results for all frequencies.

Menglin et al. [36] presented a detailed literature review on structure-soil-structure interaction. In this study, the concept of structure-soil-structure interaction was introduced which considers interaction of adjacent buildings through soil. A number of well-known and commonly used software were listed and capabilities of those were discussed. Most crucial part of this study was the suggested studies for future. Some of those suggested future studies can be listed as: dynamic interaction of deep foundations, nonlinear analysis of structure-soil-structure interaction problems, numerical analysis of full model in 3D to be able to consider structures with complicated geometries, experiments using centrifuge tests and shake tables, seismic damage data collection and development of practical simplified calculation methods.

1.2.4 Underground Structure Surface Structure Interaction

Chen [37] studied dynamic response of buried structures. This study focuses on the phenomenon of dynamic soil structure interaction by considering embedded structures. A shock impulse experimental system was developed for this thesis and small models of buried structures were tested using the developed setup. A circular plate resting on sand was tested to understand the plate vibration, the interaction between plate and soil and propagation of load into the sand. During this study, also buried structures were tested. It was concluded that stiffer structure was observed to experience less soil arching. The author also concluded that using linear elastic dynamic analysis yields consistent numerical results.

Navarro [38] presented a companion paper for [39] and extended the previously proposed seismic design of tunnels methodology to other types of structures. A numerical example was presented which includes a totally buried rectangular reinforced concrete structure. In this study a number seismic load combinations were proposed for the design of underground structures. The author concluded that in case of neighboring massive structures simplified methodologies may not yield conservative results.

Wang et al. [40] investigated the interaction between underground station and nearby pile supported superstructure. They built numerical models of the problem by considering soil layer as viscoelastic and subjected to vertically propagating shear waves. They utilized ANSYS [41] software which is a powerful finite element method software and capable of modelling both soil and structure with frequency based hysteretic damping. They studied the effects of a large number of parameters among which shear wave velocity, distance between structures, damping of soil, burial depth on horizontal acceleration magnification. They also investigated the effects of number of storeys, pile length, stiffness on horizontal acceleration magnification. The authors concluded that the system response is highly sensitive to arrangement of buildings and shaking direction.

Pitilakis et al. [42] studied the interaction between circular tunnels and ground structures. They performed dynamic time history analyses by considering tunnel response mainly. There were two structural configurations in this study, first one was a single above ground structure and second one was two above ground structures located over a circular tunnel. In this study above ground tunnels were modelled as single degree of freedom systems with mechanical properties equivalent to conventional structures. Sensitivity of several parameters were investigated among which are tunnel dimensions, burial depth and soil to tunnel relative flexibility. They concluded that the presence of the above ground structures may affect the seismic

tunnel response significantly.

Abuhajar et al. [43] studied the effect of buried box culverts on earthquake excitation. In this study, centrifuge tests were performed for uniform sandy soils with relative densities 50% and 90%. A one dimensional shaker was used in conjunction with centrifuge set up at 60g gyration. The authors investigated the interaction between sands, buried box culverts and surface foundations. They used three different earthquakes with different frequency content and amplitudes. It was observed that rocking of buried box culverts was small compared to the surface foundations due to soil confinement. The authors concluded that the interaction between soil and buried structure can lead to a decrement in peak ground acceleration up to 50%. Using experimental studies for calibration of numerical models, they also studied effect of soil cover height on the kinematic interaction between soil and buried culvert. The numerical models were prepared by using FLAC software [15] which is a finite difference based software.

Gillis [44] studied seismic response of shallow underground structures located in dense regions. In this study, a number of centrifuge tests were performed to evaluate seismic interactions between underground structure, surrounding soil and adjacent surface structure. Firstly, they performed free field test where only underground structure and surrounding soil exists. Then adjacent mid to high rise buildings were added to test model. The tests provided the data to understand the interaction between structure, soil and underground structure and to calibrate numerical models. The author concluded that presence of an adjacent mid to high rise building slightly reduces racking displacements of the underground structure while increases seismic lateral earth pressures.

Franza et al. [45] presented a simplified elastic analysis approach for piled structure-tunnel interaction problems. Their approach is a Winkler springs based approach and considers structural displacements caused by tunnel excavations. In this study, results from the presented simplified approach were compared with that of 3D finite element analyses. The authors performed a number of parametric analyses to investigate the role of tunnel-pile interaction in the general response of whole system, namely tunnel, soil and superstructure. They concluded piled foundations can increase the risk of structural damage in comparison with shallow foundations. There also simple design charts were given.

Wang et al. [46] studied the influence of surface structures on seismic response of underground structures. This study was an extension to a previous study of the authors which mainly focuses on seismic response of surface structures in contrast with current

study. Soil medium, underground structure and surface structure were modelled using a well-known finite element software ANSYS [41] which enables frequency domain hysteretic damping consideration. A number of parameters related with numerical model were investigated to shown their effect on seismic response. The authors concluded that those underground structures surrounded by surface structures with fundamental frequency close to the fundamental frequency of free field are more sensitive to the investigated parameters.

1.2.5 Design of Underground Structures

Gazetas et al. [47] studied seismic response of three underground structures located in Athens during 1999 Parnitha earthquake. The three underground structures were equipped with accelerometers before the seismic event took place. The authors utilized the recordings obtained from those accelerometers to perform numerical analyses. They concluded a number of useful findings. The authors observed that presence of excavations increases the peak free field acceleration amplitudes up to 30%. They also stated that soil-tunnel interaction caused lower internal forces despite the large displacements during Parnitha earthquake.

Ma and Brady [48] presented a case study including dynamic analysis of an underground excavation in jointed rock subjected to repeated seismic loading. They compared field observation results with numerical studies of the rock deformations. According to the authors, rock response could be reproduced by using a Distinct Element model for the rock mass, however, formation of displacements depend on the joint rock model. The authors suggest that, rock mass fatigue behavior should be considered during excavation design, since excavations become increasingly vulnerable to dynamic effects if they are subjected to earthquakes again and again during their service life time.

Hashash et al. [49] prepared a report about seismic design and analysis of underground structures. They presented approaches employed during seismic design process of underground structures. In this study, a review of both deterministic and probabilistic seismic hazard analysis approaches were given. They mentioned both simpler approaches and more sophisticated approaches used in design of underground structures. According to the authors in case of low levels of shaking, interaction between buried structure and surrounding soil can be ignored and underground structures can be designed by considering the free field ground deformations. In this study, approaches that consider interaction between underground structure and surrounding soil were also described. In this report, approaches enhanced with use of numerical methods such as finite element method and finite difference method were

also mentioned. In addition, some special design issues including the design of tunnel segment joints were also discussed.

Hatzigeorgiou and Beskos [50] presented a new methodology to calculate inelastic seismic response of three dimensional underground structure embedded in rock. They utilized both boundary element method and finite element method where the first was used to model tunnel linings and the latter was used to model rock medium. In this study, interaction between structure and surrounding medium was neglected. The tunnel linings and rock medium were modelled using inelastic material models based on continuum damage mechanics theory. The authors performed a number of parametric studies to determine the effect of some parameters on structural response.

Wang and Munfakh [51] studied the subject seismic design of tunnels. The analytical approach that they proposed was based on ovaling deformation for circular tunnels and racking deformation for rectangular tunnels. The procedure proposed for circular tunnels was developed from an existing theory, and simple design charts were given. The design charts were expressed as a function of relative stiffness between the structure and the ground. The results were validated by using finite element and finite difference method based analyses. A number of parametric analyses were also performed and some design charts for rectangular tunnels were also given.

Hosseini and Tafreshi [52] investigated buried pipes under cyclic loading by taking soil structure interaction into account. They developed a physical model and conducted a number of experiments on the model. The physical model was costing of a steel pipe lying in medium silica sand. They performed nearly 60 tests with different burial depths, different sand densities, different eccentricity of the load and different values of peak loading amplitudes. The authors concluded that the tested factors have a significant effect on the deflection behavior and the failure mechanism of the system. They also stated that leaving the surrounding soil uncompacted may cause serious damages on pipes during seismic activities. It was also suggested that a depth of twice of the pipe diameter provides the safest design for pipe buried in sand.

Huo [53] studied seismic design and analysis of rectangular underground structures. This thesis is mainly based on a case study which is related with Daikai station and its seismic response during 1995 Kobe earthquake. During the Kobe earthquake different sections of the station Daikai experienced different levels of damage or no damage. The author presented results of finite element analyses to investigate the load transfer mechanism between underground structure and surrounding soil to identify the cause of damage difference. A hysteretic nonlinear soil model was utilized for the numerical analyses. The author concluded that the stiffness ratio between the structure and the

surrounding soil and the frictional characteristics of the soil-structure interface are crucial for the response of an underground structure.

Liu and Song [54] investigated seismic behavior of a subway station buried in saturated sandy deposit by using Finite Element code DYNA Swandyne-II [55]. In this study, effect of excitation and cover depth on underground structure were examined. The authors employed a generalized plasticity model with a material model representing liquefaction properties of saturated soils. The uplift performance of buried structure was investigated for different values of cover depth. They concluded that increasing the cover depth is beneficial for underground structures with regard to liquefaction uplift. They also suggested that grouting underneath the buried structure can mitigate uplift behavior.

Nagy [56] studied the effect of blast loads to underground concrete structures by considering dynamic soil structure interaction. Numerical models were prepared by using a well-known finite element method package software ABAQUS [33]. The numerical models were capable of including the whole system instead of partitioning the problem. The fully coupled model was utilized to determine more realistic results. In this study, a number of numerical examples were also presented. The results of those numerical analyses validated through field tests and analytical solutions available in the literature.

Kontoe et al. [57] presented a case study on seismic tunnel response by using the data from Bolu highway twin tunnels. They mainly focused on the damaged part of the tunnel. The authors performed static and dynamic finite element analyses to investigate the seismic tunnel response. They also compared the numerical analyses results with field observations. They concluded that the maximum total hoop stress determined from numerical analysis exceeds the strength of shotcrete. The authors also compared the numerical analyses results with results from simplified approaches. They also concluded that the bending moment distribution around the lining differs significantly.

Singh et al. [58] presented a case study about soil structure interaction analysis of underground structures in soft, sloping soils. They developed a methodology to investigate the soil structure interaction problem. In this study, numerical models were prepared by using two software in conjunction, 3D SASSI [59] and FLAC 3D [15]. Scatter motion time histories were also derived using SASSI [59] software. The main outcome of this study was to present a novel approach for numerical modelling process of buried massive structures.

Smerzini et al. [60] presented analytical solutions for the seismic response of

underground structures subjected to SH wave propagation. The underground structure was modelled as a circular inclusions embedded in a homogenous, isotropic and linear visco-elastic medium. The underground structure was also assumed to be a cavity with/without ring shaped linings. The response of soil medium was calculated in both frequency domain and time domain. The authors also performed a parametric study to show effects of a number of critical phenomena. They concluded that this study may be used as a benchmark for dynamic soil structure interaction studies.

Liu [61] investigated dynamic performance of subway structures under blast loading effect. In this study, the author mainly focused on terrorist attacks on subways. Three dimensional Finite Element models were used to determine dynamic response and damageability of subways under internal blast loading. New York subway system was considered in the study to establish numerical models. After modelling underground structure geometry, a comparative study was carried out. In this comparative study, effect of explosive weight, soil type, burial depth and properties of blast loading were investigated. The author also investigated the effect of soil improvement by grouting on performance of underground structure. In this study, elasto-plastic behavior of tunnel linings and surrounding soil was taken into account and nonlinear interaction between soil and structure was also considered. The author concluded that small tunnels buried in soft soil with lower cover depth might experience permanent damage even in case of modest internal blast loading.

Hashash et al. [62] presented seismic design considerations for underground rectangular structures. They gave a detailed description of seismic analysis approaches for underground structures. In this study, simplified solutions were reviewed and procedures required to perform numerical analyses were described. The procedures described are based on pseudo-static and dynamic soil structure interaction approaches. Thus, some of the limitations associated with pseudo-static analyses were also given. The authors also concluded that in case of those limitations, dynamic soil structure interaction analyses need to be used.

Katona [63] presented a method to assess performance of buried culverts and cut and cover tunnels which are exposed to seismic loadings as well as static loadings. A plane strain finite element software named as CANDE-2007 [64] was utilized to analyze buried structures under static seismic loadings. In this study, results from finite element analysis compared with closed form analytical solutions. The author states that the results were in a good harmony. The author concluded that the novel method is rational and easy to apply for engineering practices.

Ma et al. [65] presented a new method to assess behavior of buried structures under

shock loading. In their study, they considered damage on devices and equipment mounted inside buried structures. They considered soil structure interaction as an interfacial damping tool and they investigated effect of soil type on behavior of buried structures. In their study, a response spectrum for shock loading was also given. Their main finding can be stated as in case of subsurface shock loading or detonation soils sites with high impedance, which means high wave propagation velocity and high mass density, are more detrimental on buried structures.

Chian and Madabhushi [66] studied effect of cover depth and buried structure diameter on uplift performance of underground structures located in liquefiable soil deposits. They conducted a number of centrifuge tests to investigate the effect of cover depth and structure diameter for circular structures. In this study, ratios were derived for cover depth and diameter to determine uplift displacement in different soil and earthquake conditions. The derived ratios yields an approximate value for uplift displacement of buried structure based on known uplift displacement of a similar case.

Sun et al. [67] studied the effect of shield tunnel construction on nearby underground structures. They monitored nearby underground structures during a metro line construction in which a shield tunneling machine was employed. In this study, lateral displacements of nearby diaphragm walls and stresses on reinforcements were monitored and seemed to be in elastic range which is far below the design values. They concluded that, the effect on nearby underground structures during shield tunnel construction is small, however, construction parameters of shield tunneling machine have great influence on lateral displacement of nearby diaphragm wall.

Chen et al. [68] investigated effect of conventional blast loads on buried arch shaped structures by considering dynamic responses. They derived analytical solutions using modal superposition method. In this study, soil structure interaction considered as an interfacial damping and different types of soils were investigated. They composed two different models for the buried structure where one of them takes curvature of the structure into account and the other does not. In this study, acceleration, velocity and displacement time histories were determined by using a simplified method and maximum moment and displacement distributions were plotted. They concluded that the protective structures should be constructed in soft soil sites where acoustic impedance is quite small.

Chen et al. [69] studied elastic responses of buried arch shaped structures under subsurface detonation loading. They obtained an exact solution for the forced vibration of circular arches under subsurface detonation forces. In this study, dynamic soil structure interaction was considered by introducing an interfacial damping

between buried structure and surrounding soil. By using simplified models, analytical solutions of the dynamic responses of the underground structures were derived. In addition to first author's previous study, arches with different opening angles, acoustic impedances and height to width ratios were analyzed and influence of those phenomena was discussed.

Debiasi et al. [70] investigated the limits of simplified methods used in design of buried box culverts and rectangular tunnels. In their comparative study, they studied the effects of the frictional behavior of the soil–structure interface, the geometry of the box structure, the overburden depth, the maximum PGA (peak ground acceleration), and the increasing soil stiffness with increasing depth. They compared the results from simplified analysis methods and non-linear static soil-structure interaction analyses. They concluded that for some specific dimension ratios, stiff shallow-buried rectangular structures are affected deeply by sliding at the soil-structure interface.

Kuhnow [71] studied effects of blasting on underground concrete structures in his thesis. In this study, blasting level estimation and techniques to control vibrations caused by blasting were given. There is also a section about structural dynamics of reinforced concrete structures under seismic loading. Based on a case study, a number of criteria were proposed to decrease effects of blasting near underground concrete structures. The author recommended use of electronic detonators and early delay detonators to achieve successful levels of vibration. And it was concluded that determining vibration frequency is very critical for analyzing the response of the underground structure.

Abdel-Motaal et al. [72] studied the interaction effect between tunnels and surrounding granular unsaturated soil. They utilized finite element method to model the interaction problem by considering nonlinear material properties. Three artificial earthquake recordings were used as input. Circular tunnels with varying densities were examined in this study. The effect of tunnel embedment depth, soil density and lining thickness were also investigated. The authors concluded that the maximum strain in tunnel linings is directly proportional to the ratio of tunnel lining stiffness and surrounding soil stiffness. They also concluded that detailed analysis required when the peak ground acceleration exceeds 0.15 g.

Akhlaghi and Nikkar [73] studied the effect of shear waves on seismic behavior of circular tunnels. They utilized both quasi-static analytical approaches and numerical methods to investigate this effect. The utilized pseudo-static approaches are based on closed-form solutions which considers the tunnel lining to experience equivalent static ovaling deformations. On the other hand, numerical method carries out

dynamic nonlinear soil structure interaction analysis. The authors compared the results gathered from both approaches and concluded that the axial forces determined using analytical solutions are in harmony with results from numerical analysis results, however the bending moments determined from the two approaches are not consistent.

Chen et al. [74] presented a novel simplified seismic design method for underground structures located in soft soils in Shanghai. The novel method was named as equivalent horizontal seismic inertial force method (EHSIFM) and intended to use for underground structures in soft soils. The presented method utilizes the quasi-static approach in which the effects of equivalent horizontal seismic inertial forces, corresponding to the dynamic effects, are imposed on the underground structures. The authors also presented a case study in which a subway station lying in a soft soil site was analyzed. They concluded that analytical results proved the efficiency of the method to reflect structural response in case of seismic action.

Koneshwaran et al. [75] studied behavior of circular tunnels subjected to surface blast loads by taking fluid structure interaction into account. They used finite element models to investigate the effect of blast load on buried structures. They visualized blast-induced shock wave propagation in both saturated and unsaturated sands. In their paper, effect of blast source distance on tunnel deformation was also investigated. As a main finding they stated that the response of tunnels buried in saturated sands are more severe for a given blast event.

Abuhajar et al. [76] studied seismic interaction between soil and buried culvert in this study as a companion of another study of the authors. They utilized experimental and numerical procedures to investigate the soil-culvert interaction. The authors performed a number of centrifuge tests by using three different earthquake recordings with varying amplitude and frequency content. The results from centrifuge test were used to calibrate and verify two dimensional finite difference numerical models. FLAC software [15] was used in this study. By using the verified models, the authors performed a number of parametric analyses to show the effect of earthquake intensity, frequency, burial depth and culvert thickness on the seismic bending moments. They also presented a number of design charts for the seismic design of box culverts.

Kumar et al. [77] studied response of semi-buried protective structures under multiple blast loading effect by considering soil structure interaction. The authors introduced soil structure interaction by using frequency independent spring-dashpot-mass system. They used Johnson-Cook material model for structural steel to be able to define strain rate sensitivity. A comparative study was carried out to understand the significance

of standoff distance, explosive amount, strain rate and provision of stiffeners on the dynamic behavior of semi-buried structure. They constructed models using ABAQUS [33] software and gathered results which indicate that the buried depth of structure, soil structure interaction and strain rate controls the dynamic behavior. They concluded a number of findings among which decreasing effect of some soil types and buried depth on peak displacement were the most important.

Hushmand et al. [78] investigated performance of buried structures in medium dense dry sand by considering structure stiffness and earthquake motion properties. In their study, they presented results of three centrifuge tests in comparison with simplified analytical methods employed in design process. Their study emerges from a simplified design assumption which considers retaining or reservoir structures as either yielding structure or rigid-unyielding structure. This assumption is used in design of reservoir structures located above ground. In case of buried reservoirs, they assumed the behavior to be between yielding and rigid-unyielding, which they named as stiff-yielding. Their main finding in this study was that any of the simplified design procedures cannot capture structural deformations for all stiffness levels.

Hushmand et al. [79] investigated the seismic performance of reservoir structures buried in dry medium dense sand and compacted partially saturated silty sand. They focused on the effect of backfill soil properties, soil cover depth and soil slope on behavior of buried structure. In their study, four centrifuge tests were conducted to observe behavior of buried structures. They concluded that, the spectral ratios of structure acceleration to far field acceleration approaches unity in case of soil confinement increase, density increase and stiffness increase. They suggested that new analytical procedures and design guidelines are required for design of underground structures.

Kawamata et al. [80] tested underground structures at E-Defense shaking facility. According to the authors, in case of large earthquake actions underground structures will survive and those structures may serve as a base for reconstructing the damaged cities. In this study, the authors investigated the performance of buried structures to assure that underground structures will survive after large seismic activities. The tests mainly focused on the inground joints and tunnels passing through an interface of soft soil layer and bedrock layer. They concluded that inground joints are prone to significant failure in case of seismic activity and at soft soil bedrock interface additional strains occur along tunnel.

Wang and Cai [81] studied seismic wave propagation in underground mines by using numerical models. They visualized the wave propagation process around mine

tunnels. They tried to capture ground motion peak particle velocity accurately for design process of mine support system. They utilized SPECFEM2D [27] software which is an advanced seismic tool based on wave propagation theory. They concluded that presence of a tunnel can alter the peak particle velocity distribution around the tunnel. This alteration can cause high and low peak particle velocity zones around the tunnel. The authors stated that the presented numerical modelling approach can be useful to prevent potential rockburst damage in a mine.

1.3 Objective of the Thesis

Considering the given literature review, it can be seen that there are not so many number of studies about the Underground Structure Surface Structure Interaction. The researchers generally considered this phenomenon by determining the variation in the ground surface responses without surface structure. Since the ground surface response would deviate in case of existence of a surface structure, the ground surface response is not sufficient alone to describe the USSSI. Thus, the main focus in this study is the interaction between an underground structure and a surface structure via the surrounding soil.

1.4 Hypothesis

There mainly two numerical model sets for evaluation of the interaction effects. In the first set, the numerical models include an underground structure, surrounding soil and a surface structure. In the second set, the numerical models include an underground structure and surrounding soil. For the first set, the interaction effects are addressed by calculating the variation in the surface structure peak drifts and peak accelerations. On the other hand, for the second set, the interaction effects are addressed by calculating the variations in the acceleration and displacement response spectra along the ground surface in the vicinity of the surface structure. Thus, modelling approaches for the USSSI problems are also compared. Besides, the most effective parameters on the interaction are addressed by performing an Artificial Neural Network (ANN) based sensitivity analyses.

2
FUNDAMENTALS

2.1 Dynamics of Structures

Static and dynamic analyses are different mainly in two aspects. The first one is the time varying nature of the dynamic loadings. The static loadings are not time dependent and only one single solution exists for any time during loading. However, the dynamic loadings have as many solutions as the number of loading steps. The second difference is the number of system properties required to solve the problem. A fixed base column is given in Figure 2.1 to be considered as a benchmark system to explain the second difference between dynamic and static analyses. In case of static loading, the analyst can determine internal forces at each point on the column by knowing only column height and static load value. On the other hand, the analyst must also know column mass and stiffness beyond dynamic load value to determine the internal forces.

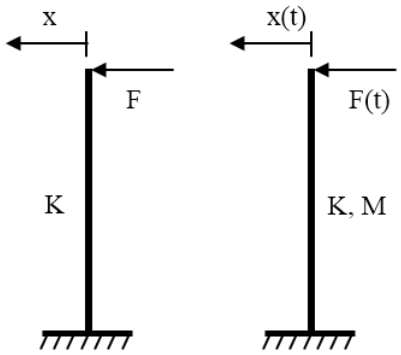

Figure 2.1 Cantilever column system

If the system deformations (i.e. deformed curve of the column) are considered, another issue emerges. Even in case of static loading the lateral deformations will vary with location along column height. On other hand, in case of dynamic loading the lateral deformations will vary not only with location but also with time. The prior problem requires solution of a second order differential equation with only on variable (i.e. location along column height). The latter problem requires solution a

partial differential equation with two variables (i.e. location and time). Therefore, geometrical discretization is generally utilized to transform the problem to a set of differential equations with one variable.

There are primarily three methods for discretizing the system geometry [82]. The most common way of discretizing the system geometry is lumping masses at some specific points. For instance, considering the column given in Figure 2.1, whole mass of the column may be concentrated at the tip of the column. On the other hand, for mediums such as soils where the masses are distributed uniformly, generalized displacements method is more preferable for discretization. In this concept, it is assumed that the deflected shape of the system can be represented as the sum of a series of predefined deflection patterns. For instance, considering the column given in Figure 2.1, the deflected shape can be represented by the sum of a series of trigonometric functions. Furthermore, a more recent method for discretization is based on the Finite Element Method. Actually, use of interpolation functions used in Finite Element Method for mass matrix construction yields the consistent mass matrix. However, if the interpolation functions are not utilized for mass matrix construction one can end up with lumped mass matrix even in Finite Element Method analysis.

The above mentioned discretization methods mainly provides the analyst to limit the number of differential equations, namely the degrees of freedom. For any dynamic problem, based on the physical properties of the problem, sufficient number of degrees of freedom (DOF) must be considered. Then, the equation of motion should be constructed with the same number of independent variables.

There are several methods for deriving the equation of motion for a structural dynamic system. However, in this section, the most common and simple procedure, which is based on d'Alembert's principle, is explained. Newton's second law of motion states that the change in momentum of any mass particle for unit time is equal to the sum of all forces acting on the mass. The differential equation for the statement above can be written as given in Equation 2.1.

$$P(t) = \frac{d}{dt}.\left(M.\frac{dX}{dt}\right) \tag{2.1}$$

In Equation 2.1, $P(t)$ is the sum of all forces acting on the mass particle, M is the amount of mass and X is the position variable. This equation can be simplified as

given in Equation 2.2.

$$P(t) = M.\left(\frac{d^2X}{dt^2}\right) \tag{2.2}$$

$$P(t) - M.\ddot{X} = 0 \tag{2.3}$$

The formulation above is the general form of the equation of motion. It should be noted that the term $P(t)$ includes possible elastic restoring forces, possible viscous damping forces and externally applied forces. Equation of motion for a SDOF system is given here to illustrate the forces acting on a structural dynamic system. The SDOF system is shown in Figure 2.2 includes a system with mass M, lateral stiffness K and a viscous damper with damping coefficient C.

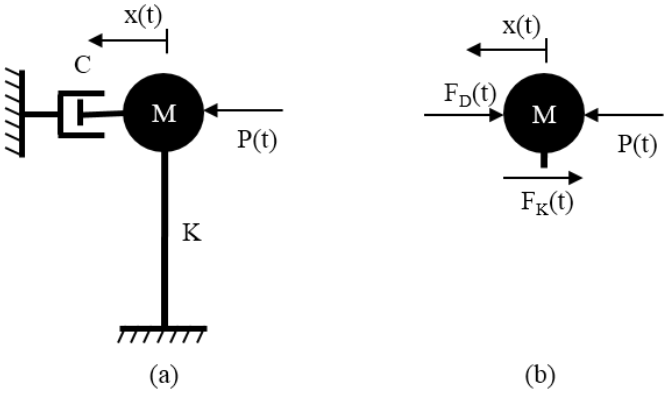

Figure 2.2 Idealized SDOF system: (a) basic components; (b) forces in equilibrium

The forces shown in Figure 2.2 (b) are parts of the total force denoted by $F(t)$. The term $F_K(t)$ represents the elastic spring force due to displacement of the mass, the term $F_D(t)$ represents the damping force due velocity of the mass and the term $P(t)$ represents the externally applied force to the mass. Introducing the force terms into Equation 2.3 yields Equation 2.4.

$$P(t) - F_D(t) - F_K(t) - M.\ddot{X} = 0 \tag{2.4}$$

The elastic spring force $F_K(t)$ is equal to $K.X$ and the damping force $F_D(t)$ is equal to $C.\dot{X}$ where $\dot{X}$ is velocity of the mass. Introducing these terms into Equation 2.4 the most well-known form of the equation of motion for SDOF systems emerges as given

in Equation 2.5.

$$K.X + C.\dot{X} + M.\ddot{X} = P(t) \tag{2.5}$$

In earthquake engineering, the external forces emerges in the form of ground accelerations. Since the structural supports (i.e. footings/foundations) are directly located on the ground surface, the external forces acts onto the supports. Thus, the external forces appear with a minus sign in the equations. The equation of motion for a structure subjected to earthquake loading is given in Equation 2.6, where $\ddot{X}_g$ represents the ground acceleration history.

$$K.X + C.\dot{X} + M.\ddot{X} = -M.\ddot{X}_g \tag{2.6}$$

As stated before, the equation of motion is a second order ordinary differential equation. This kind of equations can be solved by using analytical or numerical methods. The analytical methods are generally utilized for linear systems. The analytical solution consists of two sub-solutions as homogeneous solution and particular solution. The homogeneous solution of the equation of motion can be derived by setting the right-hand side of the Equation 2.6 to zero and is given in Equation 2.7.

$$X(t) = e^{-\xi\omega t}.(G_1.\sin(\omega_d t) + G_2.\cos(\omega_d t)) \tag{2.7}$$

In Equation 2.7, G_1 and G_2 are integration constants which should be determined based on the initial conditions. The term ω_d refers to damped radial frequency and is equal to $\omega.\sqrt{1-\xi^2}$.

The particular solution for the equation of motion can be derived by considering the equation as it is. While solutions for forcing functions with known mathematical expressions are easy to determine, more complex forcing functions require elaborate solutions. Then, general solution for dynamic loading is obtained by summing the homogeneous and particular solutions.

2.1.1 Earthquake Response Spectrum

The maximum responses of Single Degree of Freedom (SDOF) structures with varying fundamental periods and same damping ratios under a certain input ground motion

can be illustrated as a function of fundamental period. This type of illustration of the peak responses is named as the response spectrum. An earthquake response spectra can give an insight about the seismic hazard due to a specific ground motion.

The earthquake response spectra is obtained by solving the equation of motion for SDOF systems with various fundamental periods. Thus, the analyst should focus on the equation of motion for correct understanding of the spectral parameters. Any SDOF structure basically have acceleration, velocity and displacement responses. Thus, peak values of these are the spectral parameters and named as Spectral Acceleration (S_a), Spectral Velocity (S_v) and Spectral Displacement (S_d). On the other hand, there are two more spectral parameters, which are named as Pseudo Spectral Acceleration and Pseudo Spectral Velocity. The relation between spectral displacement and these parameters are given in Equation 2.8 and Equation 2.9.

$$PSA = \omega^2 . S_d \tag{2.8}$$

$$PSV = \omega . S_d \tag{2.9}$$

The relations given in Equation 2.8 and Equation 2.9 are based on the low damping assumption. On the other hand, the peak base shear calculated by multiplying the total mass and the PSA corresponds to the force that results in the SDOF displacement S_d. The PSA parameter mentioned above corresponds to the peak value of total acceleration, i.e. SDOF acceleration and ground acceleration. The general misuse of relative and total acceleration terms for PSA and SA should be avoided.

The earthquake response spectrum for 1999 Kocaeli earthquake is illustrated for 5% damping to set an example. Displacement response spectrum (S_d), pseudo velocity response spectrum (PSV) and pseudo acceleration response spectrum (PSA) are given in Figure 2.3.

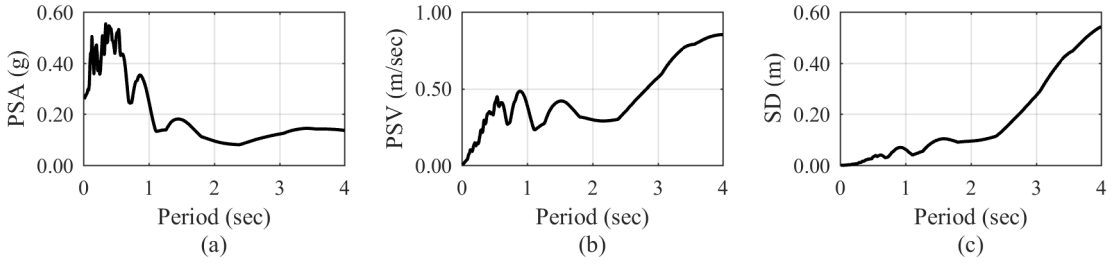

Figure 2.3 Displacement response spectrum, pseudo velocity response spectrum and acceleration response spectrum

2.2 Finite Element Method

Contrary to popular belief, Finite Element Method (FEM) is not a numerical tool for analyzing engineering structures or systems. In fact, FEM is a powerful numerical method for solving differential equations. If any engineering problem can be represented by a differential equation, then this problem can be solved under given boundary conditions or initial conditions by using FEM. The engineering problem can be a heat transfer problem, a site response analyses problem or an aerospace engineering problem etc.

On the other hand, although FEM is a powerful numerical method, it is not a magical tool for solving differential equations. The physical problem should be well defined, the boundary conditions and initial conditions should be correctly considered and the defined differential equation should be sound. The analyst also should be capable of using FEM to solve the differential equation. In engineering problems, generally determining deformations, temperature, stresses etc. is desired. These effects are generally caused by a force, thermal source etc. The relationship between these effects and causes can be represented by differential equations. Solution of these differential equations yields the distribution of the effects along the investigated body. Here, a cantilever bar is under effect of a nodal force, which is given in Figure 2.4, can set a good example. The bar length is the investigated body. The deformations along the body may be considered as the effects to be determined. The nodal force acting on the body is the causes for these effects.

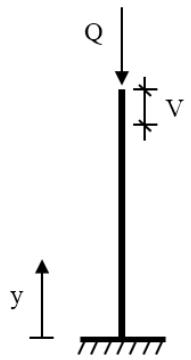

Figure 2.4 Cantilever bar with nodal force

The first step of FEM is to discretize the body and select appropriate elements for the problem. The discretization process is generally called as meshing. There are high quality software for meshing the investigated body. After meshing, nodal points and finite elements are obtained. The appropriate elements are: line elements for one-dimensional problems, triangular or quadrilateral elements for two-dimensional problems and tetrahedron or hexahedron elements for three-dimensional problems. All of the mentioned elements are illustrated in Figure 2.5 to set an example.

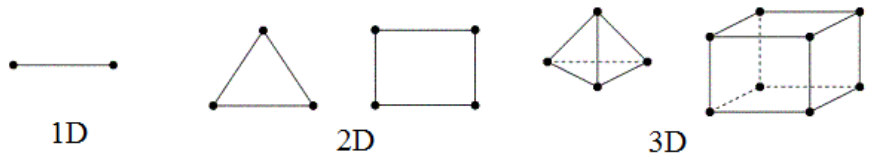

Figure 2.5 Finite element types

In the second step of FEM approximation functions for the investigated effects are selected. These functions are also named as test functions since they are possible solutions for a differential equations. The approximation functions or test functions relate the effects at nodal points to the effects at interior of a finite element. Some mathematical functions such as trigonometric functions and polynomials can be used as test functions. The requirements for a test function are not given here but have great importance. For a generic stress deformation problem, distribution of displacement (V) along a finite element can be expressed as given in Equation 2.10.

$$V = N_1 \cdot V_1 + N_2 \cdot V_2 + N_3 \cdot V_3 + ... + N_m \cdot V_m \tag{2.10}$$

In Equation 2.10, there are m nodal points on the finite element and thus there are m nodal displacements, i.e. V_1, V_2, ..., V_m. The functions N_1, N_2, ..., N_m are the approximation functions which are also called as shape functions and interpolation functions. The nodal displacements in Equation 2.10 are the unknowns for the problem and the solution will yield values of these unknowns.

The third step of FEM is constructing the relationship between gradient and unknown. For the generic stress deformation problem mentioned above, the unknowns are the nodal displacements. The gradients are the variation of the displacements with position variables, i.e. differentiation with respect to position variables. Here, another assumption is required, i.e. validity of the first order theory, but details of the assumption is not given here. In Equation 2.11, the relationship between displacement (i.e. the unknown) and strain (i.e. the gradient) is given.

$$\varepsilon = \frac{dV}{dy} \tag{2.11}$$

Since the investigated problem is a stress deformation problem, the relationship between strains and stresses must be also be defined. These kind of relationships are called as constitutive relationships. Here, linear-elastic constitutive relationship is considered for simplicity. However, considering nonlinear constitutive relationships in FEM is also possible. In Equation 2.12, the constitutive relationship is given, where

σ corresponds to stresses and E represents Young's modulus.

$$\sigma = E \cdot \varepsilon \tag{2.12}$$

In the fourth step element equations are obtained by using energy methods or residual methods. The use of energy methods requires knowledge of variational calculus, while the use of residual methods requires some specific procedures such as collocation, subdomain, least squares and Galerkin's method. Here, first variation of potential energy is utilized for constructing element equations.

The potential energy in a generic stress deformation problem corresponds to summation of internal strain energy and potential of external loads. In case of equilibrium, potential energy of the investigated system should experience a minimum. Thus, first derivative (i.e. first variation) of the potential energy in equilibrium should be zero. It must be noted that the potential energy function will include integrations along finite element and actually is a functional. Variation of such functionals corresponds to derivative of functions. The potential energy is given in Equation 2.13, where Π_p represents total potential energy, U corresponds to internal strain energy and W_p is the potential of external loads.

$$\Pi_p = U + W_p \tag{2.13}$$

Both the internal strain energy and the potential energy of external loads are functions of nodal displacements, which are unknowns. Thus, the total potential energy is also a function of nodal displacements. Taking first variation of total potential energy with respect to each unknown and equating to zero yields a set of equations. The equations are finite element equations. In Equation 2.14, the first variation of total potential energy is given briefly.

$$\delta \Pi_p = 0 \tag{2.14}$$

Equation 2.14 can be stated more clearly as:

$$\frac{\partial \Pi_p}{\partial V_i} = 0 \tag{2.15}$$

where V_i represents nodal displacements and i ranges from 1 to m.

In the fifth step, the obtained set of finite element equations are written in a matrix form. The unknowns (i.e. nodal displacements) are represented by a column vector ($\tilde{V}$), the external loads are represented by a column vector ($\tilde{Q}$) and the relating matrix is named as element property matrix ($\tilde{K}$). Since all the unknowns are nodal quantities, the external loads should be converted to nodal quantities. The element property matrix is also named as the stiffness matrix. In Equation 2.16, the element equations are given in matrix form.

$$\tilde{K} \cdot \tilde{V} = \tilde{Q} \tag{2.16}$$

The sixth step of FEM includes assembling the element equations to construct global element equations and applying boundary conditions. After meshing the investigated body there are nodal points and finite elements. These nodal points are generally the locations where adjacent elements are connected. Thus, the assemblage must be done by considering continuity issues. After constructing the global element matrices, the set of equations can be re-written as given in Equation 2.17.

$$\tilde{K}_g \cdot \tilde{V}_g = \tilde{Q}_g \tag{2.17}$$

The boundary conditions are the physical constraints or supports which means known values of some of the unknowns in the problem. There are different kind of boundary conditions such as geometric boundary conditions, homogeneous boundary conditions etc. however explanations for them is not given here. Applying boundary conditions to the set of equations given in Equation 2.17 will yield reduced element matrices and modified set of equations.

In the seventh step the set of equations are solved for the unknowns and the secondary quantities are determined by using the results. For instance, nodal displacements can be calculated by using the set of equations and internal forces can be calculated by using the nodal displacements. Finally the obtained results can be presented as a deformed shape, internal force diagram etc.

2.3 Site Response Analysis

The seismic waves departing from seismic sources travel through rock and soil stratums to reach ground surface. During this propagation, seismic waves tend to amplify, especially while passing from soft soil layers. The amplified seismic waves causes more damage on structures located on ground surface. This process is named as

soil site amplification and the response at ground surface is named as soil site response. Soil site amplification is an important phenomenon in earthquake engineering studies.

The level of amplification and the frequency content of the ground surface motion depend on the underground structure (i.e. subsurface soil layers). While softer layers below ground surface cause amplification of low frequency waves, stiffer layers below ground surface cause amplification of high frequency waves. The impedance ratio between subsurface layers controls the amplification magnitude and level of radiation damping.

There are mainly two methods for site response analyses: frequency domain solution methods and time domain solution methods. The frequency domain solution methods are capable of analyzing soil sites with linear mechanical properties. On the other hand, time domain solution methods are capable of analyzing soil sites with both linear and non-linear mechanical properties.

There is a misconception that equivalent linear site response analysis is a non-linear solution method and superior to linear site response analysis. The equivalent linear site response analysis is nothing more than a linear solution method which uses average stiffness based on the effective shear strain. Therefore, the equivalent linear site response analyses is not listed above as a site response analysis method.

In the frequency domain site response analyses, the analyst calculates Fourier transform of the input motion, then multiplies it with the transfer function of the soil deposit (i.e. dynamic system) and calculates the inverse Fourier transform to obtain the site response. In the time domain site response analyses, the analyst needs to utilize numerical methods such as Finite Element Method and Finite Difference Method. Then, incremental solution algorithms such as Newmark-β integration are employed to obtain the site response.

Besides frequency domain and time domain methods, there is an underrated method which solves the site response problem in discrete time domain. In the discrete time domain site response analysis, there is no need for numerical methods or Fourier transforms. The transfer function of frequency domain site response analysis method is also available in discrete time domain. Applying the transfer function to input motion step by step yields the site response.

The frequency domain transfer function for a single layer soil deposit lying on a rock layer is given in Equation 2.10. The transfer function of a single soil layer with 240 m/sec shear wave velocity, 1.8 t/m^3 mass density and 30 m thickness lying on a rock layer with 760 m/sec shear wave velocity and 2.0 t/m^3 mass density is illustrated in

Figure 2.6. The illustrations are depicted for viscous damping ratio of 0% and 3%.

$$F(f) = \frac{1}{\cos(kZ) + i.\alpha.\sin(kZ)} \tag{2.18}$$

In Equation 2.18 k represents the complex wave number, α represents the complex impedance ratio and H is the soil layer thickness.

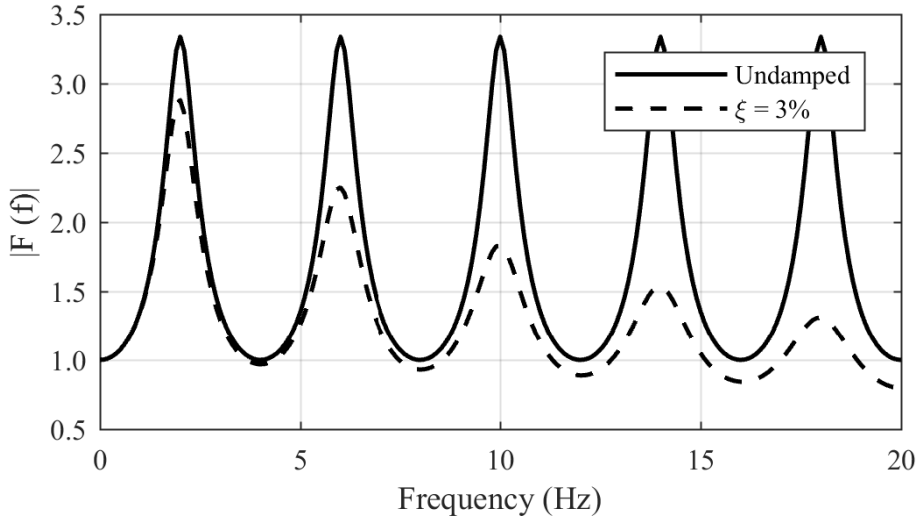

Figure 2.6 Transfer function of a single soil layer with different damping ratios

3
METHODOLOGY, DATA PROCESSING AND NUMERICAL MODELLING

In this chapter, firstly the utilized methodology for defining cases and case parameter explanations are given. Secondly, manipulation of the results obtained from the numerical analyses is explained. At the end, the numerical model properties, limitations, and components are given in detail.

3.1 Methodology

In this thesis, there are four groups of numerical models. The first model group is named as Free Field (FF) conditions. The numerical models in FF conditions includes only a single layer soil deposit. There is no underground structure and surface structure in numerical models in FF conditions. The second group is named as Unground Structure Free Field (USFF) conditions. The numerical models in this group includes an underground structure embedded in a single layer soil deposit. However, there is not a surface structure on the soil deposit. The third group is named as Surface Structure Free Field (SSFF) conditions. The numerical models in this group includes a surface structure lying on a single layer soil deposit. However, there is not an underground structure embedded in the soil layer. The last group is named as Surface Structure Underground Structure (SSUS) conditions. The numerical models in this group includes a surface structure lying on a single layer soil deposit in which an underground structure in embedded.

There are 12 numerical models in FF conditions, 216 numerical models in USFF conditions, 60 numerical models is SSFF conditions and 3240 numerical models in SSUS conditions. Thus, a total of 3528 numerical models are generated in this thesis. Schematic illustrations of the numerical model groups are given in Figure 3.1.

As stated before, 3528 numerical analyses are performed for this thesis. There are seven different parameters, which are named as case parameters, taken into account.

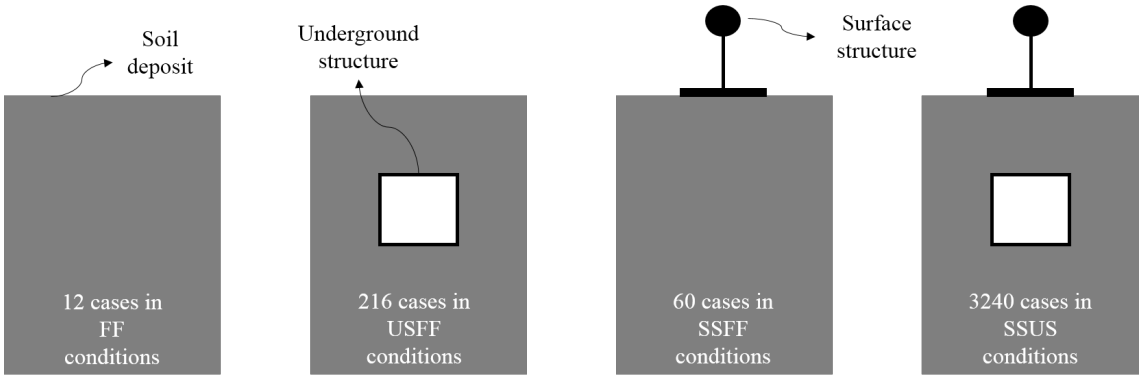

Figure 3.1 Schematic illustrations of the numerical model groups

Detailed explanations and parameter values are given in the following. The case parameters can be listed as:

- Mechanical properties of the soil site,
- Peak amplitude of the input motion,
- Underground structure burial depth,
- Underground structure dimensions,
- Underground structure wall thickness
- Surface structure horizontal location,
- Surface structure fundamental period.

3.1.1 Case Parameters

In this thesis, a large number of dynamic time history analyses are performed by using numerical models comprising of a soil deposit, an underground structure, and a surface structure. The analyses results are utilized to examine the interaction effects between the surface structure and the underground structure, with regard to several parameters. There are a number of parameters which are likely to affect this interaction, but only seven of them are investigated in this thesis. The investigated parameters and parameter ranges are given in Table 3.1.

As stated before, the aim of this study is to investigate the dynamic surface structure-underground structure interactions in different soil deposits. For this purpose, four different single layer soil deposits are considered. There are two soil mechanical properties which are controlled by the soil site parameter. The first property is average shear wave velocity of the soil deposit and the second property

Table 3.1 Investigated parameter ranges

Parameter Name, Unit	Parameter Ranges
Soil Site (SS)	Soil Site 1, Soil Site 2, Soil Site 3 and Soil Site 4
Peak amplitude of input motion acceleration (PGA, g)	0.10, 0.30 and 0.50
Depth ratio (R_D)	0.5, 1.0 and 1.5
Underground structure height (H, m)	5 and 10
Underground structure wall thickness (t_W, m)	0.50, 0.75 and 1.00
Lateral distance ratio (R_L)	0, 2, and 4
Surface structure fundamental period (T_B, sec)	0.2, 0.4, 0.6, 0.8 and 1.0

is cohesion of the soil material in undrained conditions. These mechanical parameter values are given in Table 3.2.

Table 3.2 Soil mechanical properties

Soil Site	$V_{S30}(m/sec)$	Cohesion(kPa)
Soil Site 1	100	20
Soil Site 2	200	40
Soil Site 3	350	70
Soil Site 4	500	100

The average shear wave velocity values range from 100 m/sec to 500 m/sec for the four soil sites. The soil sites 1 to 4 correspond to soil classes ZE, ZD, ZD, and ZC according to TBEC 2018 [83], respectively. The reason why there are two soil sites which correspond to ZD is to represent both lower and upper limit conditions of the soil site. The undrained cohesion value is assumed to be 1/5 of the average shear wave velocity value. A unique empirical relationship is not adopted in this study, instead an average value is considered.

Mechanical behavior of soil deposits may be altered during stronger input motions due to the soil material non-linearity. For this reason, the input motion acceleration history is scaled to three different peak acceleration values to be used as input motions. The peak amplitude of input motion acceleration values given in Table 3.1 correspond to these three values. The acceleration history is scaled to $0.10g$, $0.30g$ and $0.50g$ in order to represent weak, moderate and strong earthquake input motions, respectively.

The depth ratio (R_D) parameter corresponds to the ratio of burial depth of the underground structure to its height. The burial depth and underground structure dimensions are shown in Figure 3.2. The R_D parameter values are selected in accordance with the literature. The R_D parameter value of 0.5 corresponds to shallow

underground structures while the R_D parameter value of 1.5 corresponds to deep underground structures.

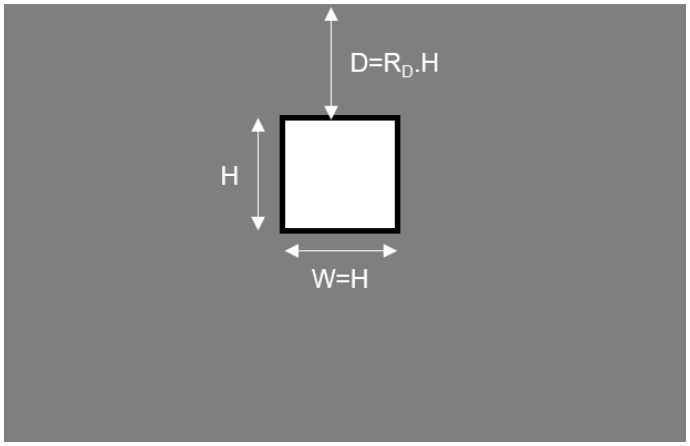

Figure 3.2 Underground structure dimensions and orientation

The underground structure height (H) parameter represents the size of the underground structure, because the shape of the underground structure is selected to be a square. It is done with the aim of controlling the dimensions of the square-shaped structure with only one parameter, i.e. H. The aspect ratio of the underground structure (i.e. the ratio between its width and height) is also considered in some studies from the literature. In this study, the aspect ratio is held constant at 1.0 (i.e. aspect ratio of a square) to have lesser number of combinations.

In the majority of the studies related to static and dynamic response of underground structures [42, 45, 84–86] a parameter named as flexibility ratio is considered. The flexibility ratio parameter corresponds to the ratio of diametric (for circular underground structures) or lateral (for rectangular underground structures) deformation stiffness of surrounding soil to that of the underground structure. In most of these studies, the variation of the flexibility ratio is generally assured by altering Young's Modulus of the underground structure material. However, in practice, Young's Modulus can only vary slightly for possible concrete materials. In fact, the variation of the flexibility ratio mainly corresponds to change in dimensions and wall cross-section of the underground structure (e.g. cross-section height contributes to underground structure stiffness with its cube). The change in the underground structure wall cross-section causes not only variation of the underground structure stiffness but also the variation of the underground structure mass. The inertial change in the underground structure is generally neglected in previous studies. There is only a limited number of studies [87, 88] that account for variation of the underground structure mass. In this study, wall thickness (t_W) and height (H) of the underground structure are directly addressed to overcome possible inaccuracies due to omission of

the mass variation effect.

The lateral distance ratio (R_L) parameter represents the ratio of the horizontal distance between the surface structure and the underground structure to the surface structure foundation width. In other words, the lateral distance ratio is a normalized measure of the distance between the surface structure and center of the underground structure. Foundation width and the lateral distance dimensions are given in Figure 3.3.

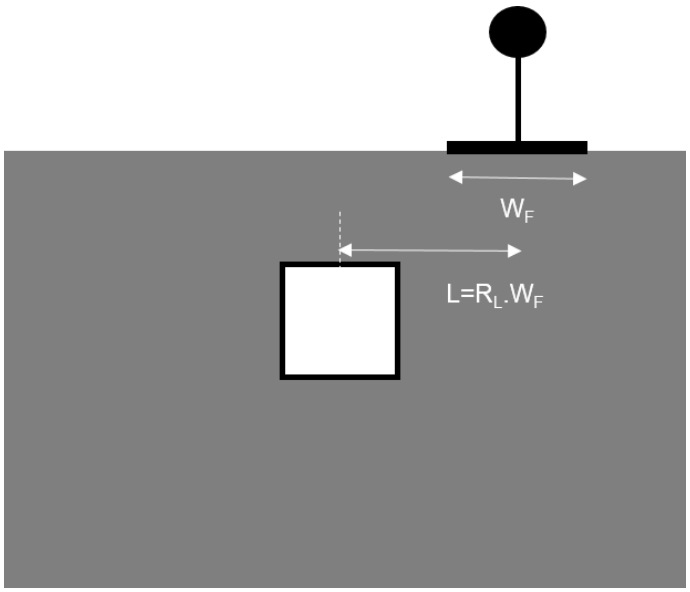

Figure 3.3 Foundation width and lateral distance ratio

The surface structure fundamental period (T_B) represents a dynamic characteristic of the surface structure. The surface structure fundamental period is also used as a parameter to control the number of stories of the surface structure. The number of stories and the fundamental period are correlated by using the approximation given in Equation 3.1. The given approximate fundamental period equation is a well-known approximation used in practice. In this equation, T_B corresponds to the fundamental period and N represents the number of stories.

$$T_B = N/10 \tag{3.1}$$

The case conditions (i.e. FF, USFF, SSFF, and SSUS) were explained previously and each case condition holds a group of case parameter combinations. Since the FF conditions do not include underground structure and surface structure, the only case parameters to combine are the Soil Site (SS) and peak amplitude of the input motion (PGA). Thus, there are 12 cases in FF conditions as a combination of four soil sites and three input motion PGA values. Similarly, in USFF conditions, there are five case parameters: Soil Site (SS), peak amplitude of the input motion (PGA), underground

structure height (H), underground structure wall thickness (t_W), and depth ratio (R_D). Thus, there are 216 cases in USFF conditions as a combination of the listed case parameter values. In SSFF conditions, there are only three case parameters: Soil Site, peak amplitude of the input motion and surface structure fundamental period (T_B). Thus, there are 60 cases in SSFF conditions as a combination of the listed case parameter values. In SSUS conditions, there are all seven case parameters which are listed in Table 3.1. Thus, there are 3240 cases in SSUS conditions as a combination of the given case parameter values. Finally, 3528 different cases are generated in the course of this thesis.

3.2 Data Processing

The previously explained 3528 cases mean 3528 numerical analyses. The analyses are performed on a workstation computer with 48 CPU cores. The total analyses time was almost two weeks and the output data is about 28 GB. Nowadays, this amount of data is quite large to store and process. However, by using MATLAB [89] scripts developed in the course of this thesis, the data is processes and illustrated.

The output types vary for different case conditions. While the ground surface acceleration histories are obtained from the cases in FF and USFF conditions, surface structure acceleration histories are obtained from the cases in SSUS and SSFF conditions. On the other hand, the foundation level accelerations are also obtained for the cases in SSUS and SSFF conditions. The acceleration histories obtained from the cases in SSUS and SSFF conditions are numerically integrated to determine displacement histories. Then, the drift ratios are calculated by subtracting surface structure foundation level displacement from its roof level displacement and dividing by total height of the surface structure. The Equation 3.2 shows the drift ratio calculation formula. In Equation 3.2, δ_{roof} represents the horizontal displacement at roof level of the surface structure and $\delta_{foundation}$ represents the horizontal displacement at foundation level of the surface structure, and Δ represents the drift ratio in percent.

$$\Delta = 100.\left(\frac{\delta_{roof} - \delta_{foundation}}{h_{tot}}\right) \tag{3.2}$$

As stated before, underground structure and surrounding soil interaction effects on surface structures are focused in this thesis. There are two methods adopted for this purpose: (1) examining the spectral responses, and (2) examining the directly modelled surface structure responses. The first method is utilized for the cases in FF

and USFF conditions. The second method is utilized for the cases in SSFF and SSUS conditions.

Pseudo Spectral Acceleration (PSA) and Spectral Displacement (S_d) values are calculated for the cases in FF and USFF conditions, for the first method. The amplification of the PSA and S_d values for the cases in USFF conditions with respect to the corresponding cases in FF conditions are considered as the measurement of the interaction. The amplifications are given as percentages and negative values represent de-amplifications.

Since all points on the ground surface yields the same response for a case in FF conditions, there is only one ground surface acceleration history per cases in FF conditions. However, the ground surface acceleration history varies with horizontal location for the cases in USFF conditions. Therefore, the ground surface response at the horizontal center of the ground surface is utilized for the amplification calculations. On the other hand, the calculated PSA and S_d values are functions of the fundamental period. Therefore, the PSA and S_d values for the periods which correspond to the surface structure fundamental periods investigated in this thesis are utilized for the amplification calculations.

The amplification values in USFF conditions with respect to FF conditions are calculated by using the relationship given in Equation 3.3 and Equation 3.4. In the equation, PSA_{USFF} corresponds to the PSA value in USFF conditions and PSA_{FF} corresponds to the PSA value in corresponding FF conditions. Similar notation is also used for S_d values. However, it should be noted that the PSA amplifications and the S_d amplifications are purely identical. The proportionality of these two terms (i.e. $PSA = \omega^2 \cdot S_d$) yields the same amplification values.

$$Amplification = 100.\left(\frac{PSA_{USFF}(T = T_B) - PSA_{FF}(T = T_B)}{PSA_{FF}(T = T_B)}\right) \tag{3.3}$$

$$Amplification = 100.\left(\frac{S_{d,USFF}(T = T_B) - S_{d,FF}(T = T_B)}{S_{d,FF}(T = T_B)}\right) \tag{3.4}$$

For the cases in SSUS and SSFF conditions, the amplification in surface structure peak acceleration and peak drift ratio values is calculated as the measure of the interaction. The amplifications are given as percentages and negative values represent de-amplifications. The amplification values in SSFF and SSUS conditions are calculated by using the relationship given in Equation 3.5 and Equation 3.6. In the equation, $\tilde{a}_{SSUS}$ represents peak acceleration value is SSUS conditions and $\tilde{a}_{SSFF}$

represents peak acceleration value in SSFF conditions. Similar notation is also used for drift ratios.

$$Amplification = 100.\left(\frac{\tilde{a}_{SSUS} - \tilde{a}_{SSFF}}{\tilde{a}_{SSFF}}\right) \tag{3.5}$$

$$Amplification = 100.\left(\frac{\tilde{\Delta}_{SSUS} - \tilde{\Delta}_{SSFF}}{\tilde{\Delta}_{SSFF}}\right) \tag{3.6}$$

The determined amplification values are presented in the next chapter. While generating output graphs, variation of the amplification values with the surface structure period (T_B) is given. This was done so as to present the results in a spectral-like way. On the other hand, variation of the minimum, the mean and the maximum amplification values with each case parameter is also calculated.

The last but not the least, sensitivity of the amplification values to the case parameters is determined by using Artificial Neural Networks (ANN). 16 different ANNs are generated by using MATLAB [89] ANN Toolbox for this purpose. 8 of these ANNs are for the peak acceleration amplifications and another 8 of these ANNs are for the peak drift ratio amplifications. The amplification values related with PSA and S_d are excluded to be have a more brief sensitivity assessment.

Each set of ANNs are created with the same procedure. For instance, the ANN set of the acceleration amplifications are generated as follows. Firstly, an ANN is generated by using the whole case parameters. Then, each case parameter is excluded and a new ANN is generated per each case parameter. Since there are seven case parameters in SSUS and SSFF conditions, 7 ANNs are generated for each parameter exclusion. Thus 8 ANNs are generated for the peak acceleration amplifications.

The coefficient of determination (R^2) which is an indicator of the fit (i.e. success of the ANN) is calculated for each ANN. Naturally, the R^2 value closest to 1.0 is obtained for the ANN which utilizes all case parameters, for each set. The decrease in the R^2 value after exclusion of a case parameter shows the importance of the excluded case parameter. The largest decrease in the R^2 value must be obtained for most important case parameter. An importance order for the case parameters is determined by using this procedure.

3.3 Numerical Modelling

In this thesis, the interaction between surface structure and underground structure is investigated by using numerical analyses. A Finite Element Method (FEM) software, OpenSees (Open System for Earthquake Engineering Simulation) [90], is employed for this purpose. The OpenSees [90] software has been developed by the Pacific Earthquake Engineering Research Center (PEER) with the support of the National Science Foundation. OpenSees [90] is a software framework for simulating structural and geotechnical systems.

The OpenSees [90] software platform enhances modularity and extensibility for handling models for mechanical behavior, solution algorithms and data manipulation. The OpenSees [90] software framework includes a set of C++ classes. These classes are data structures, models, elements, solution algorithms, integrators, equation solvers and databases. The classes are created in such a way that makes it possible to solve a large number of problems, including Soil Structure Interaction problems. Besides, the C++ classes of OpenSees [90] has been manipulated to create Python packages/modules, recently.

The original OpenSees [90] software is coded in C++ language in such a way that Tcl commands are embedded inside. Namely, all of the Tcl language commands can be used in OpenSees [90] scripts. For instance, the user can put a simple line of code to the end of OpenSees [90] script which shuts down the computer after the analysis performed. On the other hand, creating a large OpenSees [90] model script by hand is very difficult, since the whole Tcl script may have more than thousands of command lines. In this thesis, some useful MATLAB [89] codes are developed to automatically create Tcl scripts for the investigated problem.

3.3.1 Modelling Soil Deposit

In this thesis, two-dimensional (2D) FEM models are created to investigate the interaction problem. Therefore, quadrilateral elements with four nodes are used for modelling the soil deposit. Since the soil deposit is infinitely long in the direction which is perpendicular to the modelling plane, the element stress state is defined to be plane strain. The quadrilateral element thickness is defined to be 1 m to represent unit thickness.

The 'Pressure Independent Multi Yield (PIMY)' material from the OpenSees [90] library is assigned to the quadrilateral elements which are representing the soil medium. The Pressure Independent Multi Yield material is appropriate for modelling organic soils or clays under fast (i.e. undrained) loading conditions. The deviatoric

stress-strain behavior is elastic-plastic for the Pressure Independent Multi Yield material, while the volumetric stress-strain behavior is linear elastic. This material is suitable to model materials whose shear behavior is independent of the confinement pressure variation (i.e. Von Misses type of yield surfaces) [91].

The shear wave velocity and cohesion values for the considered four soil sites were given previously (see Table 3.2). However, the PIMY material requires more parameters than shear wave velocity and cohesion. The PIMY material of OpenSees [90] also requires mass density, Poisson's ratio, peak shear strain, and friction angle properties. Adopted values for the listed mechanical properties in this study are given in Table 3.3.

Table 3.3 Soil mechanical properties

Parameter	Value
Mass Density (t/m^3)	1.8
Poisson's Ratio	0.25
Peak Shear Strain	0.10
Friction Angle (°)	0

Even it is given in Table 3.3, the friction angle is not allowed for PIMY material in dynamic analyses, and it must be set to 0. The mass density, Poisson's ratio and peak shear strain values are selected as generic values. The property values given in Table 3.3 are the same for all investigated soil sites, i.e. soil sites 1 to 4. The stress-strain curve and the backbone curve obtained by using the given mechanical properties are given in Figure 3.4, Figure 3.5, Figure 3.6 and Figure 3.7 for Soil Site 1, Soil Site 2, Soil Site 3 and Soil Site 4, respectively.

The soil deposits have a height of 60 m and first fundamental periods of the soil sites are 2.4 sec, 1.2 sec, 0.686 sec and 0.48 sec, respectively. For the soil deposits, 5% viscous damping is employed, and the Rayleigh scheme is adopted to introduce the damping.

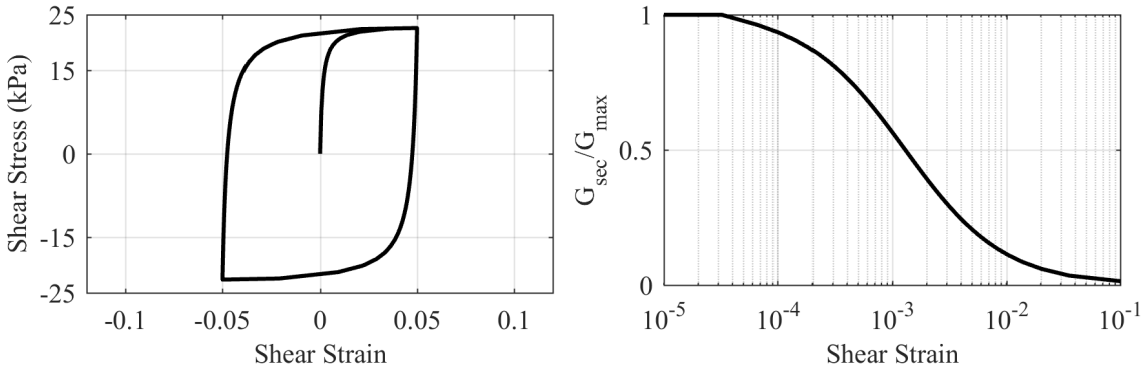

Figure 3.4 Stress-strain behavior and backbone curve for Soil Site 1

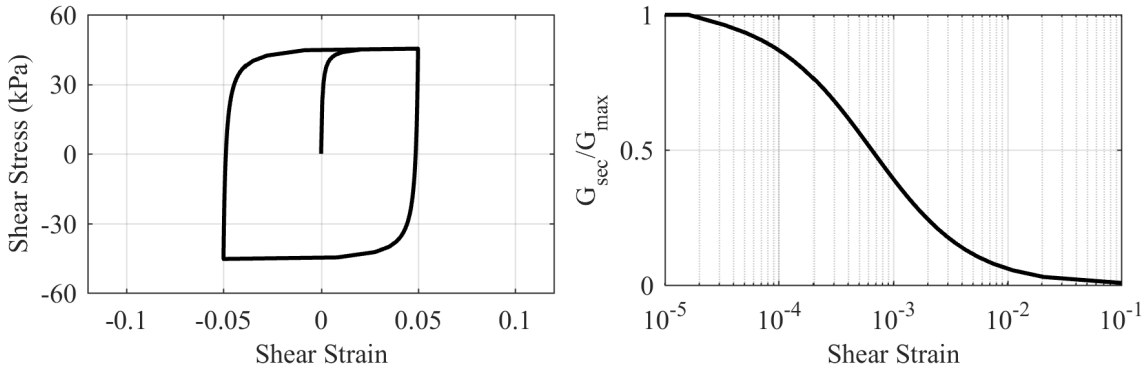

Figure 3.5 Stress-strain behavior and backbone curve for Soil Site 2

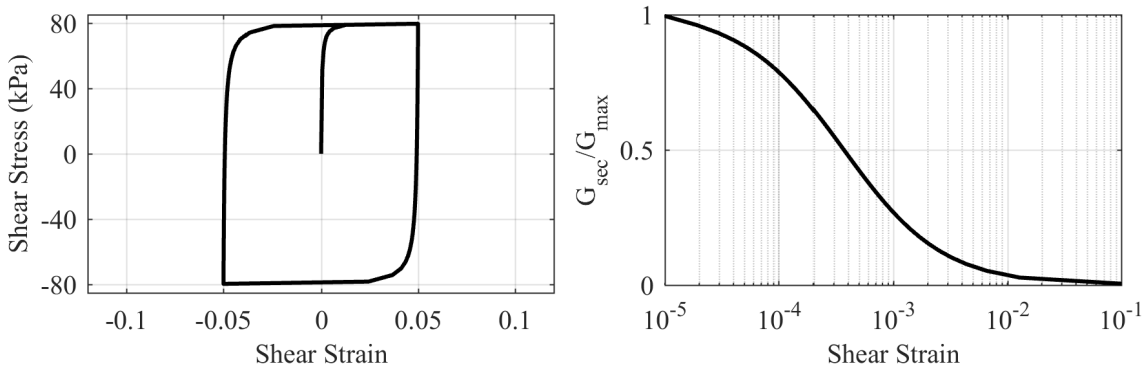

Figure 3.6 Stress-strain behavior and backbone curve for Soil Site 3

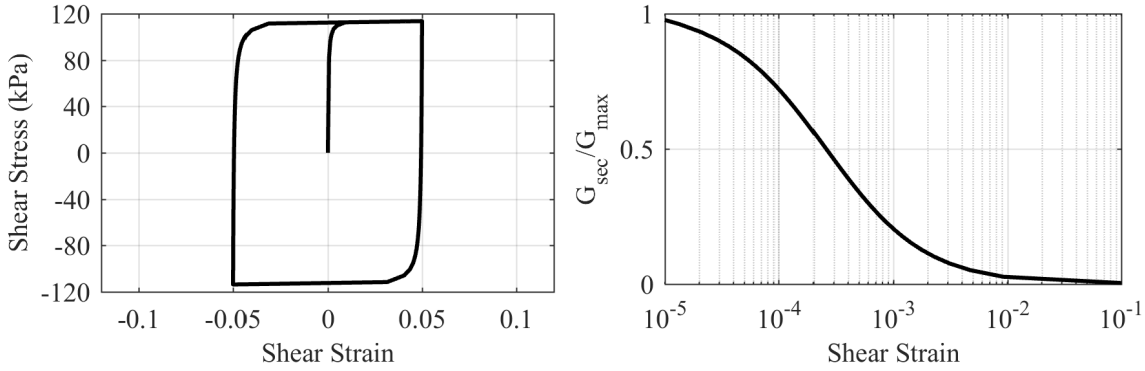

Figure 3.7 Stress-strain behavior and backbone curve for Soil Site 4

3.3.2 Modelling Structural Components

The structural components in the numerical models are the underground structure, the surface structure and its foundation. Elastic beam-column elements from the OpenSees [90] library are utilized for modelling the structural components. The surface structure is modelled as a Single Degree of Freedom (SDOF, i.e. mass and column system) system with a mat foundation. On the other hand, the underground structure is modelled as a square shaped closed frame system. For both underground structure and surface structure linear elastic material is defined.

Since the surface structure is modelled as SDOF (i.e. mass and column) system, the column stiffness and the lumped mass are representative values. Therefore, material type, concrete class, etc. cannot be mentioned. Instead, SDOF fundamental period and damping ratio can be used to identify the surface structure. In this thesis, the fundamental period of the surface structure is selected to be equal to five different values. Those values are given in Table 3.1 and represent low to mid rise residential buildings.

The surface structure have a raft foundation with a width of 16 m and a height of 1 m for all cases. The surface structure foundation is modelled so as to have a relatively rigid foundation and exclude the effects due to deformation of the foundation. The width value is selected so as to represent the width of a generic residential building. On the other hand, the mass of the foundation is accounted in the numerical models as distributed along the foundation width. The surface structure can have 2, 4, 6, 8 and 10 stories, for periods of 0.2 sec, 0.4 sec, 0.6 sec, 0.8 sec and 1.0sec, respectively. The corresponding surface structure masses are determined in accordance with current practice. Locations of the lumped SDOF masses are assumed to be at two-thirds of the total height of the surface structure (i.e. assuming triangular distribution of seismic forces along the surface structure height). The story height is assumed to be 3 m for all of the surface structures and the viscous damping ratio is assumed to be 5%. The corresponding lateral stiffness values are calculated in such a way to assure the predefined fundamental period values. The parameters used in modelling the surface structures are given in Table 3.4. A sketch representing the SDOF generation process is given in Figure 3.8.

Table 3.4 SDOF system parameters

Parameters	**Building 1**	**Building 2**	**Building 3**	**Building 4**	**Building 5**
$T_B(sec)$	0.2	0.4	0.6	0.8	1.0
$M_{str}(tons)$	28.8	67.2	105.6	144.0	182.4
$h_{eff}(m)$	4	8	12	16	20

The underground structure is modelled as a reinforced concrete structure with material mass density of 2.5 t/m^3 and Young's Modulus of 3.2×10^7 kN/m^2. The frame element cross-sectional dimensions depend on the underground structure wall thickness and the planar thickness (i.e. 1 m). For the underground structure, the element masses are defined as distributed along the frames.

3.3.3 Boundary Conditions

There are two important assumptions of one-dimensional wave propagation analysis which are violated in finite domain methods. First assumption is that the underlying

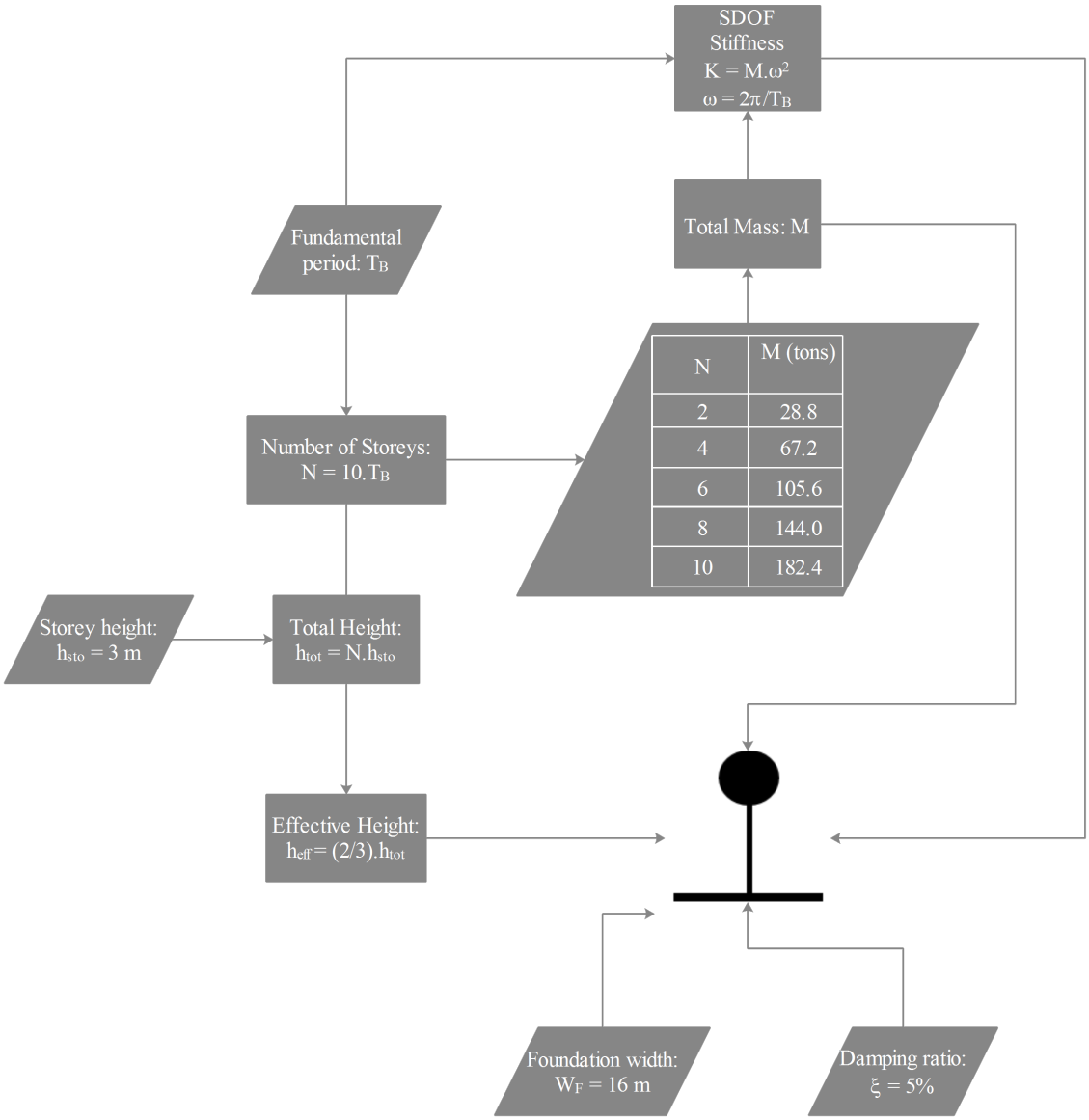

Figure 3.8 Surface structure modelling procedure

bedrock layer has a finite rigidity and an infinite thickness. And second assumptions is that the soil layers are infinitely long in horizontal direction. There are special boundary conditions to impose those assumptions to finite domain models.

As a result of the first assumption, a portion of waves reaching to the bottom boundary of the domain must be absorbed and the remaining portion must be reflected into the domain. This partial absorption can be ensured by the use of dash-pot elements at the base of the domain. In case of fixed bottom boundary, all waves reaching to this boundary will be completely reflected back into the domain. This type of boundary condition is named as Quite Boundary or Viscous Boundary [92]. The use of quite boundary condition enables FEM models to have lesser number of elements in vertical direction.

As a result of the second assumption, the FEM model should include an infinitely wide soil domain which is impossible in practice. At this stage, using Periodic Boundary Conditions on a domain with finite width yields the same results with a theoretically infinite width domain. Periodic Boundary Condition can be briefly defined as imposing the same motion to lateral boundaries of the soil domain. In FEM models for Soil Structure Interaction problems, structural part of the model is generally located at the horizontal center of the soil domain. Thus, the response on the lateral boundaries of the model is expected not to be altered by the structure at the center. The unaltered motion must be the same with the motion under free field conditions which means in-existence of any structure in the model. The periodic type of boundary condition is achieved by enforcing the lateral boundaries of the soil domain to move simultaneously (i.e. assigning equal degree of freedom in OpenSees). One dimensional shear wave propagation is ensured by introducing the periodic boundary conditions.

As stated above, implementation of Viscous Boundary Condition requires dash-pot elements on bottom boundary of the domain. The coefficient of that dash-pot is given in Equation 3 for pure shear behavior. On the other hand, lateral dash-pots may also be located at the sides of the soil domain. The use of dash-pots on lateral boundaries depends on the width of the domain and internal damping ratio. If the domain is wide enough and internal damping ratio is high enough, then there is no need for dash-pot elements on side boundaries. In this case, the waves reflecting from side boundaries are damped out by the internal damping during their propagation. However, if internal soil damping ratio is low and model width is small, then the use of dash-pot elements emerges. In this case, the waves reflecting from lateral boundaries are damped out by the dash-pot elements.

$$C_D = \rho . V_S . A \tag{3.7}$$

In Equation 3, ρ is the mass density, V_S is the shear wave velocity and A is the area represented by dash-pot element. If the dash-pot is defined for base of the model, mass density and shear wave velocity values for bedrock need to be used and the area corresponds to the base area.

On the other hand, the interfaces between soil and underground structure and the interfaces between soil and surface structure foundation should also be considered during defining boundary conditions. In this thesis, all of these contacting surfaces are defined by using bonded type constrains. It is a fact that bonded type constraints are not physically appropriate. However, numerical models with the bonded constraints

yield results for upper bound.

3.3.4 Defining Base Excitation

In wave propagation problems, incident waves start propagation from a source and travel through the whole domain. For earthquake engineering problems dealing with engineering depth, this source can be represented by the bedrock-soil interface. A well-known approach to define base excitation in FEM models is imposing velocity of seismic event from the bottom boundary. The velocity history of seismic event can be converted to force history by multiplying it with some coefficient. The coefficient for this multiplication is the same with coefficient of dash-pot at the base of domain. This procedure to exert loading at the base of soil domain was proposed by Joyner et al. [93].

All nodes at the base of domain are constrained to have the same displacement in horizontal direction and restrained in vertical direction. Thus, the force history can be applied to one node at the bottom boundary. By the way, assigning the same motion to all of the base nodes results in one-dimensional wave propagation in vertical direction. Derivation of force history is given in Equation 3.8 to Equation 3.19, by using velocity history at bedrock-soil interface.

$$V_S = \frac{dx}{dt} \tag{3.8}$$

$$\frac{d^2u}{dt^2} = V_S^2 . \frac{d^2u}{dx^2} \tag{3.9}$$

$$\gamma = \frac{du}{dx} \tag{3.10}$$

$$\tau = G.\gamma \tag{3.11}$$

$$G = \rho . V_S^2 \tag{3.12}$$

$$F = A.\tau \tag{3.13}$$

$$v = \frac{du}{dt} \tag{3.14}$$

$$\frac{dv}{dt} = \frac{d\left(\frac{G}{\rho}.\gamma\right)}{dx} \tag{3.15}$$

$$\frac{dv}{dt} = \frac{1}{\rho}.\frac{d\tau}{dx} \tag{3.16}$$

$$\rho.dx.\frac{dv}{dt} = d\tau \tag{3.17}$$

$$\rho.dx.A.\frac{dv}{dt} = dF \tag{3.18}$$

$$\rho.V_S.A.v(t) = F(t) \tag{3.19}$$

In Equation 3.19, $F(t)$ represents the force history, $v(t)$ is the outcrop velocity history, ρ is the mass density, V_S is the shear wave velocity and A is the area of the base. In these equations, while calculating the area term, thickness of the plane strain elements should be considered. As stated before, the out of plane thickness is defined to be 1 m for all models.

In this thesis, a 5 seconds long Ricker wavelet with 1 Hz dominant frequency is utilized as the input motion acceleration history. The input motion acceleration history and its Fourier Amplitude Spectrum (FAS) are given in Figure 3.9. As stated before, the input motion is scaled to three different peak amplitude values as $0.10g$, $0.30g$ and $0.50g$. Therefore, only the acceleration history with $0.10g$ peak amplitude is illustrated in Figure 3.9.

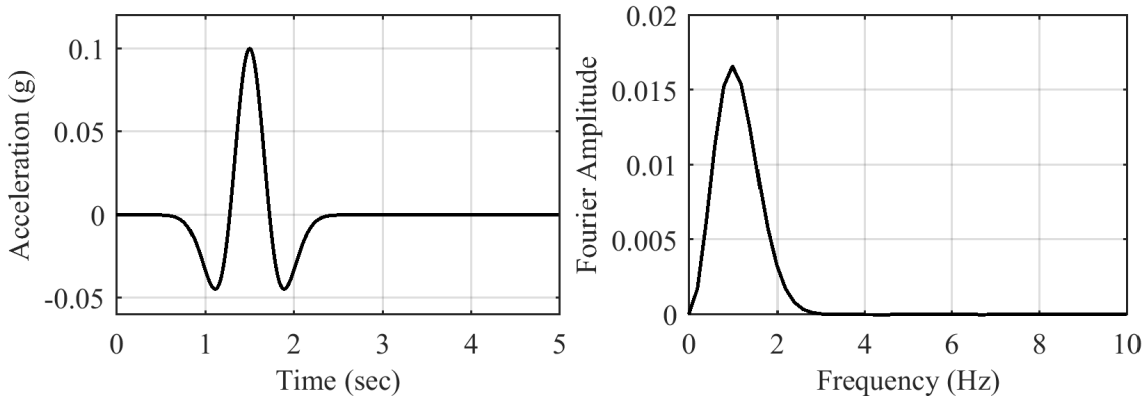

Figure 3.9 Input motion time history and FAS

The Ricker wavelet is preferred in this study to assure that the system will undergo larger deformations. Displacement response spectra of the Ricker wavelet is compared with that of a set of well-known earthquakes. In Figure 3.10, the comparison is given and it is obvious that the Ricker wavelet generally yields larger spectral displacements.

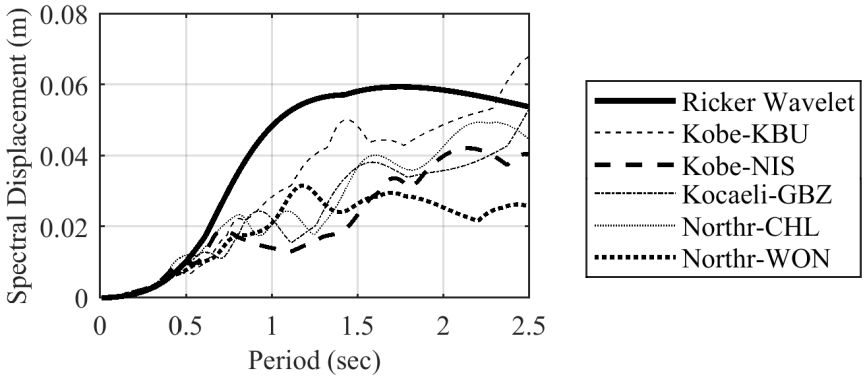

Figure 3.10 Comparison of displacement response spectra

3.4 Element Sizes, Time Step and Mesh

Element size and analysis time step are two important parameters which should be determined prior to model generation. There is a well-known relation for determination of element size based on the minimum shear wave velocity and maximum frequency of interest, given in Equation 3.20 and Equation 3.21. In these equations, l_e is the element size, λ is the minimum wavelength, $V_{S,min}$ is the minimum shear wave velocity that will propagate and f_{max} is the maximum frequency of interest. [92], suggested that the ratio should be less than 1/12 for accurate results. However, latter researches yield accurate results with larger ratios up to 1/8. In this thesis, element size is determined as 1/8 of the minimum wavelength. The maximum frequency considered in this thesis is nearly 6 Hz, the minimum propagation velocity 100 m/sec and the element size for quadrilateral elements is 2 m. However, the

element size in the vicinity of structural elements is 0.5 m due to mesh refinement.

$$\frac{l_e}{\lambda} \approx \frac{1}{8} \tag{3.20}$$

$$\lambda = \frac{V_{S,min}}{f_{max}} \tag{3.21}$$

The analysis time step is determined by using CFL criteria for wave propagation problems [94]. For the investigated problem, Courant number should be equal or less than 1, which is defined in Equation 3.22. In Equation 3.22, C_N is the Courant number, V_{min} is the minimum propagation velocity, Δx is interval length, $C_{N,max} = 1$ is the upper limit for Courant number and Δt is the analysis time step. In this study, l_e is assumed to be minimum element size, u is assumed to be maximum shear wave velocity to get a conservative analysis time step.

$$C_N = \frac{V_{min}.\Delta t}{l_e} \leq C_{N,max} \tag{3.22}$$

In general, dimensions of soil domain varies with respect to the investigated problem for numerical models in Soil Structure Interaction problems. For instance, for one-dimensional site response analysis, width of the domain can be equal to one element size. On the other hand, for two-dimensional problems, domain width depends on boundary conditions and structural components. For the investigated problem in this thesis, the model width is selected to be 500 m in accordance with preliminary convergence analyses. The numerical model utilized for convergence study includes a SDOF structure lying on a soil site in which an underground structure is embedded, i.e. a model in SSUS conditions. The model width is varied from 100 m to 700 m and top displacement of the SDOF structure is focused on for convergence. The top displacement variation with model width is illustrated in Figure 3.11 and it is obvious that the top displacement converges after 500 m model width.

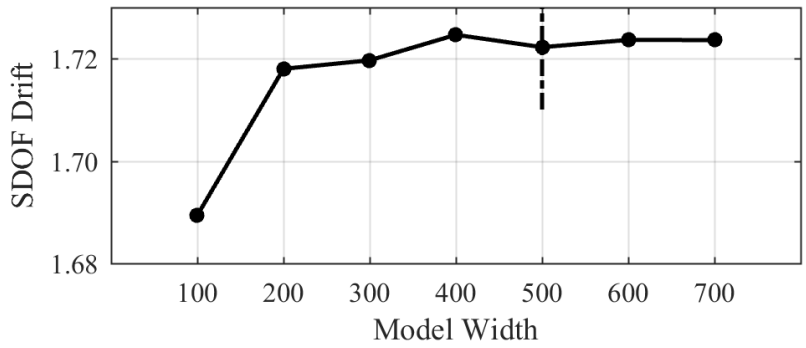

Figure 3.11 Convergence study to determine numerical model width

In this thesis, a simple mesh for FEM analysis is generated by using MATLAB [89] scripts developed during this study. The developed MATLAB [89] script generates structured meshes, and adequate for FEM analysis. There are mesh refinements in the vicinity of surface structure and underground structure. A schematic illustration for the generated mesh is given in Figure 3.12.

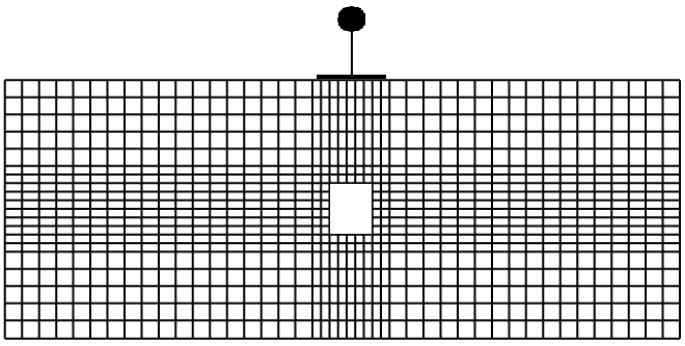

Figure 3.12 Schema of the numerical model mesh

4
NUMERICAL ANALYSIS RESULTS

In this chapter, the results obtained from numerical analyses are presented. Before presenting the results, explanations of a number of term should be given here for reading convenience.

- SSFF stands for “surface structure free field” and corresponds to the cases including a surface structure lying on a soil deposit without an underground structure.
- USFF stands for “underground structure free field” and corresponds to the cases including an underground structure embedded in a soil deposit without a surface structure.
- SSUS stands for “surface structure underground structure” and corresponds to the cases including a surface structure lying on a soil deposit with an underground structure.
- FF stands for “free field” and corresponds to the cases including only a soil deposit.

There is a large amount of response data obtained from the numerical analyses. A brief list of the obtained responses can be given as:

- Ground Surface Accelerations in FF conditions
- Ground Surface Accelerations in USFF conditions
- Surface Structure Accelerations and Drifts in SSFF
- Surface Structure Accelerations and Drifts in SSUS

By using the listed response data, acceleration and displacement response spectra for ground surface accelerations in all cases are determined. Firstly, spectral values in FF and USFF conditions are given. Secondly, surface structure accelerations and drifts in SSFF and SSUS conditions are given. The amplifications in the responses (i.e. spectral values, surface structure accelerations and drifts) are also illustrated. The amplification in the responses are calculated by dividing the responses in non-FF condition to the responses in corresponding FF condition.

Finally, the sensitivity of the surface structure acceleration and drift amplifications to the case parameters are presented.

4.1 Spectral Values in FF and USFF Conditions

Although this thesis focuses on low to mid-rise buildings, the response spectra (i.e. PSA and S_d) in FF and USFF conditions are calculated for period values up to 4 sec. The PSA values in FF conditions are given in Figure 4.1. There are 12 graphs given in four rows and three columns on this figure. The rows correspond to soil sites and columns correspond to input motion PGA values.

As seen from Figure 4.1, as a result of material non-linearity, the increase in the PSA values are not proportional to the input motion PGA values. On the other hand, the PSA values on stiffer soil sites are larger than the PSA values on softer soil sites (e.g. PSA at Soil Site 2 are larger than PSA at Soil Site 1). This is also a result of material non-linearity which causes high level of hysteretic damping during dynamic excitation.

The S_d values in FF conditions are given in Figure 4.2. There are also 12 graphs in this figure as in Figure 4.1. As seen from Figure 4.2, the increase in the S_d values are not proportional to the input motion PGA values, as it was the case for the PSA values. On the other hand, the S_d values on stiffer soil sites are generally larger than the S_d values on softer soil sites. However, for the cases where the input motion PGA is $0.10g$, the S_d values on stiffer soil sites are smaller than the S_d values on softer soil sites.

Since there are 216 cases in USFF conditions, response spectra graphs are grouped in such a way to have a total of eight figures. There are 18 graphs (i.e. corresponding to 18 different cases) on each figure and three illustrations (i.e. corresponding to three different input motion PGA values) on each graphs. For these eight figures, the corresponding case parameter values are written as titles to the graphs.

The PSA values for Soil Site 1 in USFF conditions are given in Figure 4.3. As seen from

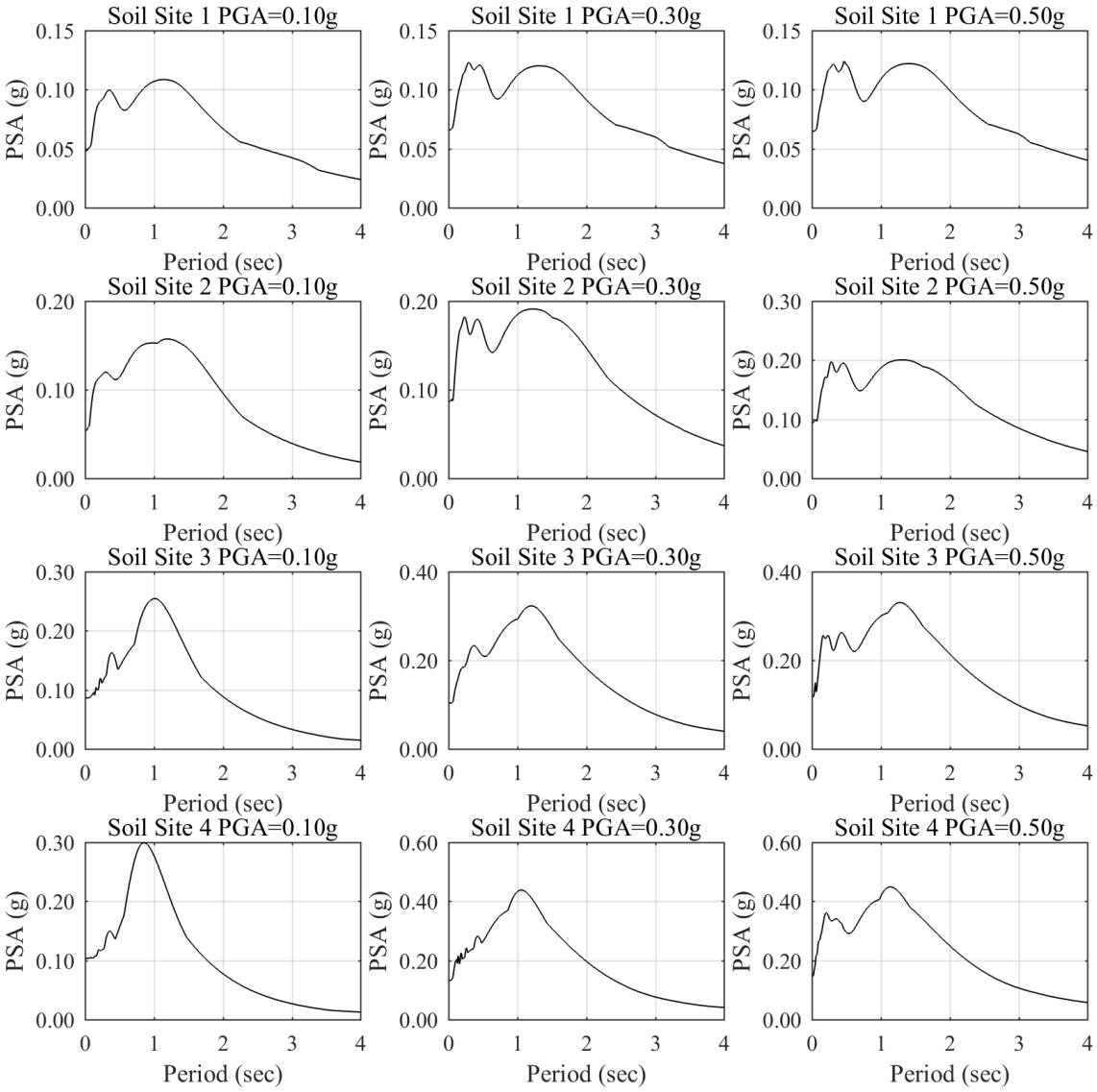

Figure 4.1 PSA values in FF conditions

Figure 4.3, the maximum PSA values are about $0.15g$, which are generally below the PSA values obtained from FF conditions. The PSA values for the cases where the input motion PGA is $0.10g$ are remarkably below the PSA values for the cases where the input motion PGA is $0.30g$ and $0.50g$. However, there is not a big difference between the PSA values for the cases where the input motion PGA is $0.30g$ and $0.50g$. On the other hand, the PSA values almost non-sensitive to the parameters R_D, H and t_W.

The PSA values for Soil Site 2 in USFF conditions are given in Figure A.1. As seen from Figure 4.4, the maximum PSA values are about $0.20g$, which are generally below the PSA values obtained from FF conditions. The PSA values for the cases where the input motion PGA is $0.10g$ are remarkably below the PSA values for the cases where the input motion PGA is $0.30g$ and $0.50g$. However, there is not a big difference between the PSA values for the cases where the input motion PGA is $0.30g$ and $0.50g$. On the

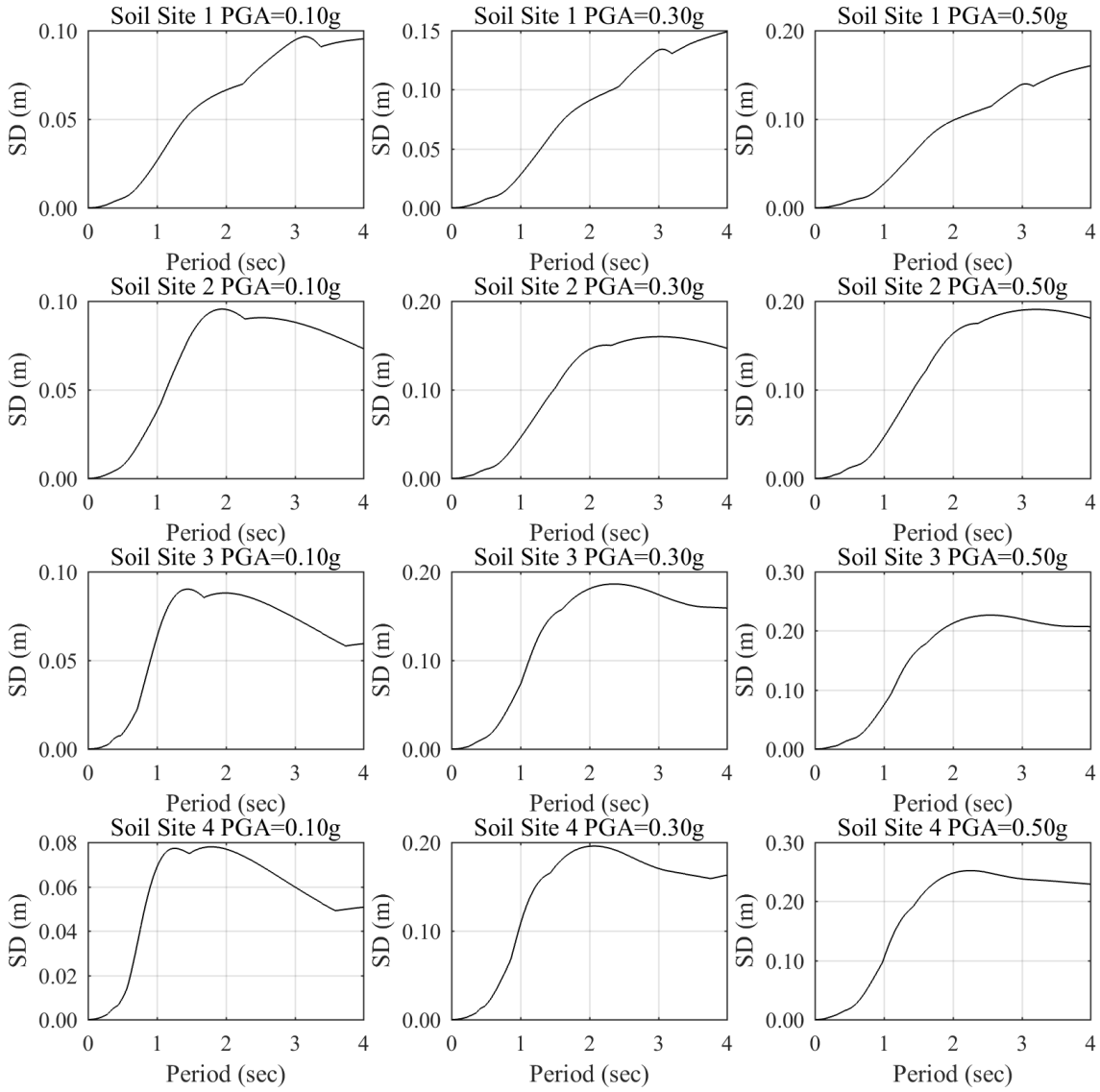

Figure 4.2 S_d values in FF conditions

other hand, the *PSA* values almost non-sensitive to the parameters R_D, H and t_W.

The *PSA* values for Soil Site 3 in USFF conditions are given in Figure A.2. As seen from Figure 4.5, the maximum *PSA* values are about $0.30g$, which are generally below the *PSA* values obtained from FF conditions. The *PSA* values for the cases where the input motion *PGA* is $0.10g$ are remarkably below the *PSA* values for the cases where the input motion *PGA* is $0.30g$ and $0.50g$. However, there is not a big difference between the *PSA* values for the cases where the input motion *PGA* is $0.30g$ and $0.50g$. On the other hand, the *PSA* values almost non-sensitive to the parameters R_D, H and t_W.

The *PSA* values for Soil Site 4 in USFF conditions are given in Figure A.3. As seen from Figure 4.6, the maximum *PSA* values are about $0.45g$, which are generally below the *PSA* values obtained from FF conditions. The *PSA* values for the cases where the input motion *PGA* is $0.10g$ are remarkably below the *PSA* values for the cases where the

input motion PGA is $0.30g$ and $0.50g$. However, there is not a big difference between the PSA values for the cases where the input motion PGA is $0.30g$ and $0.50g$. On the other hand, the PSA values almost non-sensitive to the parameters R_D, H and t_W.

The S_d values for Soil Site 1 in USFF conditions are given in Figure A.4. As seen from Figure 4.7, the maximum S_d values are about 15 cm, which are nearly the same with the S_d values obtained from FF conditions. The S_d values for the cases where the input motion PGA is $0.10g$ are remarkably below the S_d values for the cases where the input motion PGA is $0.30g$ and $0.50g$. However, there is not a big difference between the S_d values for the cases where the input motion PGA is $0.30g$ and $0.50g$. On the other hand, the S_d values almost non-sensitive to the parameters R_D, H and t_W.

The S_d values for Soil Site 2 in USFF conditions are given in Figure A.5. As seen from Figure 4.8, the maximum S_d values are about 20 cm, which are nearly the same with the S_d values obtained from FF conditions. The S_d values for the cases where the input motion PGA is $0.10g$ are remarkably below the S_d values for the cases where the input motion PGA is $0.30g$. And also the S_d values for the cases where the input motion PGA is $0.30g$ are below the S_d values for the cases where the input motion PGA is $0.50g$. On the other hand, the S_d values almost non-sensitive to the parameters R_D, H and t_W.

The S_d values for Soil Site 3 in USFF conditions are given in Figure A.6. As seen from Figure 4.9, the maximum S_d values are about 24 cm, which are nearly the same with the S_d values obtained from FF conditions. The S_d values for the cases where the input motion PGA is $0.10g$ are remarkably below the S_d values for the cases where the input motion PGA is $0.30g$. And also the S_d values for the cases where the input motion PGA is $0.30g$ are below the S_d values for the cases where the input motion PGA is $0.50g$. On the other hand, the S_d values almost non-sensitive to the parameters R_D, H and t_W.

The S_d values for Soil Site 4 in USFF conditions are given in Figure A.7. As seen from Figure 4.10, the maximum S_d values are about 26 cm, which are slightly below the S_d values obtained from FF conditions. The S_d values for the cases where the input motion PGA is $0.10g$ are remarkably below the S_d values for the cases where the input motion PGA is $0.30g$. And also the S_d values for the cases where the input motion PGA is $0.30g$ are below the S_d values for the cases where the input motion PGA is $0.50g$. On the other hand, the S_d values almost non-sensitive to the parameters R_D, H and t_W.

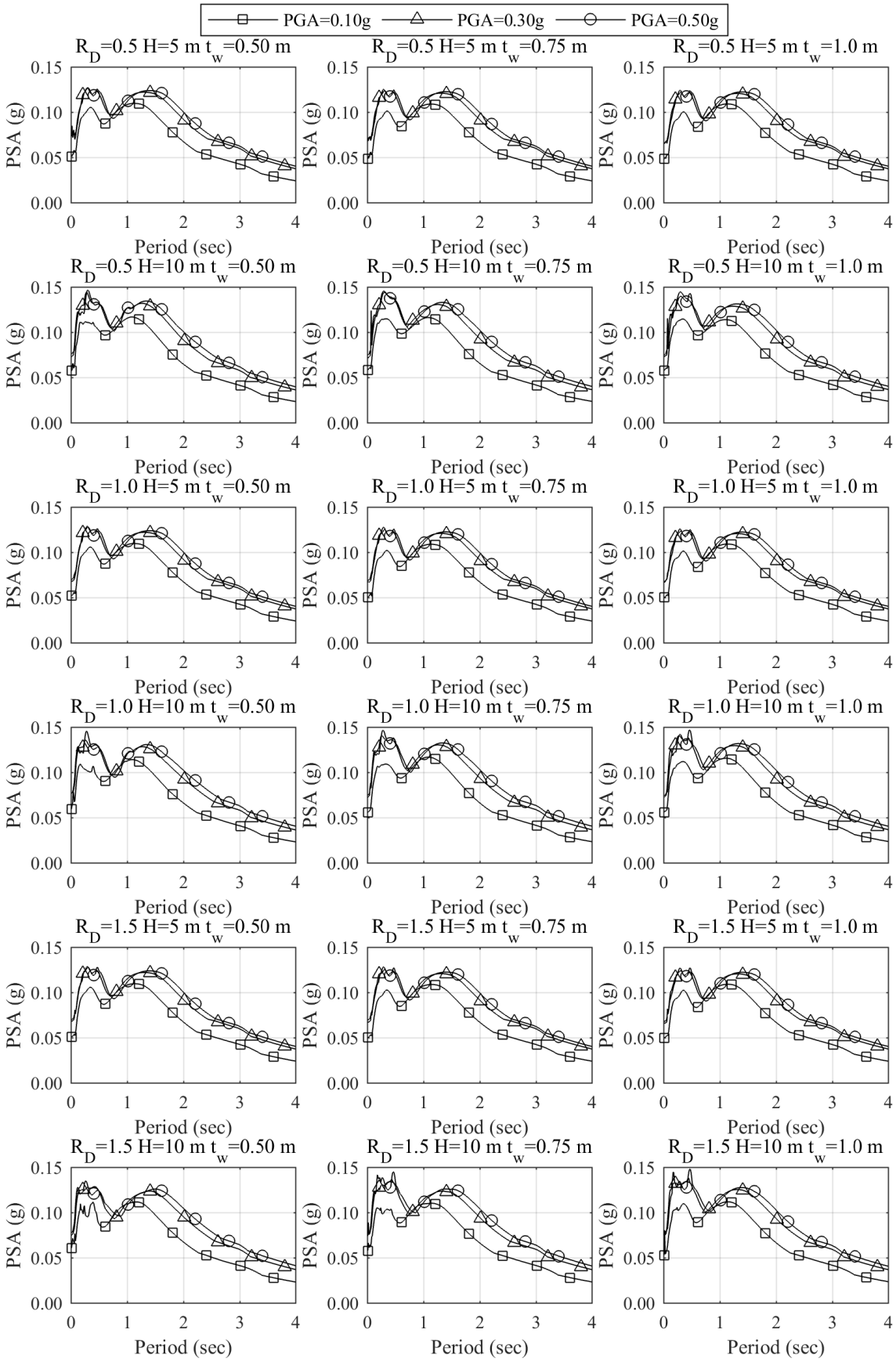

Figure 4.3 *PSA* values for Soil Site 1 in USFF conditions

4.2 Surface Structure Accelerations and Drifts in SSFF and SSUS conditions

There are totally 60 cases in SSFF conditions, which correspond to four different soil sites, three different input motion PGA values and five different surface structure fundamental period values. There are four figures for surface structure accelerations in SSFF conditions. Each of these figures consists of 15 graphs. The case parameter values are written as titles to the graphs.

The surface structure acceleration histories for Soil Site 1 in SSFF conditions are given in Figure 4.4. As seen from Figure 4.4, the maximum surface structure acceleration values are obtained for the cases where T_B is 0.2 sec. The maximum acceleration values decrease with increasing surface structure fundamental period (i.e. T_B). On the other hand, the maximum acceleration values are almost non-sensitive to the input motion PGA variation due to the hysteretic damping. The maximum surface structure acceleration value is nearly $0.11g$.

The surface structure acceleration histories for Soil Site 2 in SSFF conditions are given in Figure A.8. As seen from Figure A.8, the maximum surface structure acceleration values are obtained for the cases where T_B is 0.2 sec. The maximum acceleration values decrease with increasing surface structure fundamental period (i.e. T_B). On the other hand, the maximum acceleration values are almost non-sensitive to the input motion PGA variation due to the hysteretic damping. The maximum surface structure acceleration value is nearly $0.20g$.

The surface structure acceleration histories for Soil Site 3 in SSFF conditions are given in Figure A.9. As seen from Figure A.9, the maximum surface structure acceleration values are obtained for the cases where T_B is 0.8 sec. The maximum acceleration values are not proportional to the surface structure fundamental period (i.e. T_B). On the other hand, the maximum acceleration values are almost non-sensitive to the input motion PGA variation due to the hysteretic damping. The maximum surface structure acceleration value is nearly $0.30g$.

The surface structure acceleration histories for Soil Site 4 in SSFF conditions are given in Figure A.10. As seen from Figure A.10, the maximum surface structure acceleration values are obtained for the cases where T_B is 0.8 sec. The maximum acceleration values are not proportional to the surface structure fundamental period (i.e. T_B). On the other hand, the maximum acceleration values are almost non-sensitive to the input motion PGA variation due to the hysteretic damping. The maximum surface structure acceleration value is nearly $0.40g$.

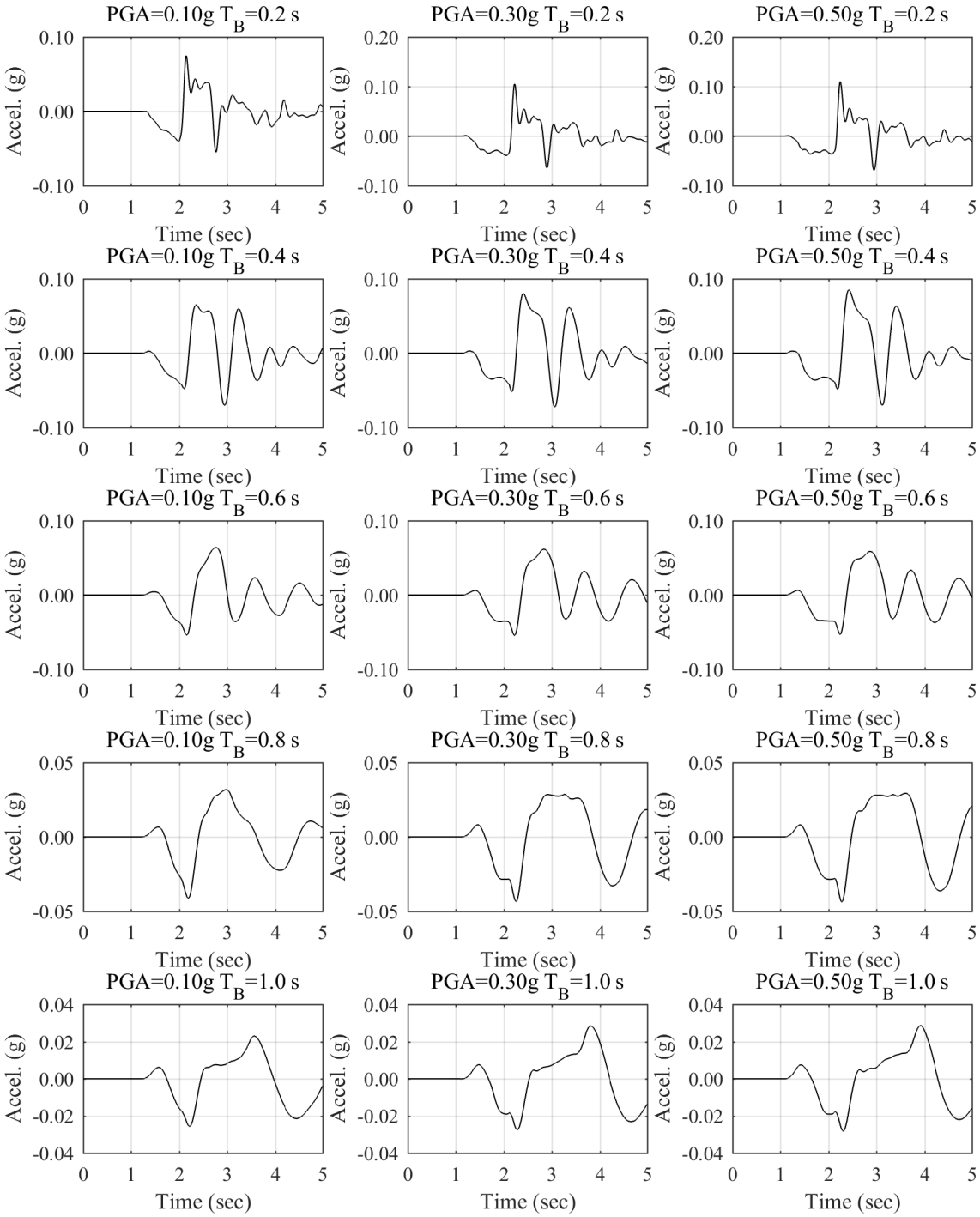

Figure 4.4 Surface structure accelerations for Soil Site 1

The surface structure drift ratios in SSFF conditions are illustrated with four figures, each corresponding to a different soil site. Each of these figures consists of 15 graphs and the case parameter values are written as titles to the graphs.

The surface structure drift histories for Soil Site 1 in SSFF conditions are given in Figure A.11. As seen from Figure A.11, the maximum surface structure drift ratio values are obtained for the cases where T_B is 0.8 sec and 1.0 sec. The maximum drift ratio values generally increases with the surface structure fundamental period (i.e. T_B). On the other hand, the maximum drift ratio values are almost non-sensitive to the input motion PGA variation due to the hysteretic damping. The maximum surface structure drift ratio value is nearly 0.55%.

The surface structure drift histories for Soil Site 2 in SSFF conditions are given in Figure A.12. As seen from Figure A.12, the maximum surface structure drift ratio values are obtained for the cases where T_B is 1.0 sec. The maximum drift ratio values increases with the surface structure fundamental period (i.e. T_B). On the other hand, the maximum drift ratio values are almost non-sensitive to the input motion PGA variation due to the hysteretic damping. The maximum surface structure drift ratio value is nearly 0.6%.

The surface structure drift histories for Soil Site 3 in SSFF conditions are given in Figure A.13. As seen from Figure A.13, the maximum surface structure drift ratio values are obtained for the cases where T_B is 1.0 sec. The maximum drift ratio values increases with the surface structure fundamental period (i.e. T_B). On the other hand, the maximum drift ratio values are almost non-sensitive to the input motion PGA variation due to the hysteretic damping. The maximum surface structure drift ratio value is nearly 0.8%.

The surface structure drift histories for Soil Site 4 in SSFF conditions are given in Figure A.14. As seen from Figure A.14, the maximum surface structure drift ratio values are obtained for the cases where T_B is 1.0 sec. The maximum drift ratio values increases with the surface structure fundamental period (i.e. T_B). On the other hand, the maximum drift ratio values are almost non-sensitive to the input motion PGA variation due to the hysteretic damping. The maximum surface structure drift ratio value is nearly 1.0%.

There are totally 3240 surface structure acceleration histories and 3240 surface structure drift histories for SSUS conditions. Even if the graphs were grouped, there would be 60 pages of figures for the SSUS conditions. Therefore, only one representative figure per soil site is given for both surface structure acceleration and drift histories. The representative case corresponds to $R_L = 2$ and $T_B = 0.60\ sec$.

The surface structure acceleration histories for Soil Site 1 in SSUS conditions are given in Figure A.15. As stated above, the representative case corresponds to $R_L = 2$ and $T_B = 0.60\,sec$. The peak surface structure acceleration value is around $0.08g$. As seen from Figure A.15, the surface structure acceleration values for the cases where the input motion PGA is $0.10g$ are slightly below the surface structure acceleration values for the cases where the input motion PGA is $0.30g$ and $0.50g$. However, there is not a big difference between the surface structure acceleration values for the cases where the input motion PGA is $0.30g$ and $0.50g$. On the other hand, effect of the parameters R_D, H and t_W on the surface structure acceleration values are almost negligible.

The surface structure acceleration histories for Soil Site 2 in SSUS conditions are given in Figure A.16. As stated above, the representative case corresponds to $R_L = 2$ and $T_B = 0.60\,sec$. As seen from Figure A.16, the peak surface structure acceleration value is around $0.19g$. The surface structure acceleration values for the cases where the input motion PGA is $0.10g$ are slightly below the surface structure acceleration values for the cases where the input motion PGA is $0.30g$ and $0.50g$. However, there is not a big difference between the surface structure acceleration values for the cases where the input motion PGA is $0.30g$ and $0.50g$. On the other hand, effect of the parameters R_D, H and t_W on the surface structure acceleration values are almost negligible.

The surface structure acceleration histories for Soil Site 3 in SSUS conditions are given in Figure A.17. As stated above, the representative case corresponds to $R_L = 2$ and $T_B = 0.60\,sec$. As seen from Figure A.17, the peak surface structure acceleration value is around $0.26g$. The surface structure acceleration values for the cases where the input motion PGA is $0.10g$ are slightly below the surface structure acceleration values for the cases where the input motion PGA is $0.30g$ and $0.50g$. However, there is not a big difference between the surface structure acceleration values for the cases where the input motion PGA is $0.30g$ and $0.50g$. On the other hand, effect of the parameters R_D, H and t_W on the surface structure acceleration values are almost negligible.

The surface structure acceleration histories for Soil Site 4 in SSUS conditions are given in Figure A.18. As stated above, the representative case corresponds to $R_L = 2$ and $T_B = 0.60\,sec$. As seen from Figure A.18, the peak surface structure acceleration value is around $0.34g$. The surface structure acceleration values for the cases where the input motion PGA is $0.10g$ are slightly below the surface structure acceleration values for the cases where the input motion PGA is $0.30g$ and $0.50g$. However, there is not a big difference between the surface structure acceleration values for the cases where the input motion PGA is $0.30g$ and $0.50g$. On the other hand, effect of the parameters R_D, H and t_W on the surface structure acceleration values are almost negligible.

The surface structure drift histories for Soil Site 1 in SSUS conditions are given in Figure A.19. As stated above, the representative case corresponds to $R_L = 2$ and $T_B = 0.60\ sec$. As seen from Figure A.19, the peak surface structure drift ratio is around 0.6%. The surface structure drift values for the cases where the input motion PGA is $0.10g$ are slightly below the surface structure acceleration values for the cases where the input motion PGA is $0.30g$ and $0.50g$. However, there is not a big difference between the surface structure acceleration values for the cases where the input motion PGA is $0.30g$ and $0.50g$. On the other hand, effect of the parameters R_D, H and t_W on the surface structure acceleration values are almost negligible.

The surface structure drift histories for Soil Site 2 in SSUS conditions are given in Figure A.20. As stated above, the representative case corresponds to $R_L = 2$ and $T_B = 0.60\ sec$. As seen from Figure A.20, the peak surface structure drift ratio is around 0.32%. The surface structure drift values for the cases where the input motion PGA is $0.10g$ are slightly below the surface structure acceleration values for the cases where the input motion PGA is $0.30g$ and $0.50g$. However, there is not a big difference between the surface structure acceleration values for the cases where the input motion PGA is $0.30g$ and $0.50g$. On the other hand, effect of the parameters R_D, H and t_W on the surface structure acceleration values are almost negligible.

The surface structure drift histories for Soil Site 3 in SSUS conditions are given in Figure A.21. As stated above, the representative case corresponds to $R_L = 2$ and $T_B = 0.60\ sec$. As seen from Figure A.21, the peak surface structure drift ratio is around 0.45%. The surface structure drift values for the cases where the input motion PGA is $0.10g$ are slightly below the surface structure acceleration values for the cases where the input motion PGA is $0.30g$ and $0.50g$. However, there is not a big difference between the surface structure acceleration values for the cases where the input motion PGA is $0.30g$ and $0.50g$. On the other hand, effect of the parameters R_D, H and t_W on the surface structure acceleration values are almost negligible.

The surface structure drift histories for Soil Site 4 in SSUS conditions are given in Figure A.22. As stated above, the representative case corresponds to $R_L = 2$ and $T_B = 0.60\ sec$. As seen from Figure A.22, the peak surface structure drift ratio is around 0.5%. The surface structure drift values for the cases where the input motion PGA is $0.10g$ are slightly below the surface structure acceleration values for the cases where the input motion PGA is $0.30g$ and $0.50g$. However, there is not a big difference between the surface structure acceleration values for the cases where the input motion PGA is $0.30g$ and $0.50g$. On the other hand, effect of the parameters R_D, H and t_W on the surface structure acceleration values are almost negligible.

4.3 Amplifications in Drifts and Accelerations

As stated before, the interaction between underground structures and surface structures was investigated by using different methods. Therefore, amplification of the surface structure accelerations are presented along with amplification of the *PSA* values obtained from the ground surface accelerations. Besides, amplification of the surface structure drifts are also presented.

4.3.1 Ground Surface Spectral Values

There are 216 different cases in USFF conditions and 12 different cases in FF conditions. The amplification graphs are grouped in such a way to have 18 graphs on a figure and three illustrations on each graphs. Thus, there is one figure per soil site for *PSA* amplifications. The parameter values for each case are written as titles to each graph. Despite both acceleration and displacement response spectra are given previously, S_d amplifications are not presented. Since the *PSA* and S_d values are proportional, the amplifications in S_d values are identical with the *PSA* amplifications.

Amplifications of the *PSA* values for Soil Site 1 in USFF conditions are illustrated in Figure 4.27. As seen from Figure 4.27, the maximum *PSA* amplification is about 24% and the maximum de-amplification is about 2%. It is obvious that amplification values for the cases where underground structure height is smaller (i.e. $H = 5\ m$) are lower than the amplification values for the cases where $H = 10\ m$. Effects of the other case parameters on *PSA* amplification are slightly complicated.

Amplifications of the *PSA* values for Soil Site 2 in USFF conditions are illustrated in Figure 4.28. As seen from Figure 4.28, the maximum *PSA* amplification is about 16% and de-amplification is not observed. It is obvious that amplification values for the cases where underground structure height is smaller (i.e. $H = 5$ m) are lower than the amplification values for the cases where $H = 10\ m$. Effects of the other case parameters on *PSA* amplification are slightly complicated.

Amplifications of the *PSA* values for Soil Site 3 in USFF conditions are illustrated in Figure 4.29. As seen from Figure 4.29, the maximum *PSA* amplification is about 10% and the maximum de-amplification is about 2%. It is obvious that amplification values for the cases where underground structure height is smaller (i.e. $H = 5$ m) are lower than the amplification values for the cases where $H = 10\ m$. Effects of the other case parameters on *PSA* amplification are slightly complicated.

Amplifications of the *PSA* values for Soil Site 4 in USFF conditions are illustrated in Figure 4.30. As seen from Figure 4.30, the maximum *PSA* amplification is about 6%

and the maximum de-amplification is about 3%. It is obvious that amplification values for the cases where underground structure height is smaller (i.e. $H = 5m$) are lower than the amplification values for the cases where $H = 10\ m$. Effects of the other case parameters on PSA amplification are slightly complicated.

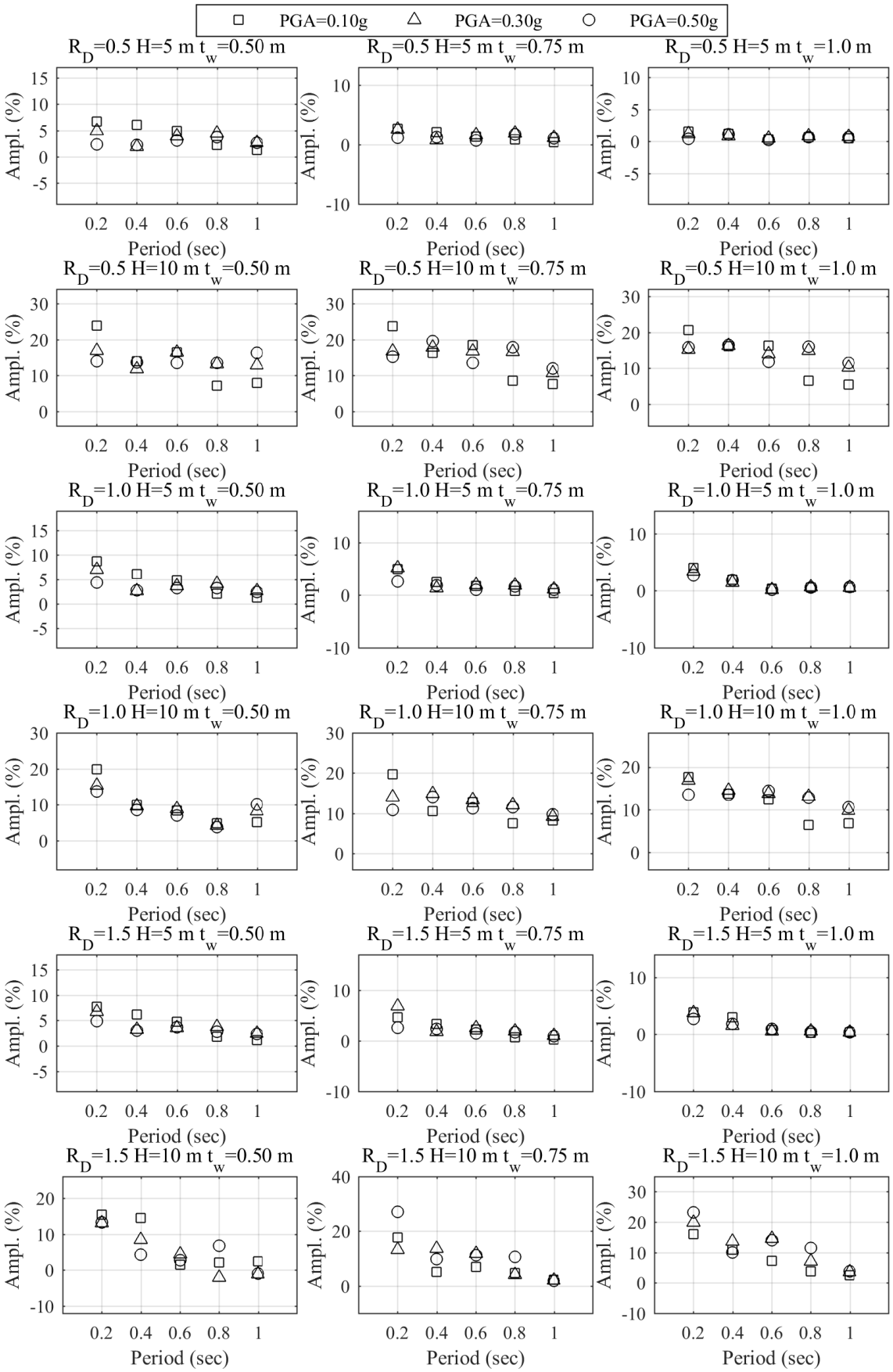

Figure 4.5 *PSA* amplifications for Soil Site 1

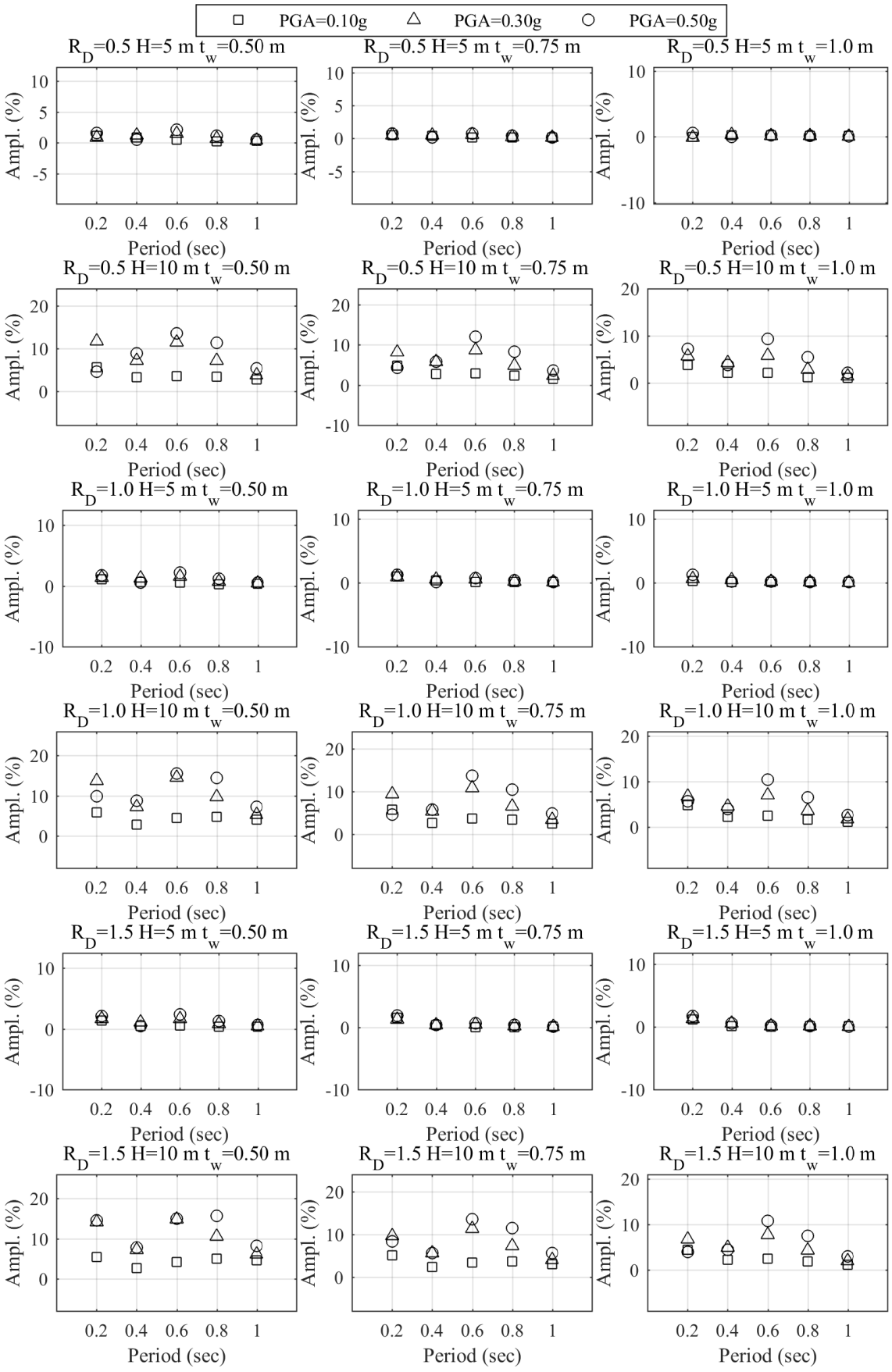

Figure 4.6 *PSA* amplifications for Soil Site 2

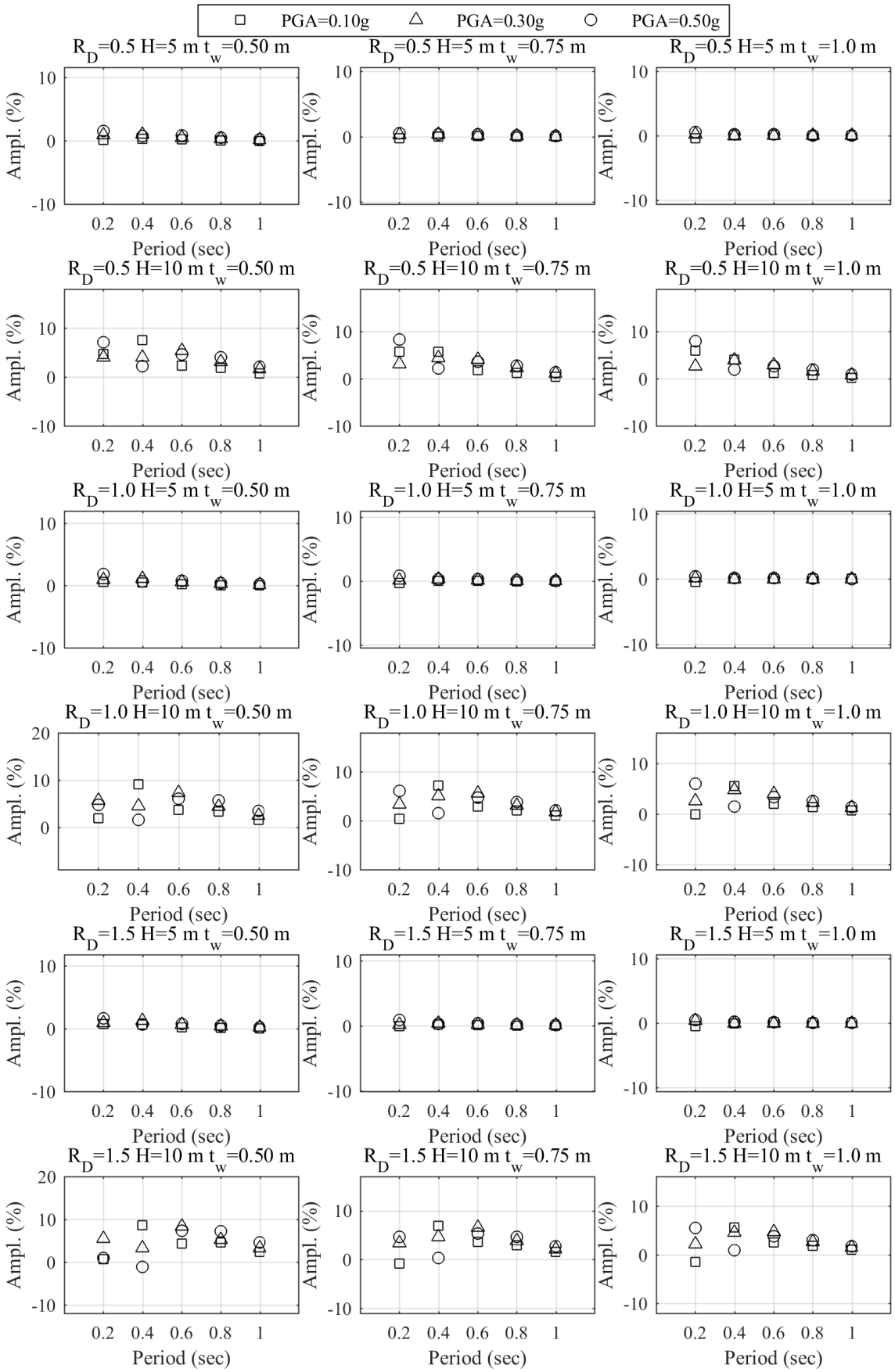

Figure 4.7 *PSA* amplifications for Soil Site 3

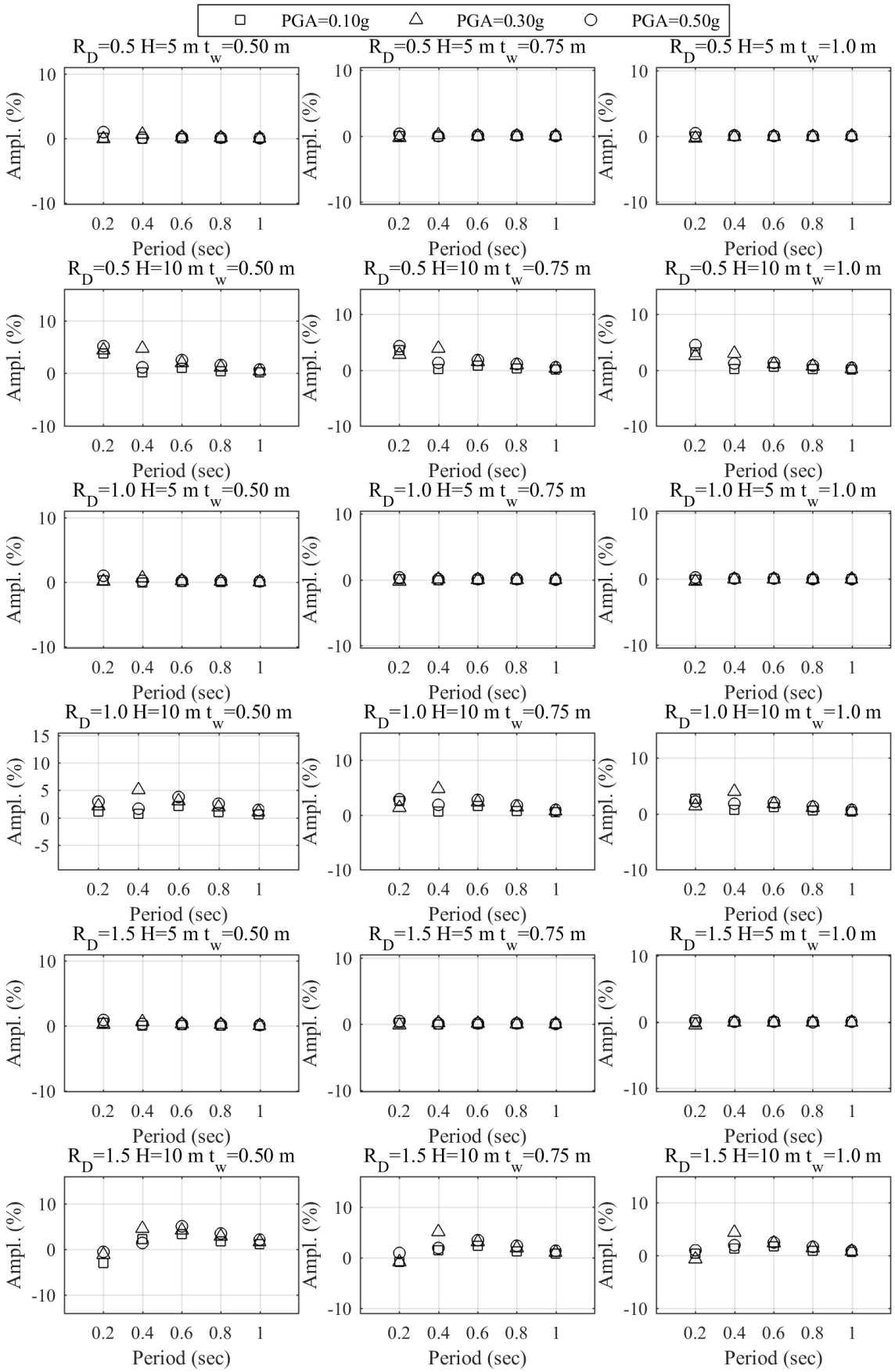

Figure 4.8 *PSA* amplifications for Soil Site 4

4.3.2 Surface Structure Responses

As stated before there are 3240 cases in SSUS conditions. Therefore, surface structure peak acceleration and drift amplifications are presented in 24 figures, i.e. 12 figures for acceleration amplifications and 12 figures for drift amplifications. In each figure, there are 18 graphs and in graph there is one plot per input motion *PGA* value. The surface structure fundamental period values are also given in horizontal axes. The 12 figures per response type corresponds to three different R_L values and four different soil sites.

The peak surface structure acceleration amplifications due to existence of an underground structure for $R_L = 0$ and Soil Site 1 are given in Figure 4.9. As seen from Figure 4.9, the maximum acceleration amplification value is about 91% and the maximum acceleration de-amplification value is about 47%. There is not a straight forward relationship between the case parameters and the acceleration amplification values. However, it can be said that the acceleration amplification values generally increase with increasing surface structure fundamental period.

The peak surface structure acceleration amplifications due to existence of an underground structure for $R_L = 2$ and Soil Site 1 are given in Figure A.23. As seen from Figure A.23, the maximum acceleration amplification value is about 33% and the maximum acceleration de-amplification value is about 51%. There is not a straight forward relationship between the case parameters and the acceleration amplification values. However, it can be said that the acceleration amplification values generally increase with increasing surface structure fundamental period.

The peak surface structure acceleration amplifications due to existence of an underground structure for $R_L = 4$ and Soil Site 1 are given in Figure A.24. As seen from Figure A.24, the maximum acceleration amplification value is about 19% and the maximum acceleration de-amplification value is about 17%. There is not a straight forward relationship between the case parameters and the acceleration amplification values. However, it can be said that the acceleration amplification values generally increase with increasing surface structure fundamental period.

The peak surface structure acceleration amplifications due to existence of an underground structure for $R_L = 0$ and Soil Site 2 are given in Figure A.25. As seen from Figure A.25, the maximum acceleration amplification value is about 15% and the maximum acceleration de-amplification value is about 29%. There is not a straight forward relationship between the case parameters and the acceleration amplification values. However, it can be said that the acceleration amplification values generally increase with increasing surface structure fundamental period.

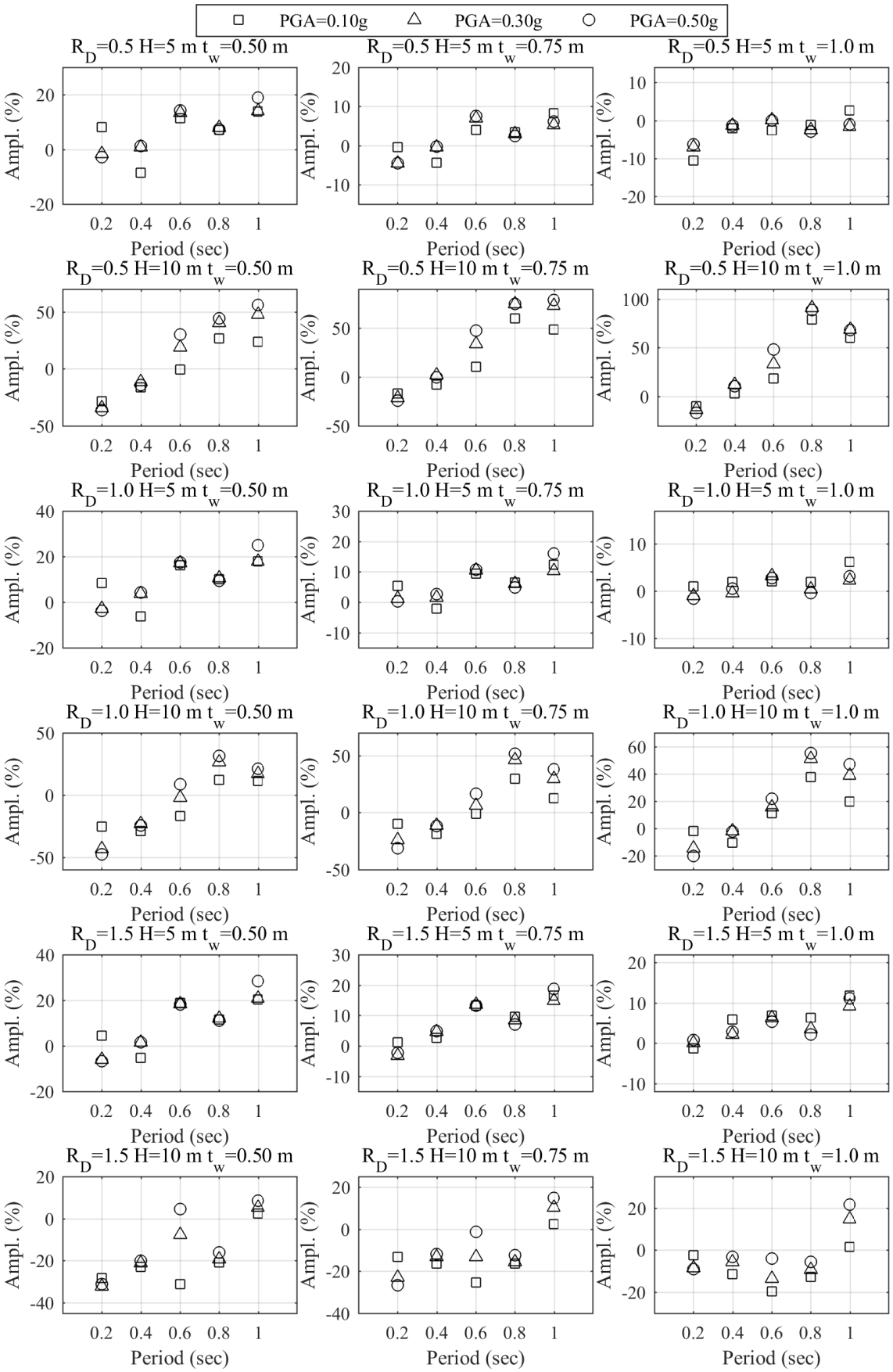

Figure 4.9 Peak acceleration amplifications for $R_L = 0$ and Soil Site 1

The peak surface structure acceleration amplifications due to existence of an underground structure for $R_L = 2$ and Soil Site 2 are given in Figure A.26. As seen from Figure A.26, the maximum acceleration amplification value is about 11% and the maximum acceleration de-amplification value is about 12%. There is not a straight forward relationship between the case parameters and the acceleration amplification values. However, it can be said that the acceleration amplification values generally increase with increasing surface structure fundamental period. On the other hand, the acceleration amplification values are lower for the cases where underground structure height is smaller.

The peak surface structure acceleration amplifications due to existence of an underground structure for $R_L = 4$ and Soil Site 2 are given in Figure A.27. As seen from Figure A.27, the maximum acceleration amplification value is about 17% and the maximum acceleration de-amplification value is about 5%. There is not a straight forward relationship between the case parameters and the acceleration amplification values. However, it can be said that the acceleration amplification values generally decrease with increasing surface structure fundamental period. On the other hand, the acceleration amplification values are lower for the cases where underground structure height is smaller.

The peak surface structure acceleration amplifications due to existence of an underground structure for $R_L = 0$ and Soil Site 3 are given in Figure A.28. As seen from Figure A.28, the maximum acceleration amplification value is about 3% and the maximum acceleration de-amplification value is about 14%. There is not a straight forward relationship between the case parameters and the acceleration amplification values. However, the acceleration amplification values are lower for the cases where underground structure height is smaller.

The peak surface structure acceleration amplifications due to existence of an underground structure for $R_L = 2$ and Soil Site 3 are given in Figure A.29. As seen from Figure A.29, the maximum acceleration amplification value is about 10% and the maximum acceleration de-amplification value is about 15%. There is not a straight forward relationship between the case parameters and the acceleration amplification values. However, the acceleration amplification values are lower for the cases where underground structure height is smaller.

The peak surface structure acceleration amplifications due to existence of an underground structure for $R_L = 4$ and Soil Site 3 are given in Figure A.30. As seen from Figure A.30, the maximum acceleration amplification value is about 8% and the maximum acceleration de-amplification value is about 9%. There is not a straight

forward relationship between the case parameters and the acceleration amplification values. However, the acceleration amplification values are lower for the cases where underground structure height is smaller.

The peak surface structure acceleration amplifications due to existence of an underground structure for $R_L = 0$ and Soil Site 4 are given in Figure A.31. As seen from Figure A.31, the maximum acceleration amplification value is about 2% and the maximum acceleration de-amplification value is about 10%. There is not a straight forward relationship between the case parameters and the acceleration amplification values. However, the acceleration amplification values are lower for the cases where underground structure height is smaller.

The peak surface structure acceleration amplifications due to existence of an underground structure for $R_L = 2$ and Soil Site 4 are given in Figure A.32. As seen from Figure A.32, the maximum acceleration amplification value is about 5% and the maximum acceleration de-amplification value is about 5%. There is not a straight forward relationship between the case parameters and the acceleration amplification values. However, the acceleration amplification values are lower for the cases where underground structure height is smaller.

The peak surface structure acceleration amplifications due to existence of an underground structure for $R_L = 4$ and Soil Site 4 are given in Figure A.33. As seen from Figure A.33, the maximum acceleration amplification value is about 2% and the maximum acceleration de-amplification value is about 9%. There is not a straight forward relationship between the case parameters and the acceleration amplification values. However, the acceleration amplification values are lower for the cases where underground structure height is smaller.

The peak surface structure drift amplifications due to existence of an underground structure for $R_L = 0$ and Soil Site 1 are given in Figure A.34. As seen from Figure A.34, the maximum drift amplification value is about 34% and the maximum drift de-amplification value is about 80%. There is not a straight forward relationship between the case parameters and the drift amplification values. However, the drift amplification values are lower for the cases where underground structure height is smaller. On the other hand, the drift amplification values generally increase with increasing surface structure fundamental period, i.e. T_B.

The peak surface structure drift amplifications due to existence of an underground structure for $R_L = 2$ and Soil Site 1 are given in Figure A.35. As seen from Figure A.35, the maximum drift amplification value is about 163% and the maximum drift de-amplification value is about 4%. There is not a straight forward relationship

between the case parameters and the drift amplification values. However, the drift amplification values are lower for the cases where underground structure height is smaller. On the other hand, the drift amplification values generally decrease with increasing surface structure fundamental period, i.e. T_B.

The peak surface structure drift amplifications due to existence of an underground structure for $R_L = 4$ and Soil Site 1 are given in Figure A.36. As seen from Figure A.36, the maximum drift amplification value is about 53% and the maximum drift de-amplification value is about 5%. There is not a straight forward relationship between the case parameters and the drift amplification values. However, the drift amplification values are lower for the cases where underground structure height is smaller. On the other hand, the drift amplification values generally decrease with increasing surface structure fundamental period, i.e. T_B.

The peak surface structure drift amplifications due to existence of an underground structure for $R_L = 0$ and Soil Site 2 are given in Figure A.37. As seen from Figure A.37, the maximum drift amplification value is about 11% and the maximum drift de-amplification value is about 67%. There is not a straight forward relationship between the case parameters and the drift amplification values. However, the drift amplification values are lower for the cases where underground structure height is smaller. On the other hand, the drift amplification values generally increase with increasing surface structure fundamental period, i.e. T_B.

The peak surface structure drift amplifications due to existence of an underground structure for $R_L = 2$ and Soil Site 2 are given in Figure A.38. As seen from Figure A.38, the maximum drift amplification value is about 64% and the maximum drift de-amplification value is about 7%. There is not a straight forward relationship between the case parameters and the drift amplification values. However, the drift amplification values are lower for the cases where underground structure height is smaller. On the other hand, the drift amplification values generally decrease with increasing surface structure fundamental period, i.e. T_B.

The peak surface structure drift amplifications due to existence of an underground structure for $R_L = 4$ and Soil Site 2 are given in Figure A.39. As seen from Figure A.39, the maximum drift amplification value is about 42% and the maximum drift de-amplification value is about 5%. There is not a straight forward relationship between the case parameters and the drift amplification values. However, the drift amplification values are lower for the cases where underground structure height is smaller. On the other hand, the drift amplification values generally decrease with increasing surface structure fundamental period, i.e. T_B.

The peak surface structure drift amplifications due to existence of an underground structure for $R_L = 0$ and Soil Site 3 are given in Figure A.40. As seen from Figure A.40, the maximum drift amplification value is about 1% and the maximum drift de-amplification value is about 43%. There is not a straight forward relationship between the case parameters and the drift amplification values. However, the drift amplification values are lower for the cases where underground structure height is smaller. On the other hand, the drift amplification values generally increase with increasing surface structure fundamental period, i.e. T_B.

The peak surface structure drift amplifications due to existence of an underground structure for $R_L = 2$ and Soil Site 3 are given in Figure A.41. As seen from Figure A.41, the maximum drift amplification value is about 25% and the maximum drift de-amplification value is about 1%. There is not a straight forward relationship between the case parameters and the drift amplification values. However, the drift amplification values are lower for the cases where underground structure height is smaller. On the other hand, the drift amplification values generally decrease with increasing surface structure fundamental period, i.e. T_B.

The peak surface structure drift amplifications due to existence of an underground structure for $R_L = 4$ and Soil Site 3 are given in Figure A.42. As seen from Figure A.42, the maximum drift amplification value is about 13% and the maximum drift de-amplification value is about 3%. There is not a straight forward relationship between the case parameters and the drift amplification values. However, the drift amplification values are lower for the cases where underground structure height is smaller. On the other hand, the drift amplification values generally decrease with increasing surface structure fundamental period, i.e. T_B.

The peak surface structure drift amplifications due to existence of an underground structure for $R_L = 0$ and Soil Site 4 are given in Figure A.43. As seen from Figure A.43, the maximum drift amplification value is about 2% and the maximum drift de-amplification value is about 21%. There is not a straight forward relationship between the case parameters and the drift amplification values. However, the drift amplification values are lower for the cases where underground structure height is smaller. On the other hand, the drift amplification values generally increase with increasing surface structure fundamental period, i.e. T_B.

The peak surface structure drift amplifications due to existence of an underground structure for $R_L = 2$ and Soil Site 4 are given in Figure A.44. As seen from Figure A.44, the maximum drift amplification value is about 14% and there is no drift de-amplification. There is not a straight forward relationship between the case

parameters and the drift amplification values. However, the drift amplification values are lower for the cases where underground structure height is smaller. On the other hand, the drift amplification values generally decrease with increasing surface structure fundamental period, i.e. T_B.

The peak surface structure drift amplifications due to existence of an underground structure for $R_L = 4$ and Soil Site 4 are given in Figure A.45. As seen from Figure A.45, the maximum drift amplification value is about 8% and the maximum drift de-amplification value is about 2%. There is not a straight forward relationship between the case parameters and the drift amplification values. However, the drift amplification values are lower for the cases where underground structure height is smaller. On the other hand, the drift amplification values generally decrease with increasing surface structure fundamental period, i.e. T_B.

4.4 Sensitivity of the Amplifications/De-amplifications to the Case Parameters

The Artificial Neural Network based sensitivity analysis results are given here for surface structure accelerations and drifts obtained from the cases in SSUS conditions. The sensitivity analysis procedure is explained in the previous chapter. The importance order for the case parameters is obtained as an outcome of the sensitivity analyses.

The sensitivity of the surface structure accelerations to the case parameters is illustrated in Figure 4.10. The figure shows the coefficient of determination (R^2) comparison for different neural networks. As seen from Figure 4.10, the coefficient of determination is 0.83 for the neural network which uses all case parameters as inputs. The neural networks with case parameter exclusions always have lower coefficient of determination values. The maximum decrement in the coefficient of determination is observed for the neural networks which excluded soil site parameter and surface structure parameter. This makes these two parameters the most effective case parameters. The importance order for the surface structure acceleration is obtained as: $T_B > V_{S30} > R_L > H > R_D > t_W > PGA$.

The sensitivity of the surface structure drifts to the case parameters is illustrated in Figure 4.11. The figure shows the coefficient of determination (R^2) comparison for different neural networks. As seen from Figure 4.11, the coefficient of determination is 0.94 for the neural network which uses all case parameters as inputs. The neural networks with case parameter exclusions always have lower coefficient of determination values. The maximum decrement in the coefficient of determination is

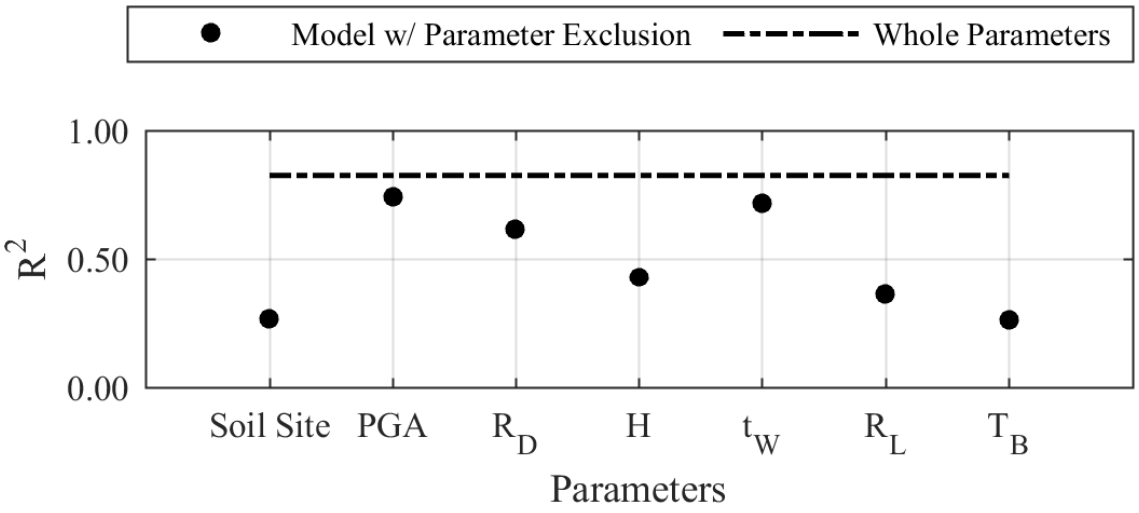

Figure 4.10 Sensitivity of the surface structure accelerations to the case parameters

observed for the neural network which excluded surface structure location parameter. This makes the parameter the most effective case parameter. The importance order for the surface structure drift is obtained as: $R_L > H > T_B > V_{S30} > PGA > t_W > R_D$.

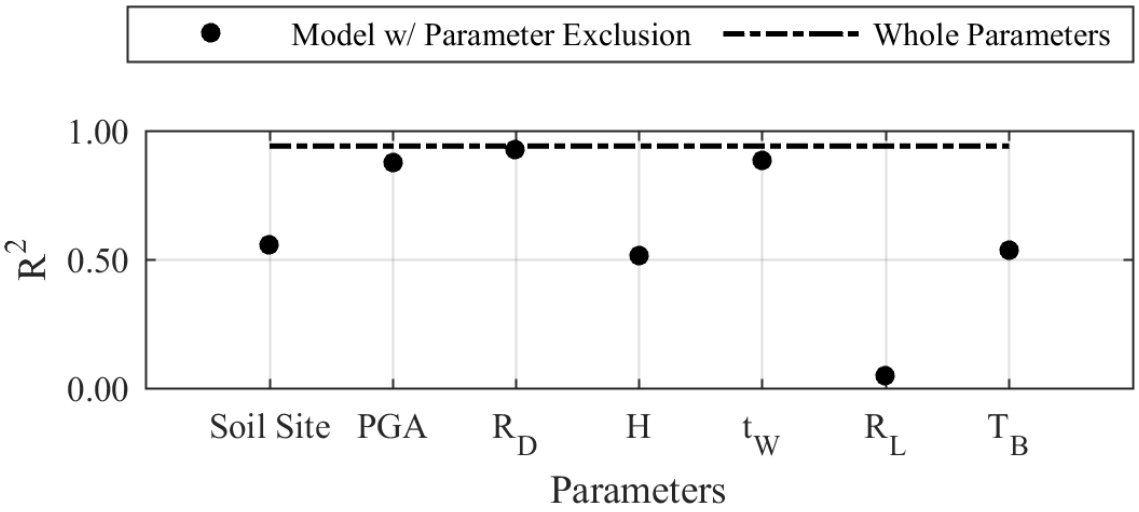

Figure 4.11 Sensitivity of the surface structure drifts to the case parameters

5
RESULTS AND DISCUSSION

The data obtained from the numerical analyses and the results obtained by manipulating the data are presented in Chapter 4. The conclusions related with the presented results are given in this chapter. Firstly, the two methods utilized for modelling the interaction problem are compared. The pros and cons of modelling the SSI directly is explained. Secondly, peak drift ratio amplification values are examined. The variation of maximum amplification values with respect to case parameters is addressed. The same explanations are also given for the peak acceleration amplification values. Finally, the importance order of the case parameters obtained via the sensitivity analyses are presented. The conclusions drawn from the results and some recommendations are given below.

As stated before, the investigated interaction problem is modelled by using two different approaches. In the first approach, the numerical model does not include the surface structure. Instead, the ground surface acceleration histories are used to calculate PSA and S_d responses. In the second approach, the numerical model includes also the surface structure. Thus, peak values of structural acceleration and drifts can be obtained directly. Here are the key conclusions about modelling approaches:

- Not directly including the surface structure in the numerical model causes exclusion of the radiation damping and yields inaccurate responses.
- Not directly including the surface structure in the numerical model causes exclusion of the rocking mode of foundation and yields inaccurate responses.
- Not directly including the surface structure in the numerical model for stiff soil sites yields accurate responses due to low radiation damping and negligible rocking mode of foundation.

Prior to evaluation of effect of the case parameters on the surface structure responses, a brief explanation of the mechanisms behind the response variations is given here.

The underground structure located inside a soil deposit can be thought as a fictitious soil layer inside the soil deposit. In this case, the fictitious soil layer would have the same lateral stiffness and mass density (i.e. the same dynamic impedance) with the underground structure. On the other hand, the surface structure and its foundation system can be thought as another fictitious soil layer. The impedance ratios among the actual soil layer and these two fictitious soil layers are key to the response variations.

Beyond the impedance ratios, presence of a lumped mass inside a continuous medium causes scattering of the propagating waves. Thus, depending on the amount of located mass and the medium characteristics, the surface structure responses vary.

The soil non-linearity is another important phenomenon which is effective on the surface structure responses. High level of soil non-linearity results in high level of hysteretic energy dissipation. The seismic input energy reaching to the ground surface varies with varying level of soil linearity. Thus, the surface structure responses vary with the level of soil non-linearity.

As stated above, the surface structure can be considered as a fictitious soil layer. Depending on the impedance ratio between the surface structure and the soil layer the amount of radiation damping varies. The additional damping results in variations of the surface structure responses. Besides, it causes different variation patterns for drift responses and acceleration responses (i.e. when the drifts are amplified the accelerations may be de-amplified). As it is known from the dynamics of the structures theory, the peak drift values are proportional to the peak acceleration values (i.e. $\omega^2 \cdot S_d = PSA$ and $PSA \approx S_a$, where ω: radial frequency, S_d: spectral displacement, PSA: Pseudo Spectral Acceleration and SA: Spectral Acceleration) in case of lower damping ratios. Addition of high level of radiation damping to the dynamic systems breaks down this proportionality.

It is shown in the literature that the underground structures create a 'shadow zone' [14] on the ground surface for the propagating shear waves. Namely, if a surface structure is located on the shadow zone, response of the structure generally decreases. It is similar to the propagation paths of the body waves through the earth's mantle. The shear waves cannot propagate through the outer core which is in liquid form and this creates a shadow zone on the earth's crust. As stated before, locating a lumped mass inside a continuous medium causes scattering of the propagating waves. The scattered waves then concentrate at the ground surface. However, the concentration level varies for different lateral distances from the lumped mass (i.e. underground structure) location. Thus, the surface structure responses vary with their lateral distance to the underground structure.

As stated above, the underground structure located inside a soil deposit can be thought as a fictitious soil layer inside the soil deposit. Due to the impedance difference between the actual soil layer and the fictitious one, shear waves can be trapped between the ground surface and the underground structure. And depending on height of the trapping zone, frequency characteristics of the trapped waves vary. Thus, the surface structures with different frequency characteristics yield different response variations.

The key conclusions related to variation of the drift amplification values with each case parameter (i.e. Soil Site, PGA, R_D, H, t_W, R_L and T_B) are listed below:

- The drift amplification values for softer soil sites are higher than the drift amplification values for stiffer soil sites. The maximum drift amplification values are 164%, 65%, 25% and 15% for Soil Site 1, Soil Site 2, Soil Site 3 and Soil Site 4, respectively.
- The drift amplification values increase with increasing input motion PGA values. The maximum drift amplification values are 78%, 136%, and 164% for PGA values of $0.10g$, $0.30g$, and $0.50g$, respectively.
- The drift amplification values increase with increasing depth ratio (i.e. R_D) values. The maximum drift amplification values are 155%, 159%, and 164% for R_D values of 0.5, 1.0, and 1.5, respectively.
- The drift amplification values increase dramatically with increasing underground structure height (i.e. H) values. The maximum drift amplification values are 19% and 164% for H values of 5 m and 10 m, respectively.
- The drift amplification values decrease with increasing underground structure wall thickness (i.e. t_W) values. The maximum drift amplification values are 164%, 129% and 92% for t_W values of 0.50 m, 0.75m and 1.0 m, respectively.
- The drift amplification values firstly increase with increasing lateral distance ratio (i.e. R_L) values, then decrease with increasing R_L values. The maximum drift amplification values are 34%, 164% and 53% for R_L values of 0, 2 and 4, respectively.
- The drift amplification values firstly decrease with increasing surface structure fundamental period (i.e. T_B) values, then increase with increasing T_B values. The maximum drift amplification values are 164%, 117%, 56%, 26% and 54% for T_B values of 0.2 sec, 0.4 sec, 0.6 sec, 0.8 sec and 1.0 sec, respectively.

The key conclusions related to variation of the acceleration amplification values with each case parameter (i.e. Soil Site, PGA, R_D, H, t_W, R_L and T_B) are listed below:

- The acceleration amplification values for softer soil sites are higher than the acceleration amplification values for stiffer soil sites. The maximum acceleration amplification values are 91%, 18%, 10% and 6% for Soil Site 1, Soil Site 2, Soil Site 3 and Soil Site 4, respectively.
- The acceleration amplification values firstly increase with increasing input motion PGA values, then converge to a specific value. The maximum acceleration amplification values are 79%, 91%, and 89% for PGA values of $0.10g$, $0.30g$, and $0.50g$, respectively.
- The acceleration amplification values decrease with increasing depth ratio (i.e. R_D) values. The maximum acceleration amplification values are 91%, 55%, and 33% for R_D values of 0.5, 1.0, and 1.5, respectively.
- The acceleration amplification values dramatically increase with increasing underground structure height (i.e. H) values. The maximum acceleration amplification values are 28% and 91% for H values of 5 m and 10 m, respectively.
- The acceleration amplification values increase with increasing underground structure wall thickness (i.e. t_W) values. The maximum acceleration amplification values are 56%, 79% and 91% for t_W values of 0.5 m, 0.75 m and 1.0 m, respectively.
- The acceleration amplification values decrease with increasing lateral distance ratio (i.e. R_L) values. The maximum acceleration amplification values are 91%, 33% and 19% for R_L values of 0, 2 and 4, respectively.
- The variation of acceleration amplification values with the surface structure fundamental period (i.e. T_B) is quite complex. The maximum acceleration amplification values are 18%, 12%, 49%, 91% and 79% for T_B values of 0.2 sec, 0.4 sec, 0.6 sec, 0.8 sec and 1.0 sec, respectively.

The importance order of the case parameters on the surface structure accelerations was obtained as: T_B, Soil Site, R_L, H, R_D, t_W, PGA. On the other hand, the importance order of the case parameters on the surface structure drifts was obtained as: R_L, H, T_B, Soil Site, PGA, t_W, R_D. The parameters PGA, t_W, and R_D may be considered as the least important cases parameters. These parameters can be excluded from the further studies to be able to focus on the more important parameters. For instance, new cases

which are combinations of the parameters T_B, Soil Site, R_L and H can be generated in the future studies. Since the number of parameters declined, number of cases may be increased.

Since the number of cases are reduced, new cases, in which vertical input ground motions considered, may be included in the future studies. Since vertical seismic events are also considered in the current seismic code, a comprehensive comparison can be presented. On the other hand, the surface structure model, which is modelled as a SDOF system, can be modelled in more detail. It is known that modelling the surface structures with larger fundamental periods as SDOF systems is not much appropriate. For instance, surface structures with 1.0 sec fundamental period can be modelled as multi degree of freedom systems to be more accurate.

References

[1] G. Hayes T. Crone. (Accessed on Oct. 6, 2020). At what depth do earthquakes occur? what is the significance of the depth? [Online]. Available: https://www.usgs.gov/faqs/what-depth-do-earthquakes-occur-what-significance-depth?qt-news_science_products=3#qt-news_science_products.

[2] S. L. Kramer, *Geotechnical Earthquake Engineering*. Upper Saddle River, N.J.: Prentice Hall, 1996.

[3] M.-u. Zaman, C. S. Desai, E. C. Drumm, "Interface model for dynamic soil-structure interaction," *Journal of Geotechnical Engineering*, vol. 110, no. 9, pp. 1257–1273, 1987.

[4] Y. Ayvaz, A. Daloğlu, A. Doğangün, "Application of a modified vlasov model to earthquake analysis of plates resting on elastic foundations," *Journal of Sound and Vibration*, vol. 212, no. 3, pp. 499–509, 1998.

[5] Y. Ayvaz K. Özgan, "Application of modified vlasov model to free vibration analysis of beams resting on elastic foundations," *Journal of Sound and Vibration*, vol. 255, no. 1, pp. 111–127, 2002.

[6] Z. Ş. Garip, "Deprem etkisindeki betonarme yapılarda yapı-zemin etkileşimi," Master's thesis, Sakarya University, Sakarya, Turkey, Jan. 2005.

[7] CSI, *Sap2000 integrated software for structural analysis and design*, Computers and Structures Incorporation, Berkeley, California.

[8] H. El-Ganainy M. El-Naggar, "Seismic performance of three-dimensional frame structures with underground stories," *Soil Dynamics and Earthquake Engineering*, vol. 29, no. 9, pp. 1249–1261, 2009.

[9] R. Mutlu, "Esnek veya sert bir tabakaya oturan yapının dinamik yapı-zemin etkileşimi problemi," Master's thesis, İstanbul Technical University, İstanbul, Turkey, Jun. 2010.

[10] M. Kirkit, "Investigation of dynamic soil – pile – structure interaction in clayey soils by numerical analysis," PhD thesis, Yildiz Technical University, İstanbul, Turkey, May 2015.

[11] S. Kiliçer, "Yapi zemin etkileşiminin betonarme yapilarin tasarimina etkisi," Master's thesis, Karadeniz Technical University, Trabzon, Turkey, Dec. 2016.

[12] J. M. Crichlow, "The effect of underground structure on seismic motions of the ground surface," *Geophysical Journal of the Royal Astronomical Society*, vol. 70, pp. 563–575, 1982.

[13] M. Dravinski, "Ground motion amplification due to elastic inclusions in a half-space," *Earthquake Engineering and Structural Dynamics*, vol. 11, no. 3, pp. 313–335, 1983.

[14] P. Yiouta-Mitra, G. Kouretzis, G. Bouckovalas, A. Sofianos, "Effect of underground structures in earthquake resistant design of surface structures," in *Proceedings Book*, 2007, pp. 1–10.

[15] I. C. G. Inc., *Flac — fast lagrangian analysis of continua*, Itasca Consulting Group Incorporation, Minneapolis, Minnesota.

[16] C. Smerzini, J. Aviles, R. Paolucci, F. J. Sanchez-Sesma, "Effect of underground cavities on surface earthquake ground motion under sh wave propagation," *Earthquake Engineering and Structural Dynamics*, vol. 38, no. 12, pp. 1441–1460, 2009.

[17] L. Hao, V. W. Lee, L. Jianwen, "Anti-plane (sh) waves diffraction by an underground semi-circular cavity: Analytical solution," *Earthquake Engineering and Engineering Vibration*, vol. 9, no. 3, pp. 385–396, 2010.

[18] O. Abuhajar, H. E. Naggar, T. Newson, "Effects of underground structures on amplification of seismic motion for sand with varying density," in *Proceedings Book*, 2011, pp. 1–6.

[19] G. Sgarlato, G. Lombardo, R. Rigano, "Evaluation of seismic site response nearby underground cavities using earthquake and ambient noise recordings: A case study in catania area, italy," *Engineering Geology*, vol. 122, no. 3, pp. 281–291, 2011.

[20] V. Besharat, M. Davoodi, M. K. Jafari, "Effect of underground structures on free-field ground motion during earthquakes," in *Proceedings Book*, 2012, pp. 1–10.

[21] J. Liang, J. Zhang, Z. Ba, "The effect of underground cavities on design seismic ground motion," in *Proceedings Book*, 2012, pp. 1–9.

[22] S. Sica, A. D. Russo, F. Rotili, A. L. Simonelli, "Ground motion amplification due to shallow cavities in nonlinear soils," *Natural Hazards*, vol. 71, pp. 1913–1935, 2014.

[23] M. Hudson, I. Idriss, M. Beikae, *QUAD4M: A Computer Program to Evaluate the Seismic Response of Soil Structures Using Finite Element Procedures and Incorporating a Compliant Base*. Center for Geotechnical Modeling, Department of Civil and Environmental Engineering, University of California, Davis, 1994.

[24] M. H. Baziar, M. R. Moghadam, D.-S. Kim, Y. W. Choo, "Effect of underground tunnel on the ground surface acceleration," *Tunnelling and Underground Space Technology*, vol. 44, pp. 10–22, 2014.

[25] H. Alielahi, M. Kamalian, M. Adampira, "Seismic ground amplification by unlined tunnels subjected to vertically propagating sv and p waves using bem," *Soil Dynamics and Earthquake Engineering*, vol. 71, pp. 63–79, 2015.

[26] X. Wang M. Cai, "Influence of wavelength-to-excavation span ratio on ground motion around deep underground excavations," *Tunnelling and Underground Space Technology*, vol. 49, pp. 438–453, 2015.

[27] J. Tromp, D. Komatitsch, Q. Liu, "Spectral-element and adjoint methods in seismology," *Communications in Computational Physics*, vol. 3, no. 1, pp. 1–32, 2008.

[28] H. Alielahi M. Adampira, "Effect of twin-parallel tunnels on seismic ground response due to vertically in-plane waves," *International Journal of Rock Mechanics and Mining Sciences*, vol. 85, pp. 67–83, 2016.

[29] H. Alielahi, M. Kamalian, M. Adampira, "A bem investigation on the influence of underground cavities on the seismic response of canyons," *Acta Geotechnica*, vol. 11, pp. 391–413, 2016.

[30] H. Alielahi M. Adampira, "Site-specific response spectra for seismic motions in half-plane with shallow cavities," *Soil Dynamics and Earthquake Engineering*, vol. 80, pp. 163–167, 2016.

[31] M. H. Baziar, M. R. Moghadam, Y. W. Choo, D.-s. Kim, "Tunnel flexibility effect on the ground surface acceleration response," *Earthquake Engineering and Engineering Vibration*, vol. 15, no. 3, pp. 457–476, 2016.

[32] A. Rostami, M. A. Ziarati, B. Shahi, S. Jahani, "Evaluation of seismic behavior and earth's surface acceleration, by interaction of tunnels with different shapes and different types of soils," *Open Journal of Civil Engineering*, vol. 6, pp. 242–253, 2016.

[33] M. Smith, *ABAQUS/Standard User's Manual, Version 6.9*. Providence, Rhode Island: Dassault Systèmes Simulia Corp, 2009.

[34] J. Qian D. E. Beskos, "Dynamic interaction between 3-d rigid surface foundations and comparison with the atc-3 provisions," *Earthquake Engineering and Structural Dynamics*, vol. 24, pp. 419–437, 1995.

[35] ATC-3, *Tentative provisions for the development of seismic regulations for buildings*, Applied Technology Council, 1st ed. 1978, 2nd ed. 1984.

[36] L. Menglin, W. Huaifeng, C. Xi, Z. Yongmei, "Structure-soil-structure interaction: Literature review," *Soil Dynamics and Earthquake Engineering*, vol. 31, pp. 1724–1731, 2011.

[37] H.-L. Chen, "Dynamic response of embedded structures," PhD thesis, Northwestern University, Evanston, Illinois, Jun. 1989.

[38] C. Navarro, "Seismic analysis of underground structures," in *Proceedings Book*, 1992, pp. 1939–1944.

[39] I. V. Constantopoulos et al., "Dynamic analysis of tunnels," in *Proceedings Book of 3rd International Conference on Numerical Methods in Geomechanics*, Aachen, Germany, 1979.

[40] H. Wang, M. Lou, X. Chen, Y. Zhai, "Structure–soil–structure interaction between underground structure and ground structure," *Soil Dynamics and Earthquake Engineering*, vol. 54, pp. 31–38, 2013.

[41] G. J. DeSalvo J. A. Swanson, *ANSYS Engineering Analysis System User's Manual*. Houston, Texas: Swanson Analysis Systems, 1985.

[42] K. Pitilakis, G. Tsinidis, A. Leanza, M. Maugeri, "Seismic behaviour of circular tunnels accounting for above ground structures interaction effects," *Soil Dynamics and Earthquake Engineering*, vol. 67, pp. 1–15, 2014.

[43] O. Abuhajar, H. El Naggar, T. Newson, "Experimental and numerical investigations of the effect of buried box culverts on earthquake excitation," *Soil Dynamics and Earthquake Engineering*, vol. 79, pp. 130–148, 2015.

[44] K. M. Gillis, "Seismic response of shallow underground structures in dense urban environments," PhD thesis, University of Colorado, Boulder, Colorado, Jun. 2015.

[45] A. Franza, A. M. Marshall, T. Haji, A. O. Abdelatif, S. Carbonari, M. Morici, "A simplified elastic analysis of tunnel-piled structure interaction," *Tunnelling and Underground Space Technology*, vol. 61, pp. 104–121, 2017.

[46] H. Wang, M. Lou, R. Zhang, "Structure-soil-structure interaction: Literature review," *Soil Dynamics and Earthquake Engineering*, vol. 100, pp. 131–143, 2017.

[47] G. Gazetas, N. Gerolymos, I. Anastasopoulos, "Response of three athens metro underground structures in the 1999 parnitha earthquake," *Soil Dynamics and Earthquake Engineering*, vol. 25, pp. 617–633, 2005.

[48] M. Ma B. H. Brady, "Analysis of the dynamic performance of an underground excavation in jointed rock under repeated seismic loading," *Geotechnical and Geological Engineering*, vol. 17, pp. 1–20, 1999.

[49] Y. M. Hashash, J. J. Hook, B. Schmidt, J. I.-C. Yao, "Seismic design and analysis of underground structures," *Tunnelling and Underground Space Technology*, vol. 16, pp. 247–293, 2001.

[50] G. D. Hatzigeorgiou D. E. Beskos, "Inelastic response of 3-d underground structures in rock under seismic loading," *Transactions on the Built Environment*, vol. 57, pp. 599–608, 2001.

[51] J. Wang G. Munfakh, "Seismic design of tunnels," *Transactions on the Built Environment*, vol. 57, pp. 589–598, 2001.

[52] S. M. Hosseini S. N. Tafreshi, "Soil-structure interaction of buried pipes under cyclic loading conditions," *IJE Transactions B: Applications*, vol. 15, no. 2, pp. 117–124, 2002.

[53] H. Huo, "Seismic design and analysis of rectangular underground structures," PhD thesis, Purdue University, West Lafayette, Indiana, Aug. 2005.

[54] H. Liu E. Song, "Seismic response of large underground structures in liquefiable soils subjected to horizontal and vertical earthquake excitations," *Computers and Geotechnics*, vol. 32, pp. 223–244, 2005.

[55] A. H. C. Chan, *User manual for DIANA SWANDYNE-II*. Birmingham, England: University of Birmingham, 1993.

[56] N. M. A. Nagy, "Dynamic soil structure interaction of buried concrete structures under the effect of blast loads," PhD thesis, University of Bradford, Bradford, England, Jun. 2007.

[57] S. Kontoe, L. Zdravkovic, D. M. Potts, C. O. Menkiti, "Case study on seismic tunnel response," *Canadian Geotechnical Journal*, vol. 45, no. 12, pp. 1743–1764, 2008.

[58] P. Singh, W. Chen, S. Vahdani, "Soil-structure interaction analysis for buried structures in soft, sloping soils - bart san francisco transition structure," in *Proceedings Book*, 2008, pp. 1–8.

[59] J. Lysmer, M. Tabatabaie-Raissi, F. Tajirian, S. Vahdani, F. Ostadan, *SASSI: A System for Analysis of Soil-Structure Interaction*. University of California Berkeley, 1981.

[60] C. Smerzini, J. Avilés, F. J. Sánchez-Sesma, R. Paolucci, A. Santini, N. Moraci, "Analytical solutions for the seismic response of underground structures under SH wave propagation," in *AIP Conference Proceedings*, 2008, pp. 674–683.

[61] H. Liu, "Dynamic analysis of subway structures under blast loading," *Geotechnical and Geological Engineering*, vol. 27, pp. 699–711, 2009.

[62] Y. Hashash, K. Karina, D. Koutsoftas, N. O'Riordan, "Seismic design considerations for underground box structures," in *Proceedings Book*, 2010, pp. 620–637.

[63] M. G. Katona, "Seismic design and analysis of buried culverts and structures," *Journal of Pipeline Systems Engineering and Practice*, vol. 1, no. 3, pp. 111–119, 2010.

[64] T. R. Board, E. National Academies of Sciences, Medicine, *Modernize and Upgrade CANDE for Analysis and LRFD Design of Buried Structures*. Washington, DC: The National Academies Press, 2008.

[65] G. Ma, H. Zhou, K. Chong, "In-structure shock assessment of underground structures with consideration of rigid body motion," *Journal of Engineering Mechanics*, vol. 137, no. 12, pp. 797–806, 2011.

[66] S. Chian S. Madabhushi, "Effect of buried depth and diameter on uplift of underground structures in liquefied soils," *Soil Dynamics and Earthquake Engineering*, vol. 41, pp. 181–190, 2012.

[67] Y. Sun, Y. S. Xu, S. L. Shen, W. J. Sun, "Field performance of underground structures during shield tunnel construction," *Tunnelling and Underground Space Technology*, vol. 28, pp. 272–277, 2012.

[68] H. L. Chen, Z. C. Xia, J. N. Zhou, H. L. Fan, F. N. Jin, "Dynamic responses of underground arch structures subjected to conventional blast loads: curvature effects," *Archives of Civil and Mechanical Engineering*, vol. 13, pp. 322–333, 2013.

[69] H. L. Chen, F. N. Jin, H. L. Fan, "Elastic responses of underground circular arches considering dynamic soil-structure interaction: A theoretical analysis," *Acta Mechanica Sinica*, vol. 29, no. 1, pp. 110–122, 2013.

[70] E. Debiasi, A. Gajo, D. Zonta, "On the seismic response of shallow-buried rectangular structures," *Tunnelling and Underground Space Technology*, vol. 38, pp. 99–113, 2013.

[71] F. B. Kuhnow, "Vibration effects on underground concrete structures," Master's thesis, University of Utah, Salt Lake City, Utah, May 2013.

[72] M. A. Abdel-Motaal, F. M. El-Nahhas, A. T. Khiry, "Mutual seismic interaction between tunnels and the surrounding granular soil," *Housing and Building National Research Center*, vol. 10, pp. 265–278, 2014.

[73] T. Akhlaghi A. Nikkar, "Effect of vertically propagating shear waves on seismic behavior of circular tunnels," *The Scientific World Journal*, vol. 14, pp. 1–10, 2014.

[74] Z. Y. Chen, W. Y. Li, L. D. Yang, "Simplified Seismic Design Method for Shanghai Underground Structures in Soft Soils," *Indian Geotechnical Journal*, vol. 44, no. 2, pp. 149–155, 2014.

[75] S. Koneshwaran, D. P. Thambiratnam, C. Gallage, "Performance of buried tunnels subjected to surface blast incorporating fluid-structure interaction," *Journal of Performance of Constructed Facilities*, vol. 29, no. 3, pp. 1–16, 2015.

[76] O. Abuhajar, H. E. Naggar, T. Newson, "Seismic soil – culvert interaction," *Canadian Geotechnical Journal*, vol. 52, pp. 1649–1667, 2015.

[77] M. Kumar, M. D. Goel, V. A. Matsagar, K. Rao, "Response of Semi-Buried Structures Subjected to Multiple Blast Loading Considering Soil–Structure Interaction," *Indian Geotechnical Journal*, vol. 45, no. 3, pp. 243–253, 2015.

[78] A. Hushmand, S. Dashti, C. Davis, B. Hushmand, M. Zhang., M. Ghayoomi, J. S. McCartney, Y. Lee, J. Hu, "Seismic performance of underground reservoir structures: Insight from centrifuge modeling on the influence of structure stiffness," *Journal of Geotechnical and Geoenvironmental Engineering*, vol. 142, no. 7, pp. 1–13, 2016.

[79] A. Hushmand, S. Dashti, C. Davis, B. Hushmand, J. S. McCartney, J. Hu, Y. Lee, "Seismic performance of underground reservoir structures: Insight from centrifuge modeling on the influence of backfill soil type and geometry," *Journal of Geotechnical and Geoenvironmental Engineering*, vol. 142, no. 11, pp. 1–11, 2016.

[80] Y. Kawamata, M. Nakayama, I. Towhata, S. Yasuda, "Dynamic behaviors of underground structures in E-Defense shaking experiments," *Soil Dynamics and Earthquake Engineering*, vol. 82, pp. 24–39, 2016.

[81] X. Wang M. Cai, "Numerical modeling of seismic wave propagation and ground motion in underground mines," *Tunnelling and Underground Space Technology*, vol. 68, pp. 211–230, 2017.

[82] R. W. Clough J. Penzien, *Dynamics of Structures*. Berkeley, CA: Computers and Structures Inc., 1995.

[83] TBEC-2018, *Turkish building earthquake code*, Disaster and Emergency Management Presidency, Ankara, Turkey, 2018.

[84] G. Tsinidis, "Response characteristics of rectangular tunnels in soft soil subjected to transversal ground shaking," *Tunnelling and Underground Space Technology*, vol. 62, pp. 1–22, 2017.

[85] G. Tsinidis, "Response of urban single and twin circular tunnels subjected to transversal ground seismic shaking," *Tunnelling and Underground Space Technology*, vol. 76, pp. 177–193, 2018.

[86] G. Tsinidis K. Pitilakis, "Improved r-f relations for the transversal seismic analysis of rectangular tunnels," *Soil Dynamics and Earthquake Engineering*, vol. 107, pp. 48–65, 2018.

[87] R. Sisman Y. Ayvaz, "Effect of mass ratio on racking ratios of underground structures under seismic loading," in *Proceedings Book of International Civil Engineering and Architecture Conference 2019*, Trabzon, Turkey, 2019.

[88] Z. Xu, X. Du, C. Xu, H. Hao, K. Bi, J. Jiang, "Numerical research on seismic response characteristics of shallow buried rectangular underground structure," *Soil Dynamics and Earthquake Engineering*, vol. 116, pp. 242–252, 2019.

[89] Mathworks Inc., *MATLAB 2017a v9.2*. Natick, Massachusetts: Mathworks Incorporation, 2017.

[90] F. McKenna, M. H. Scott, G. L. Fenves, "Nonlinear finite-element analysis software architecture using object composition," *Journal of Computing in Civil Engineering*, vol. 24, no. 1, pp. 95–107, 2010.

[91] OpenSees. (Accessed on Oct. 7, 2020). Pressure independ multiyield material, [Online]. Available: `https://opensees.berkeley.edu/wiki/index.php/PressureIndependMultiYield_Material`.

[92] J. Lysmer R. L. Kuhlemeyer, "Finite dynamic model for infinite media," *Journal of Engineering Mechanics Division*, vol. 95, pp. 859–878, 1969.

[93] W. B. Joyner A. T. F. Chen, "Calculation of nonlinear ground response in earthquakes," *Bulletin of the Seismological Society of America*, vol. 65, no. 5, pp. 1315–1336, 1975.

[94] R. Courant, K. Friedrichs, H. Lewy, "On the partial difference equations of mathematical physics," *IBM Journal*, vol. 3, pp. 215–234, 1967.

A
ADDITIONAL FIGURES

This appendix contains some of the full-page figures which are referred in Chapter 4. The figures are not given in the related chapter due to drafting restrictions.

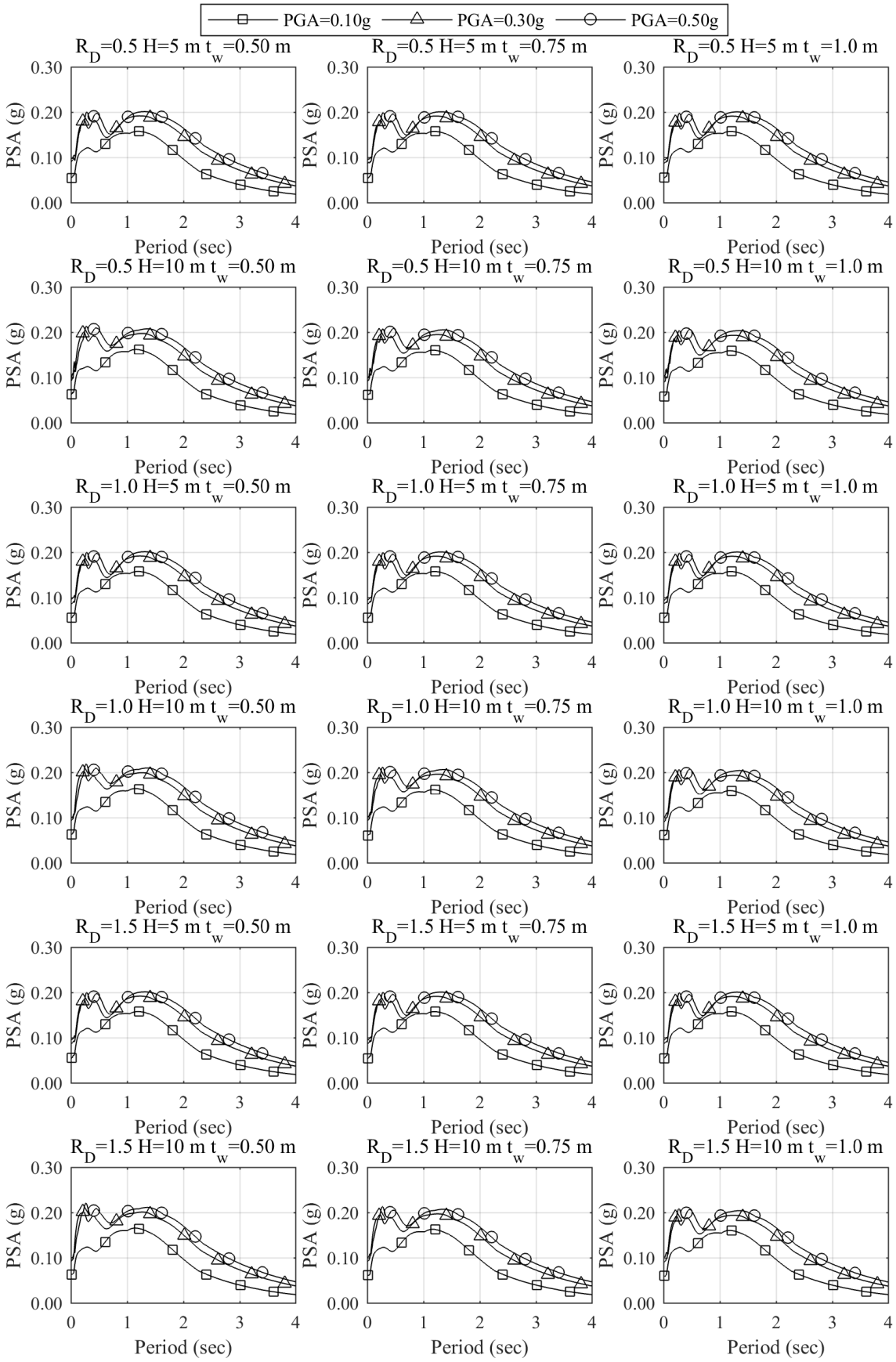

Figure A.1 *PSA* values for Soil Site 2 in USFF conditions

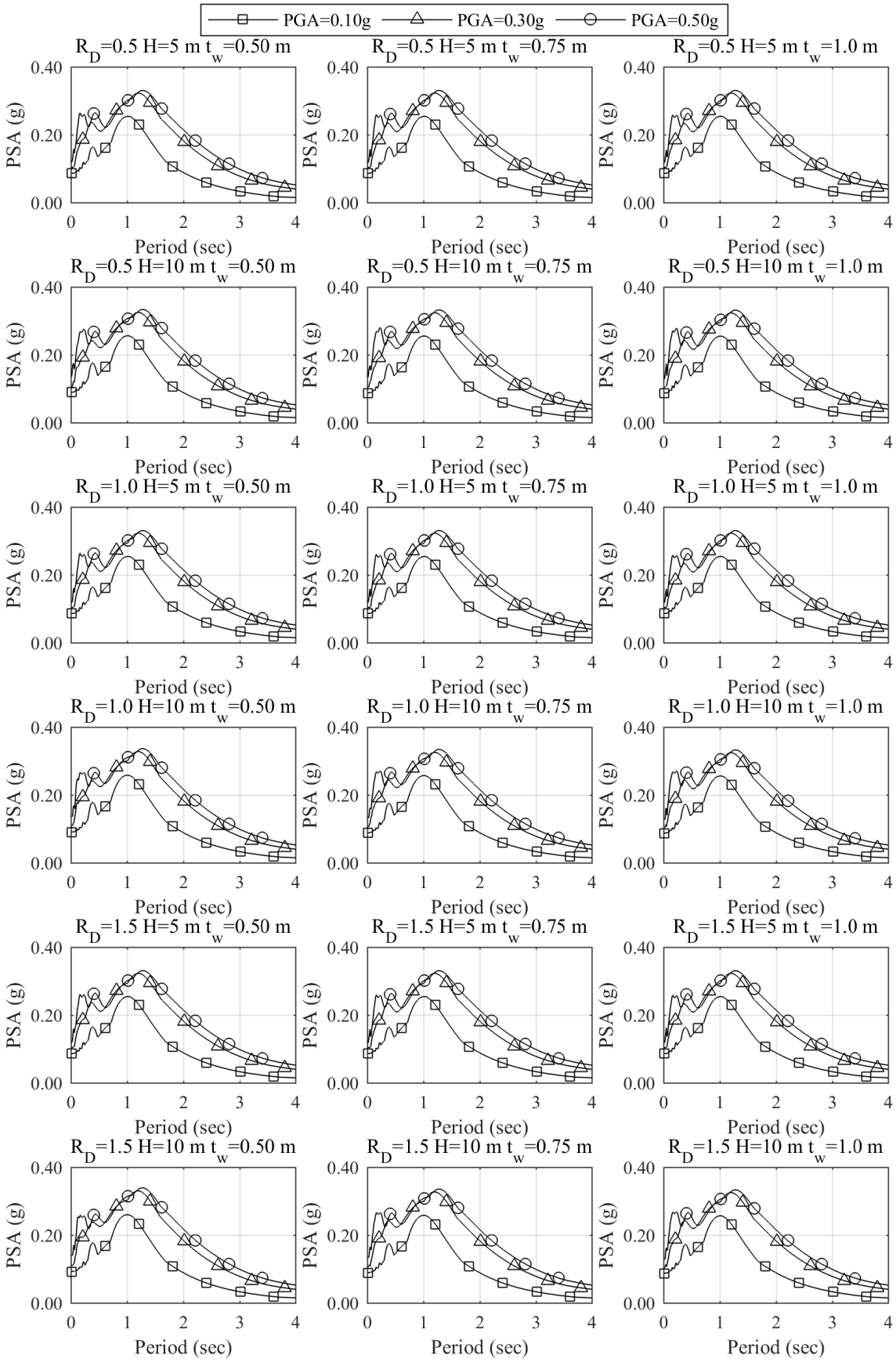

Figure A.2 *PSA* values for Soil Site 3 in USFF conditions

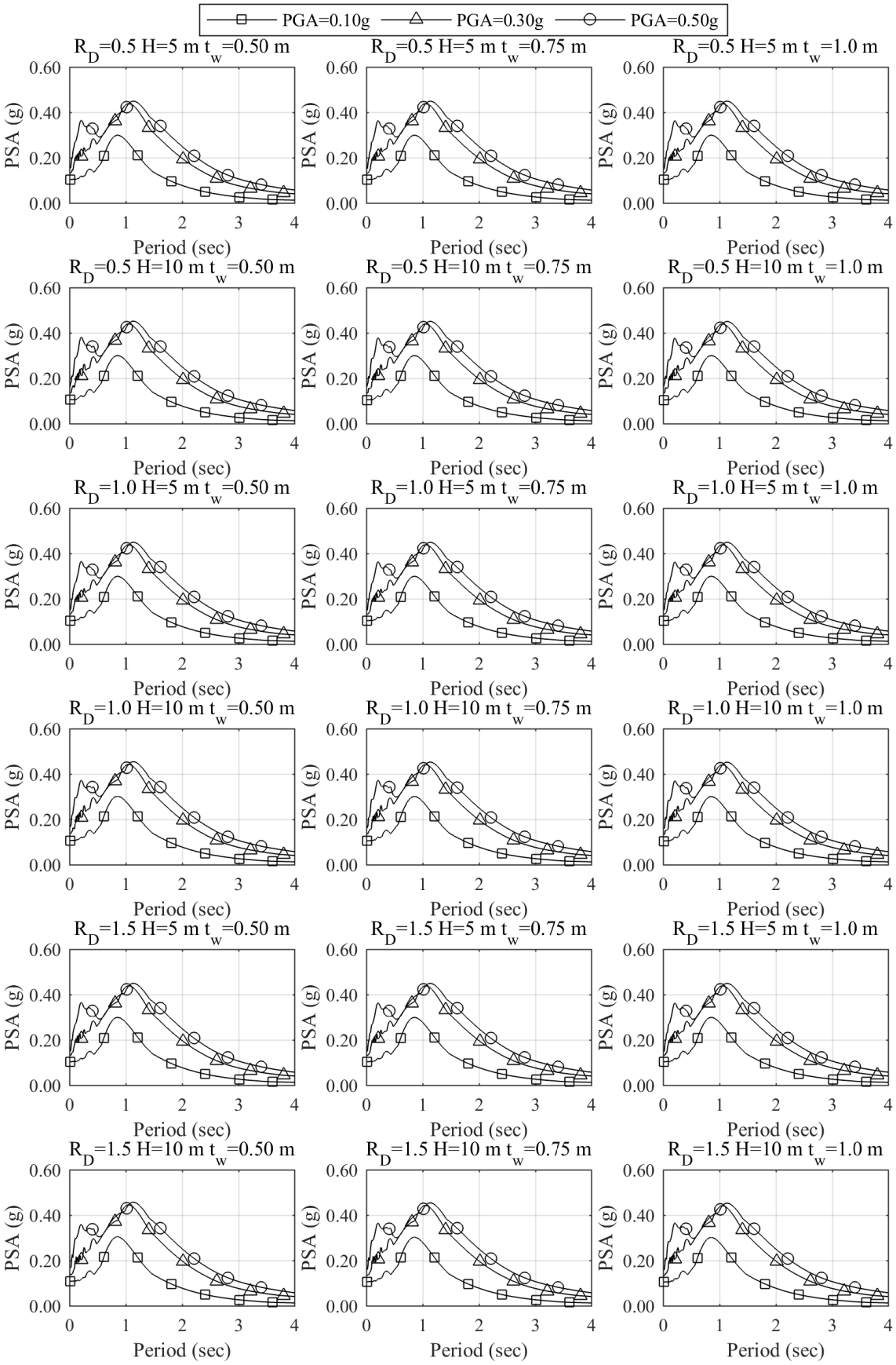

Figure A.3 *PSA* values for Soil Site 4 in USFF conditions

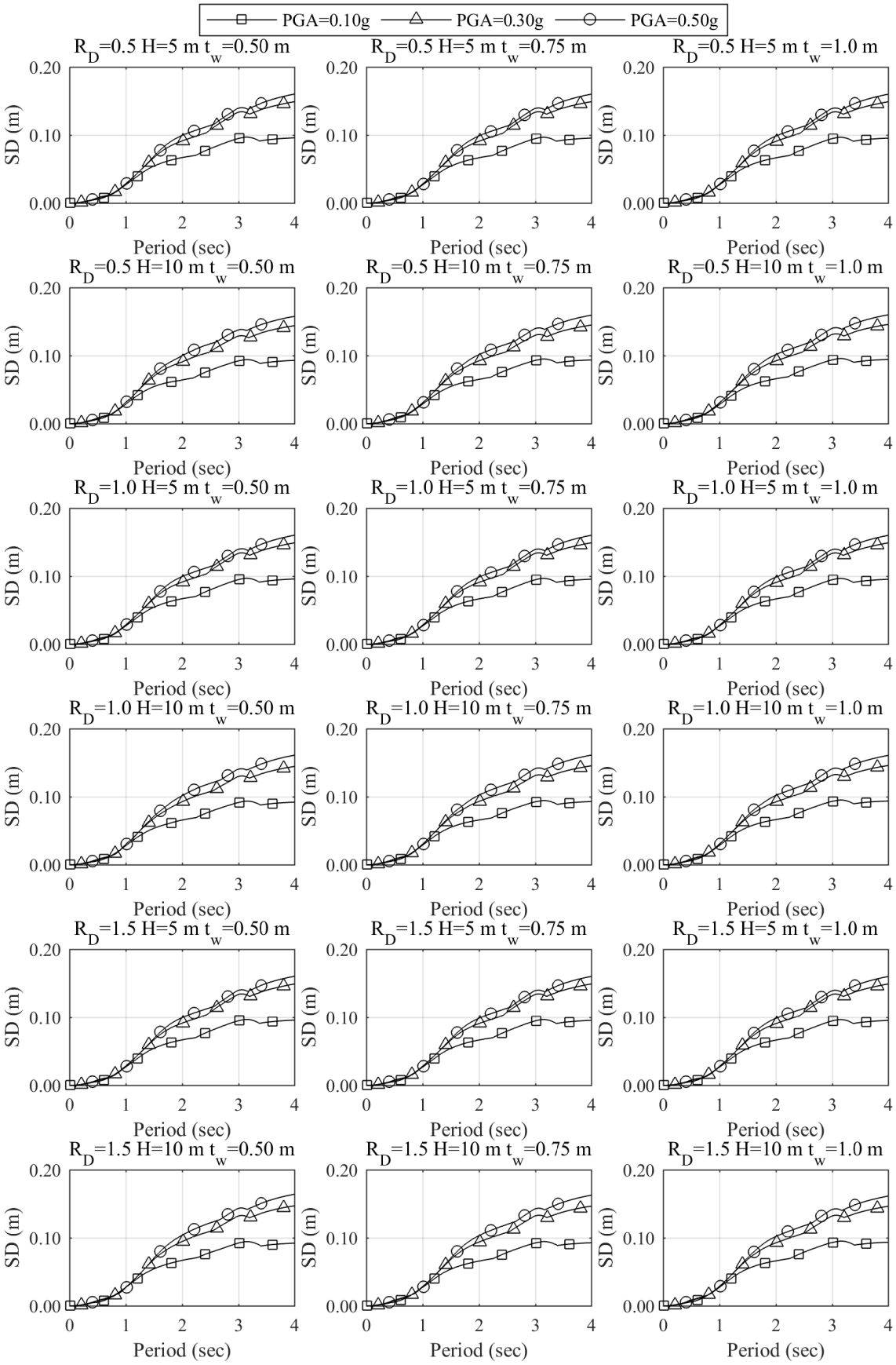

Figure A.4 S_d values for Soil Site 1 in USFF conditions

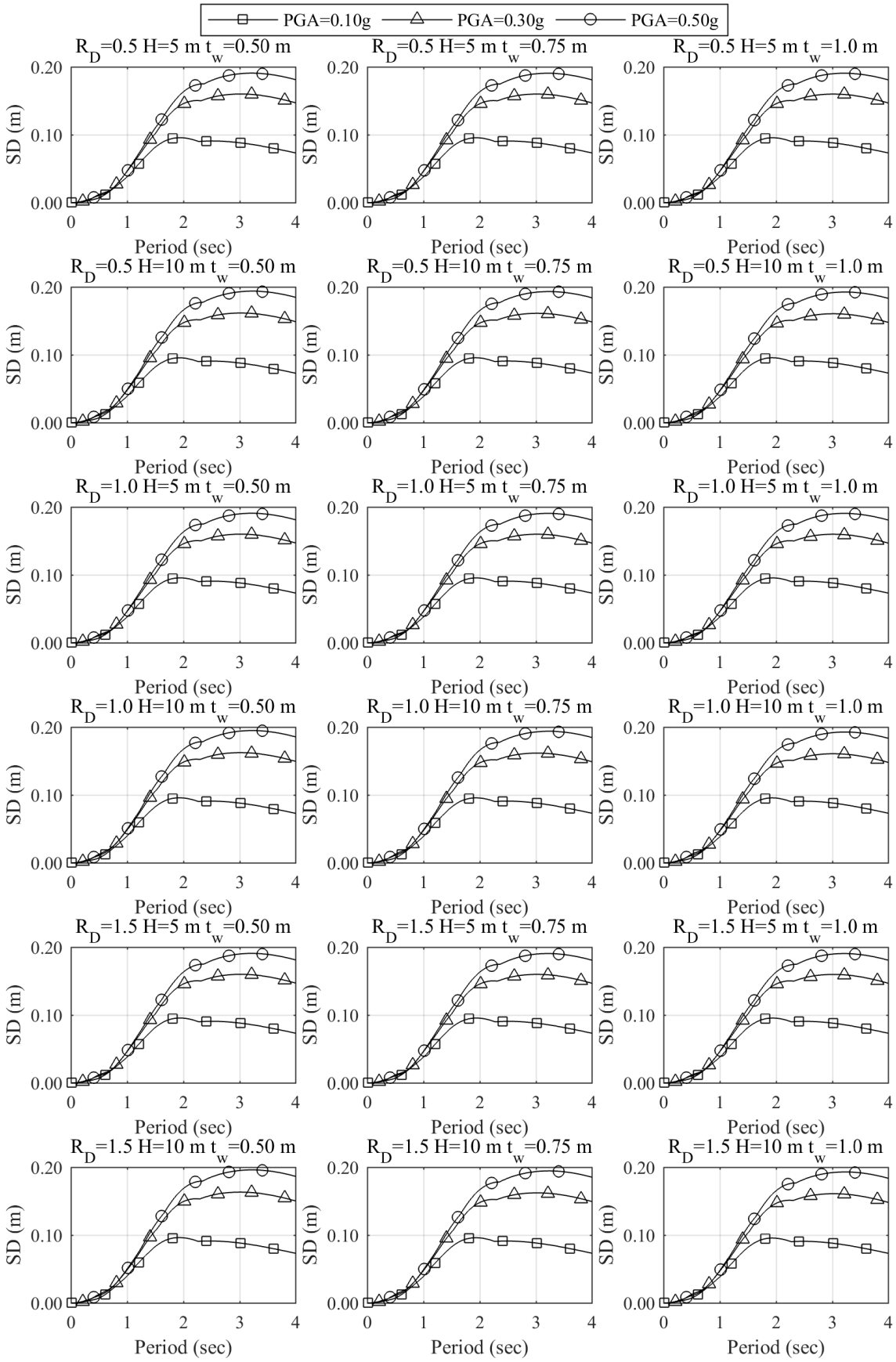

Figure A.5 S_d values for Soil Site 2 in USFF conditions

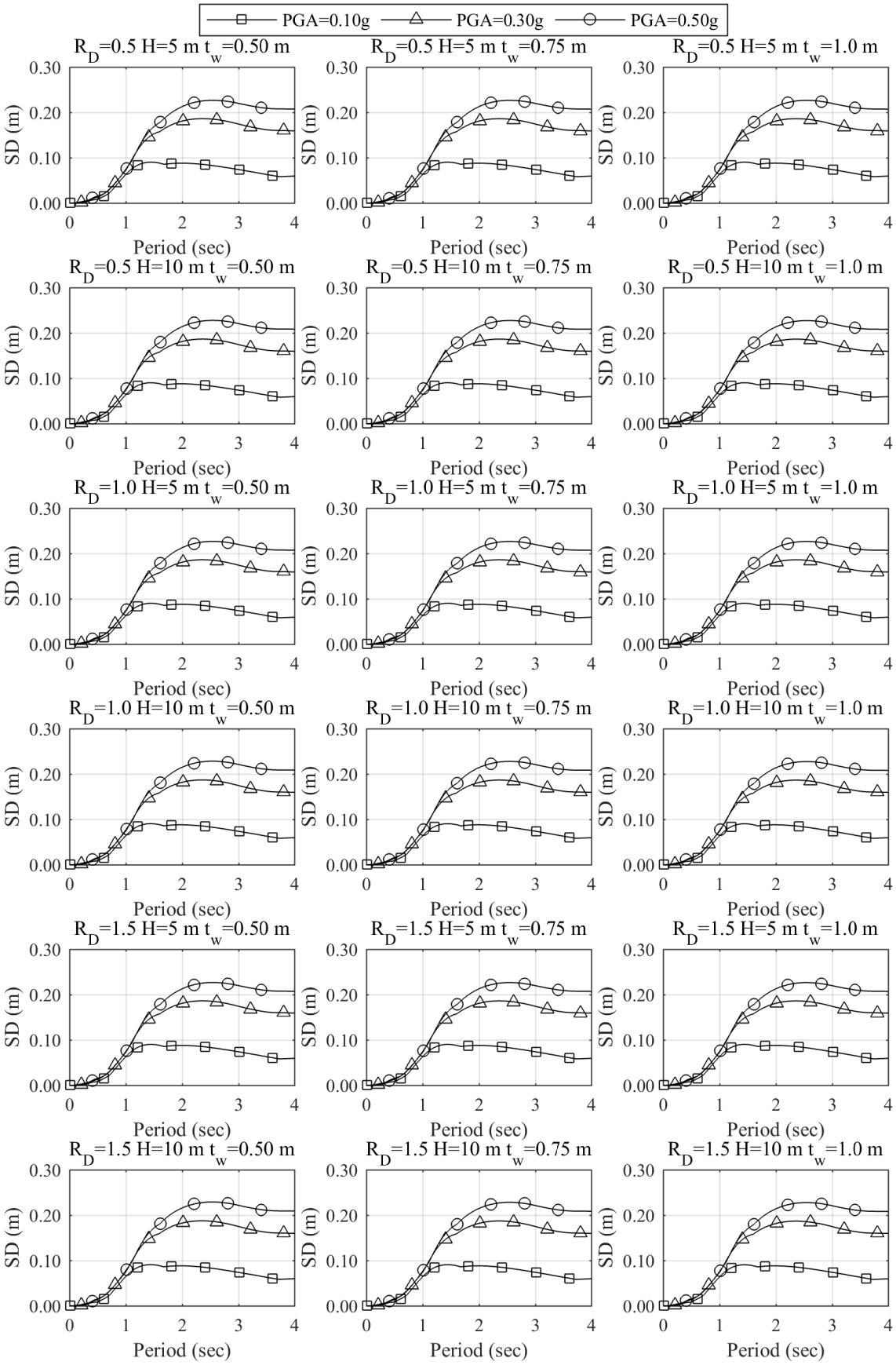

Figure A.6 S_d values for Soil Site 3 in USFF conditions

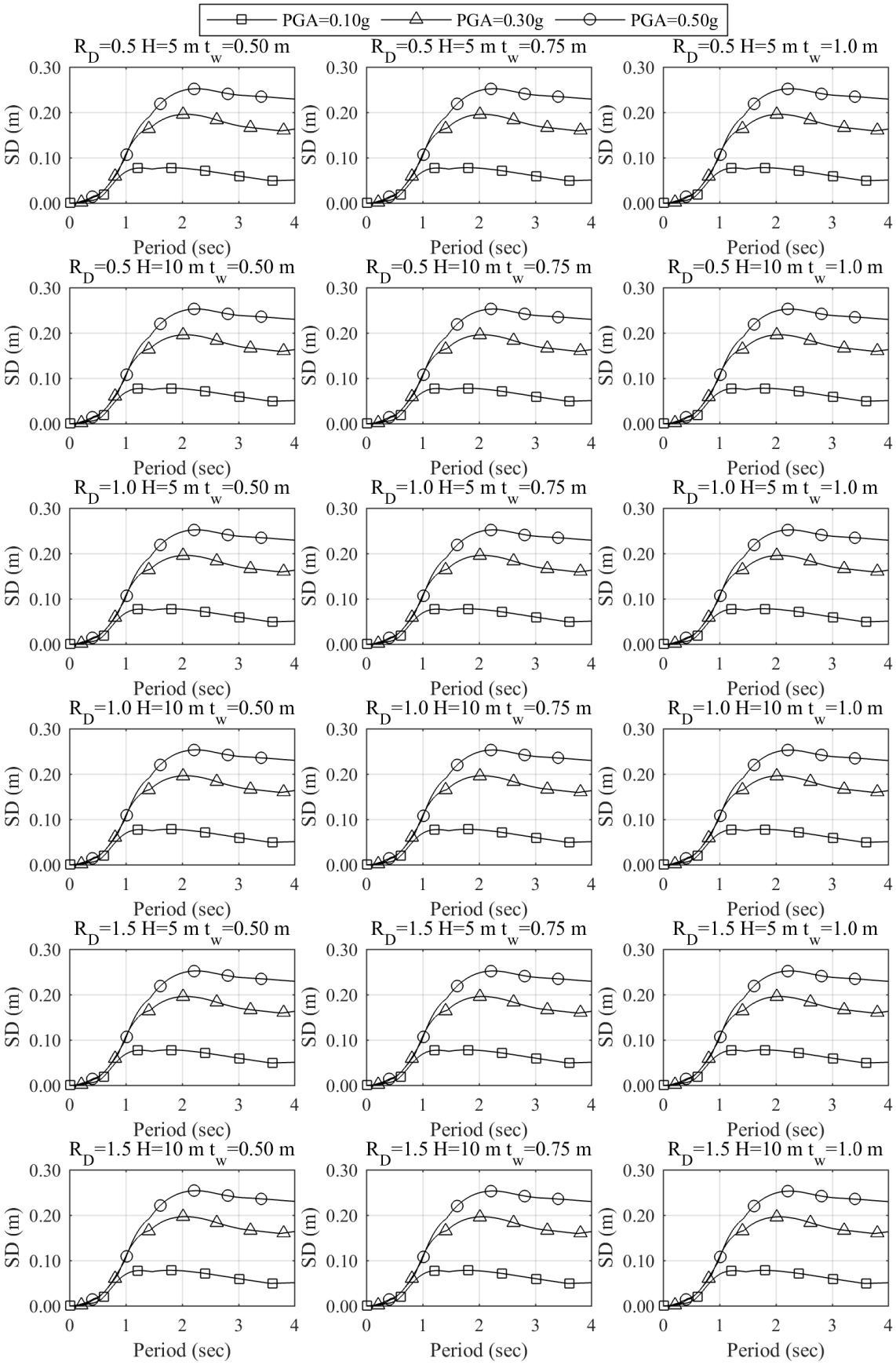

Figure A.7 S_d values for Soil Site 4 in USFF conditions

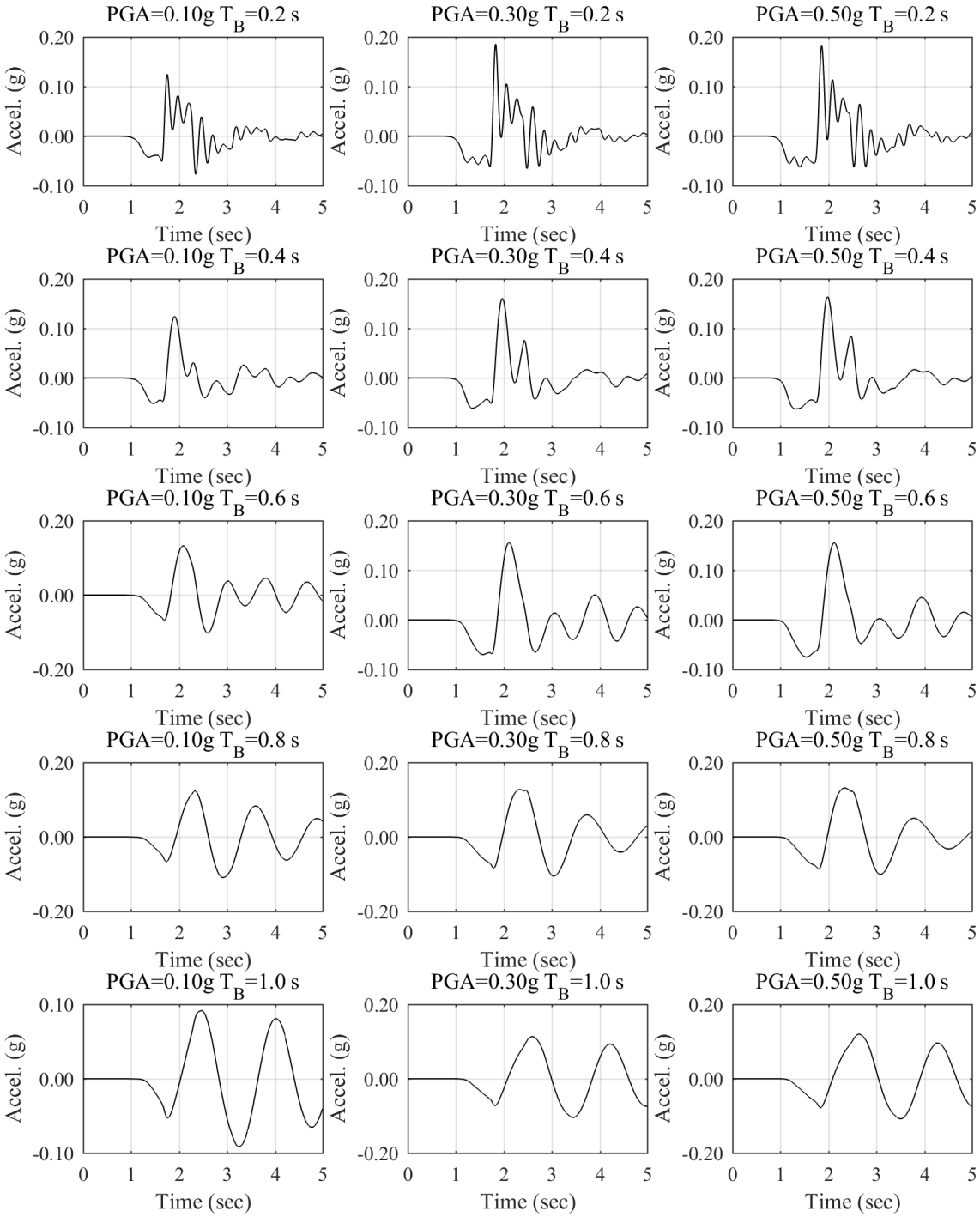

Figure A.8 Surface structure accelerations for Soil Site 2

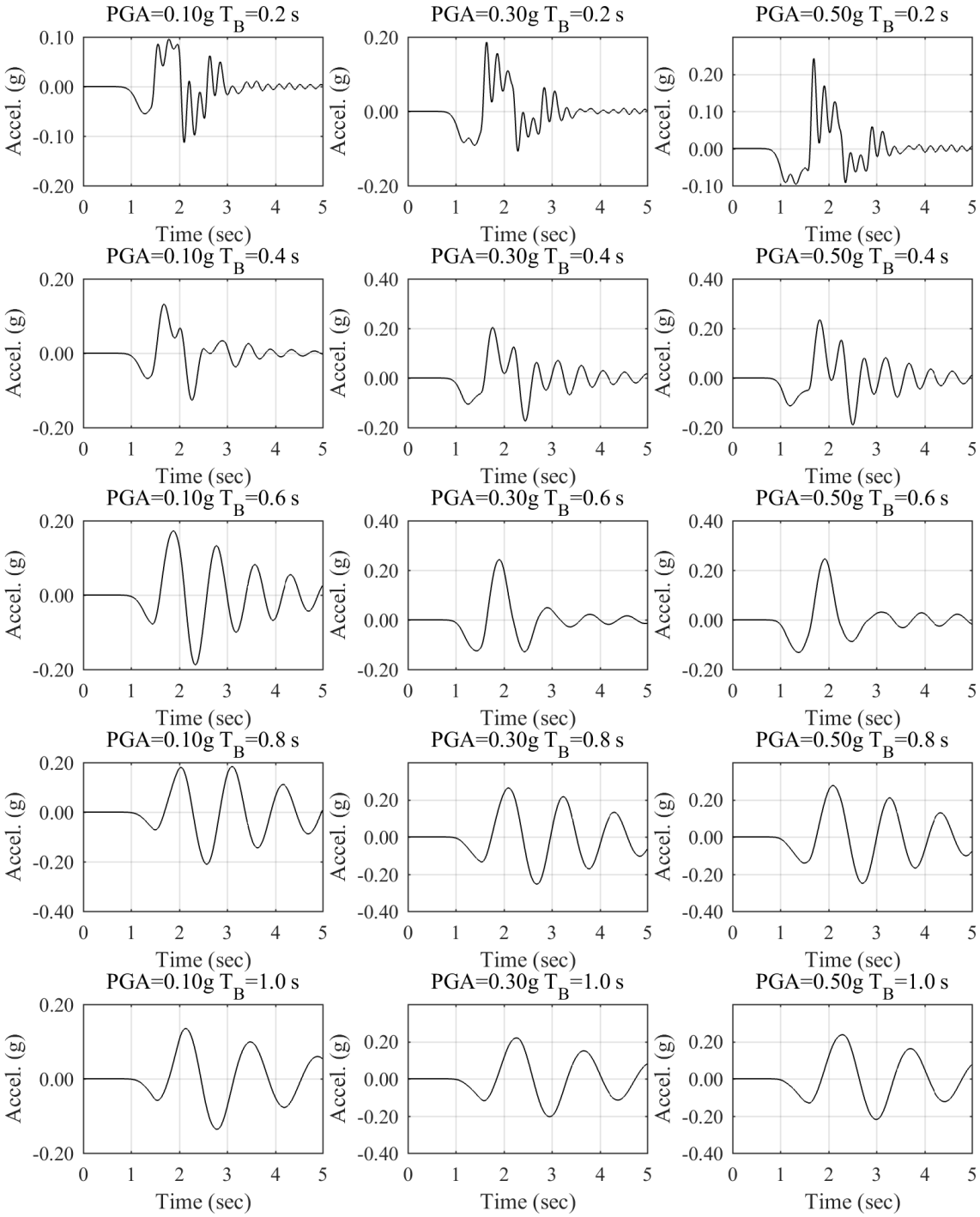

Figure A.9 Surface structure accelerations for Soil Site 3

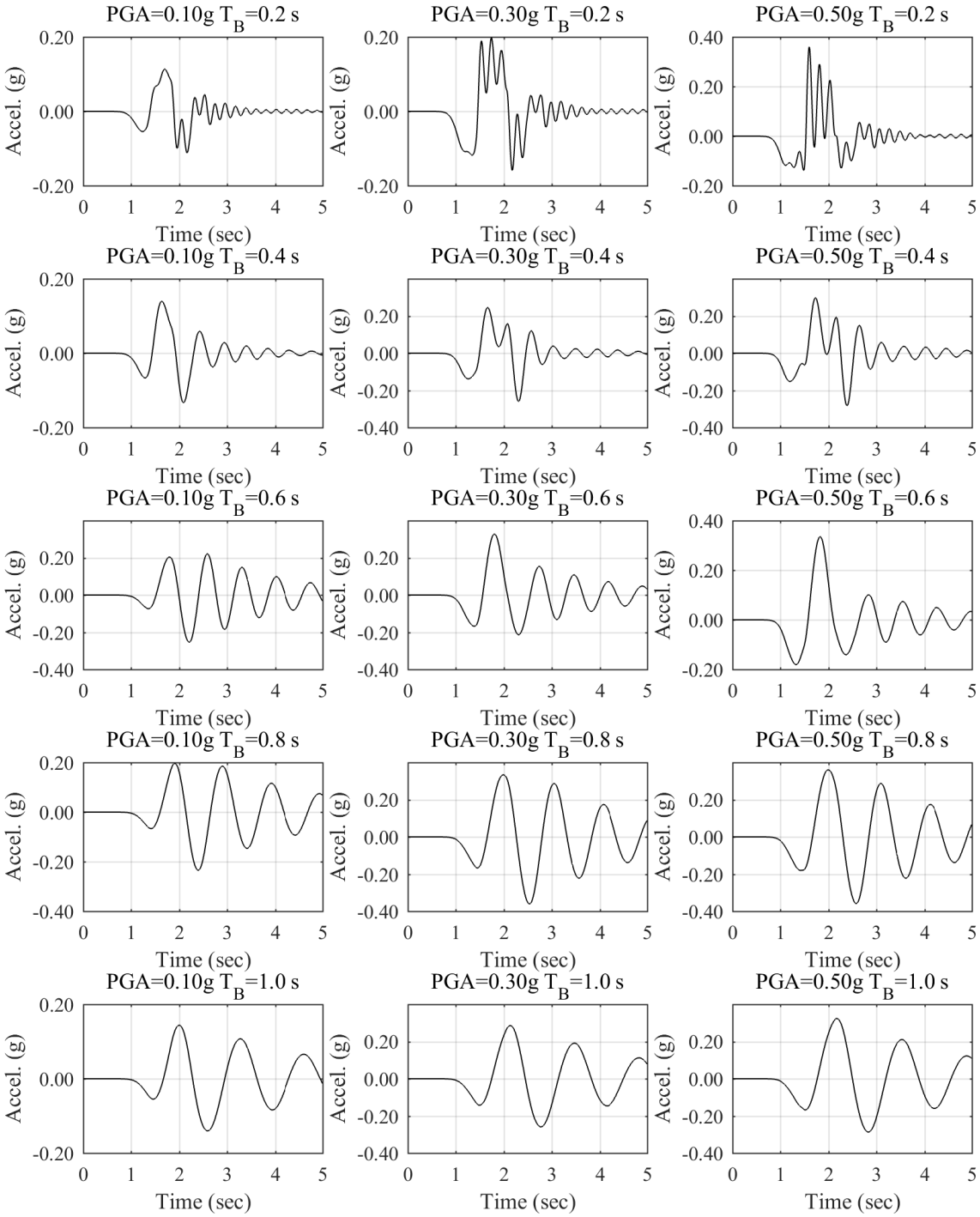

Figure A.10 Surface structure accelerations for Soil Site 4

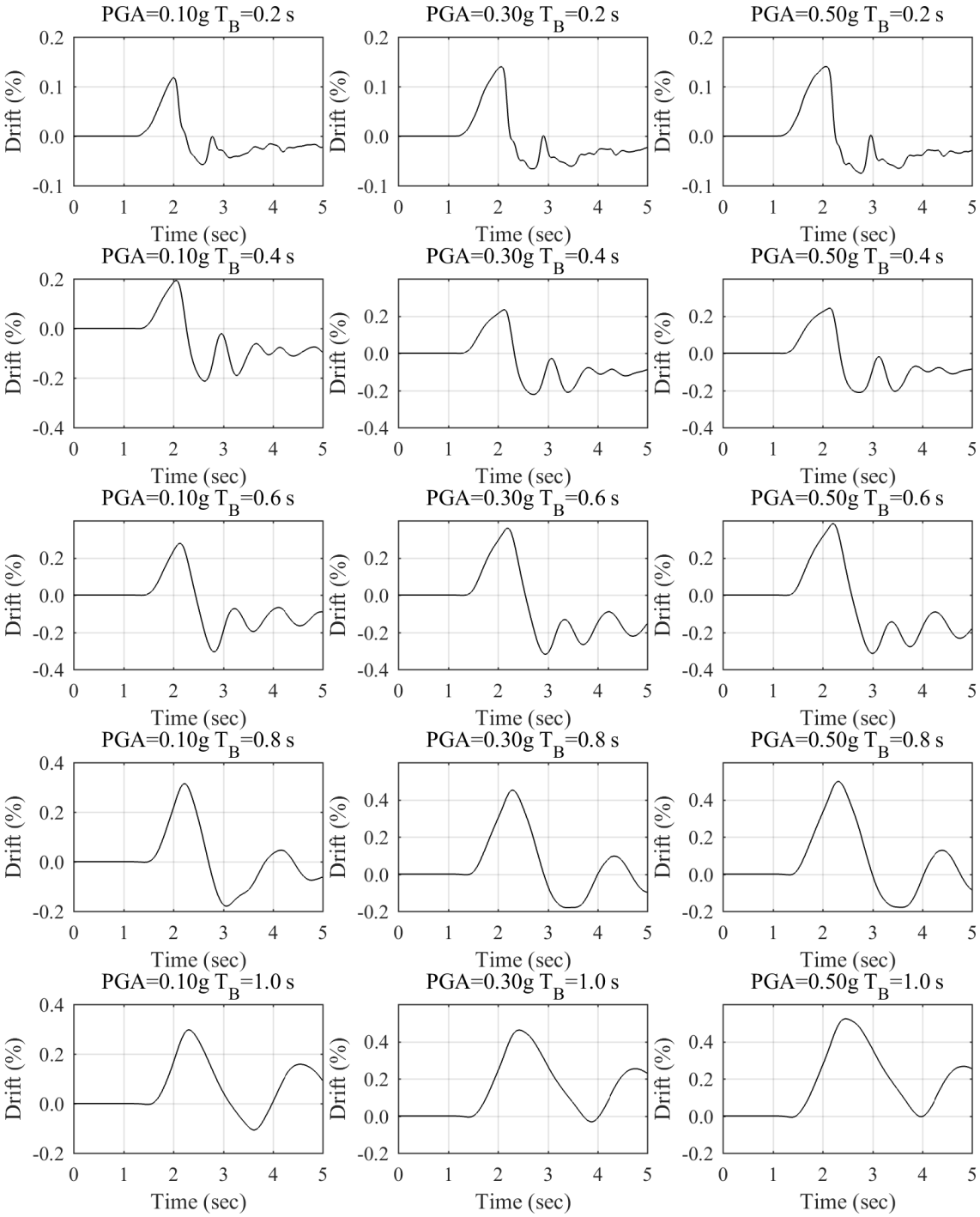

Figure A.11 Surface structure drifts for Soil Site 1

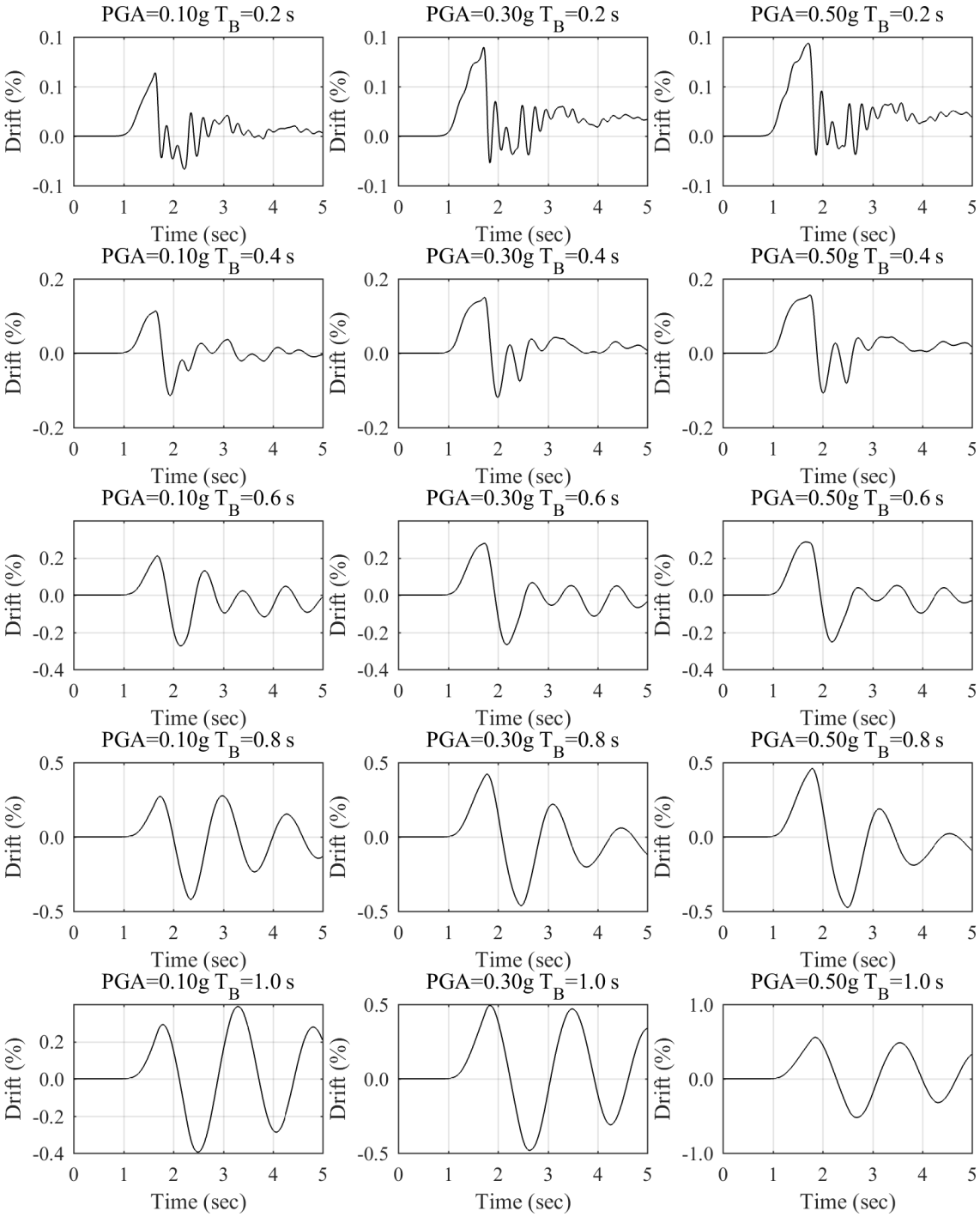

Figure A.12 Surface structure drifts for Soil Site 2

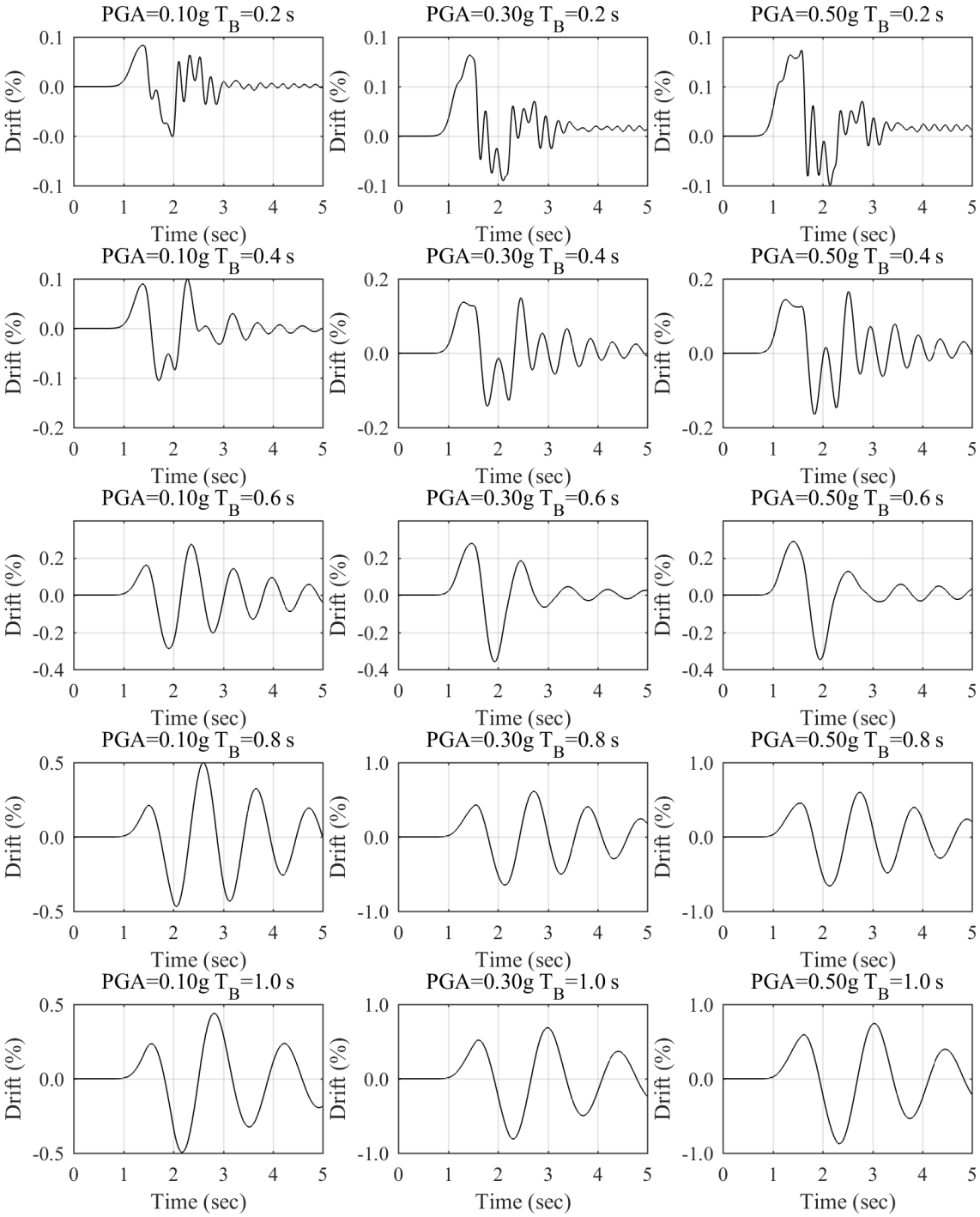

Figure A.13 Surface structure drifts for Soil Site 3

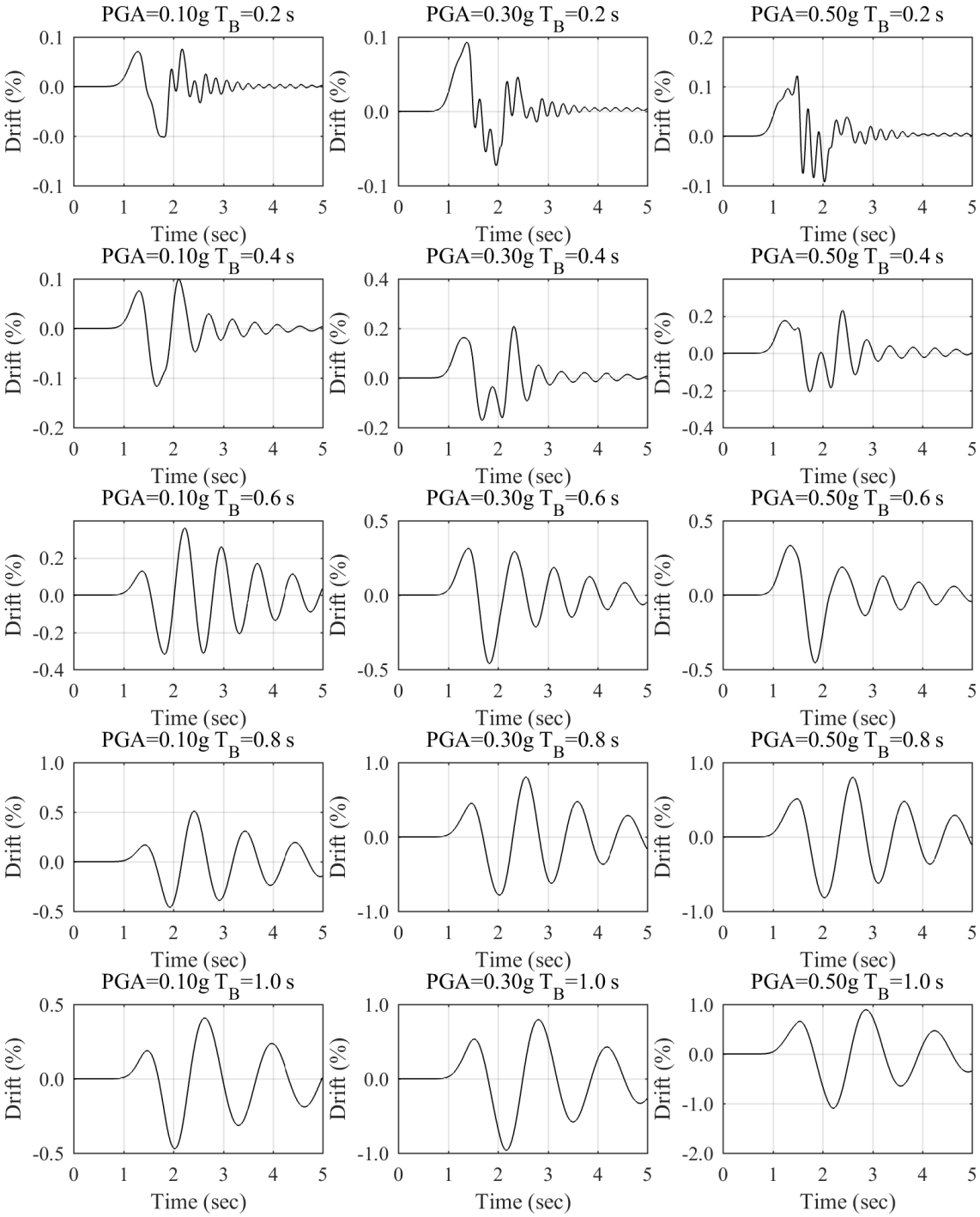

Figure A.14 Surface structure drifts for Soil Site 4

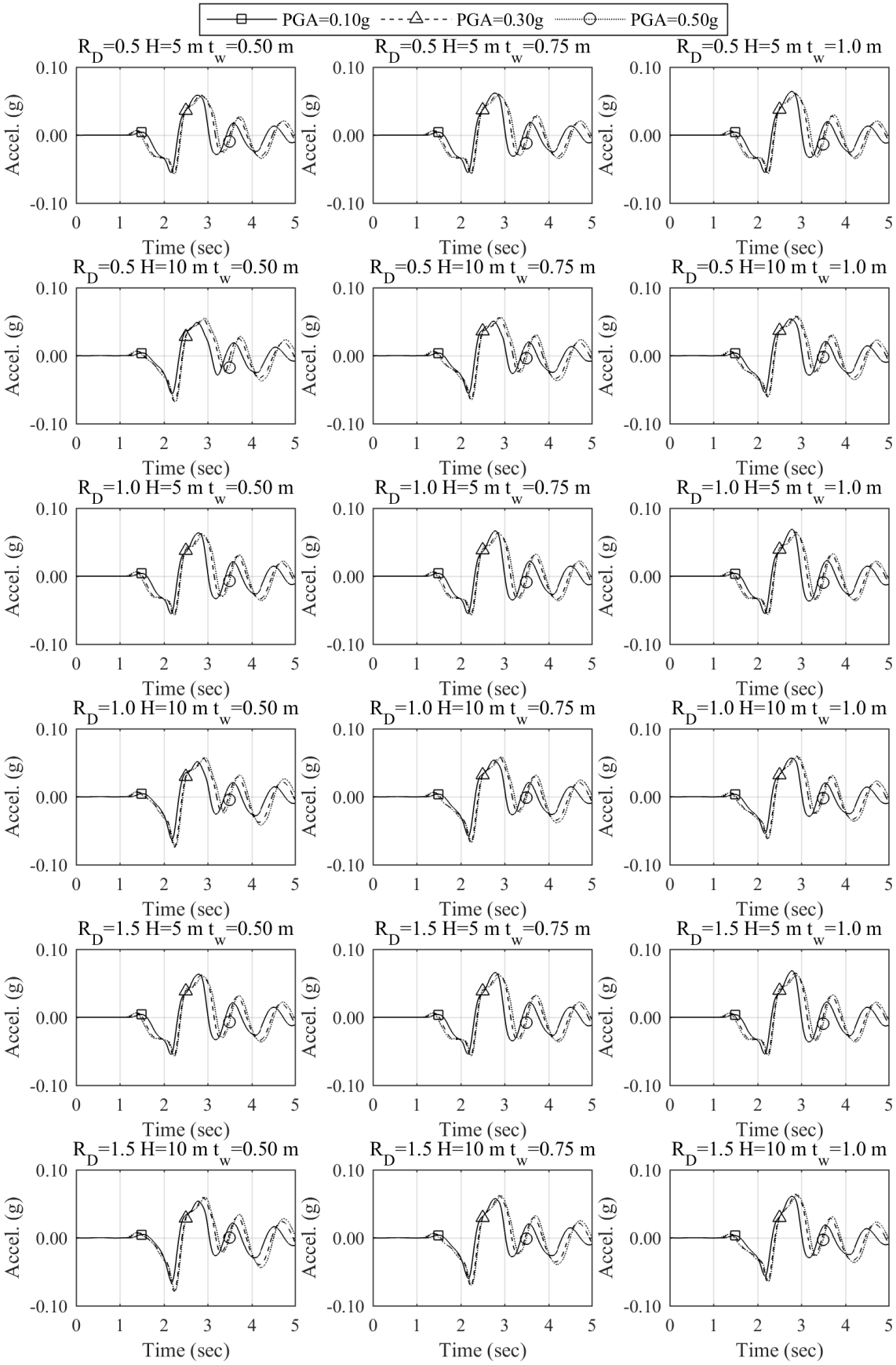

Figure A.15 Surface structure accelerations for Soil Site 1

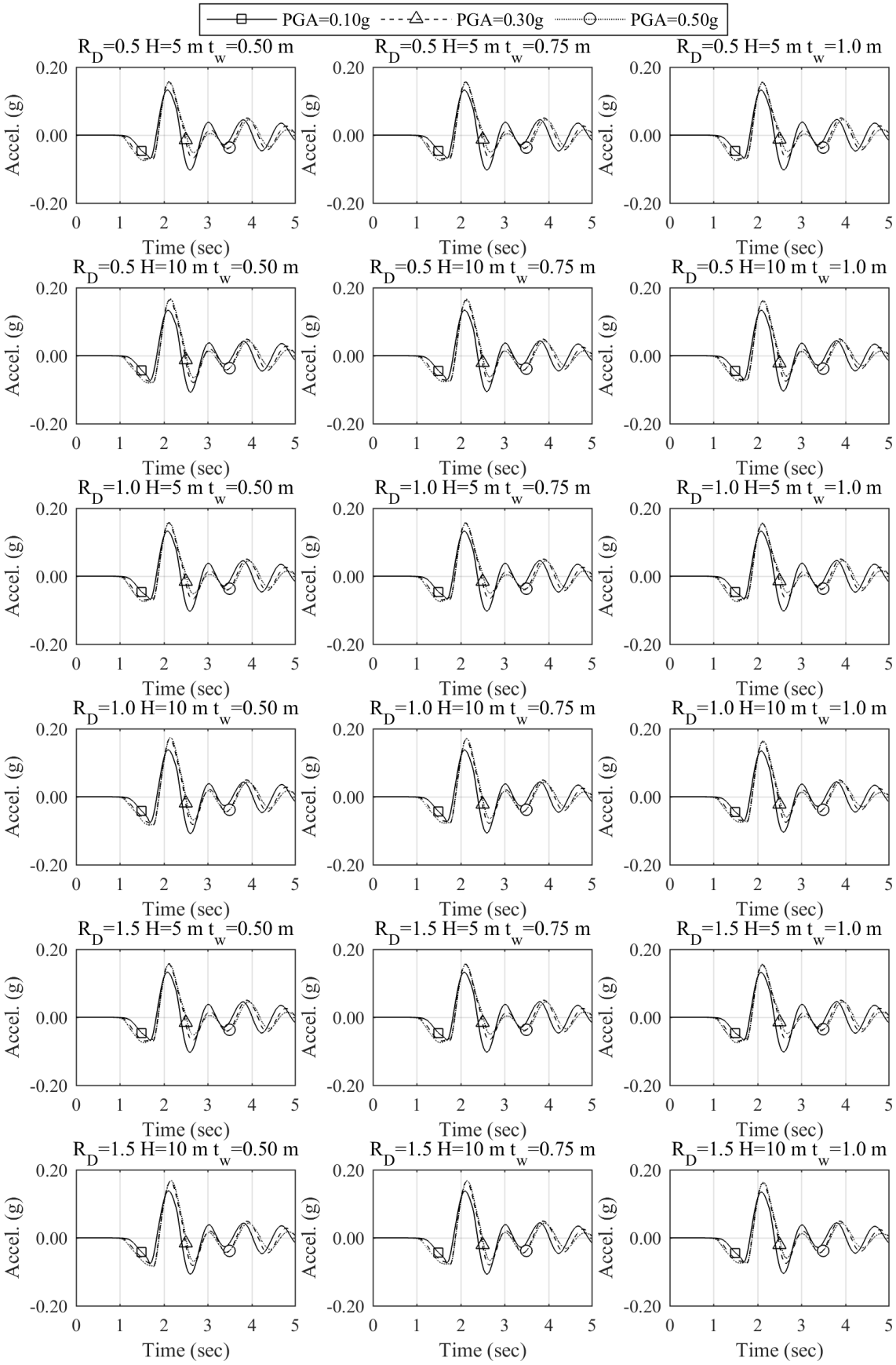

Figure A.16 Surface structure accelerations for Soil Site 2

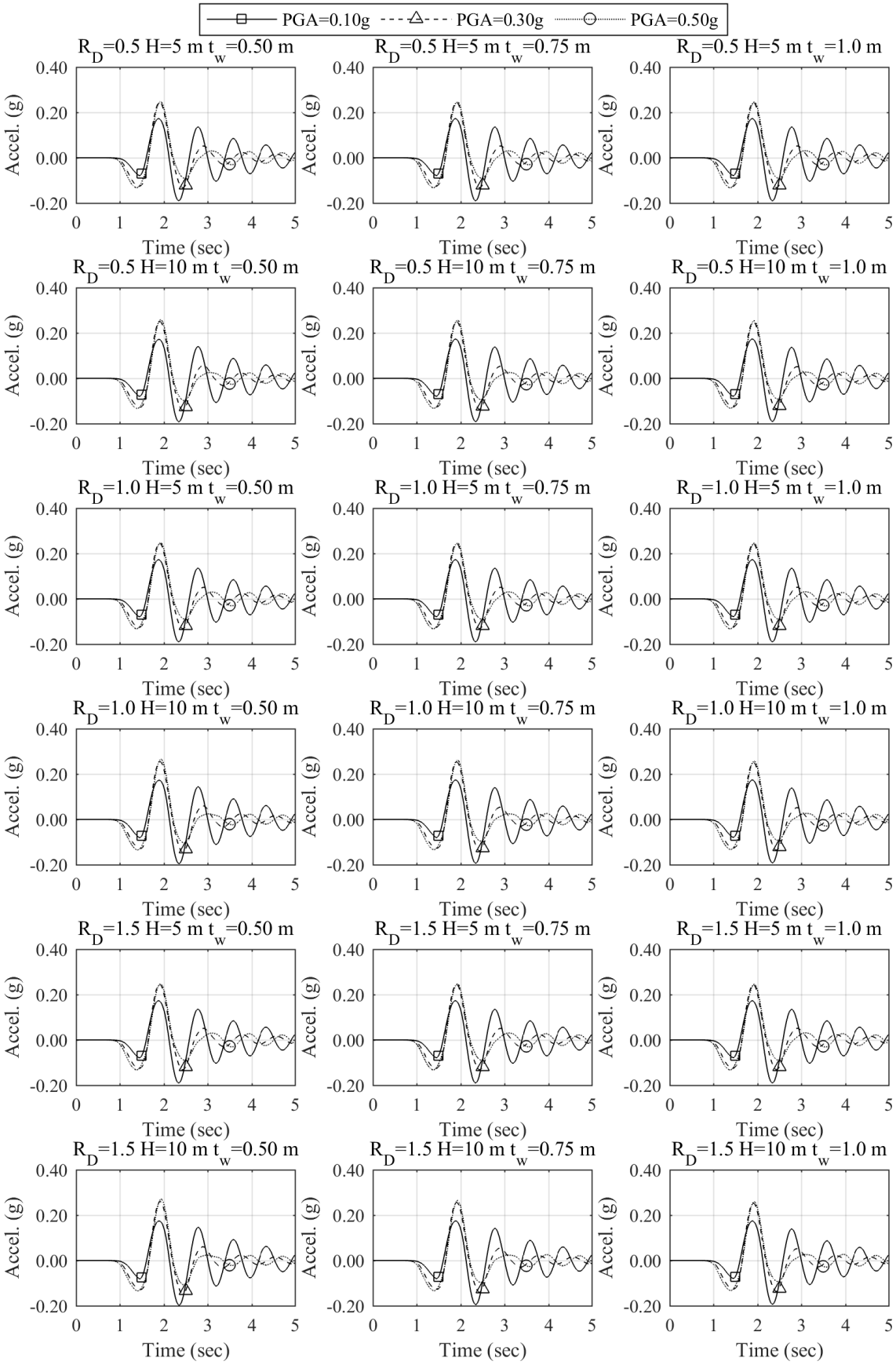

Figure A.17 Surface structure accelerations for Soil Site 3

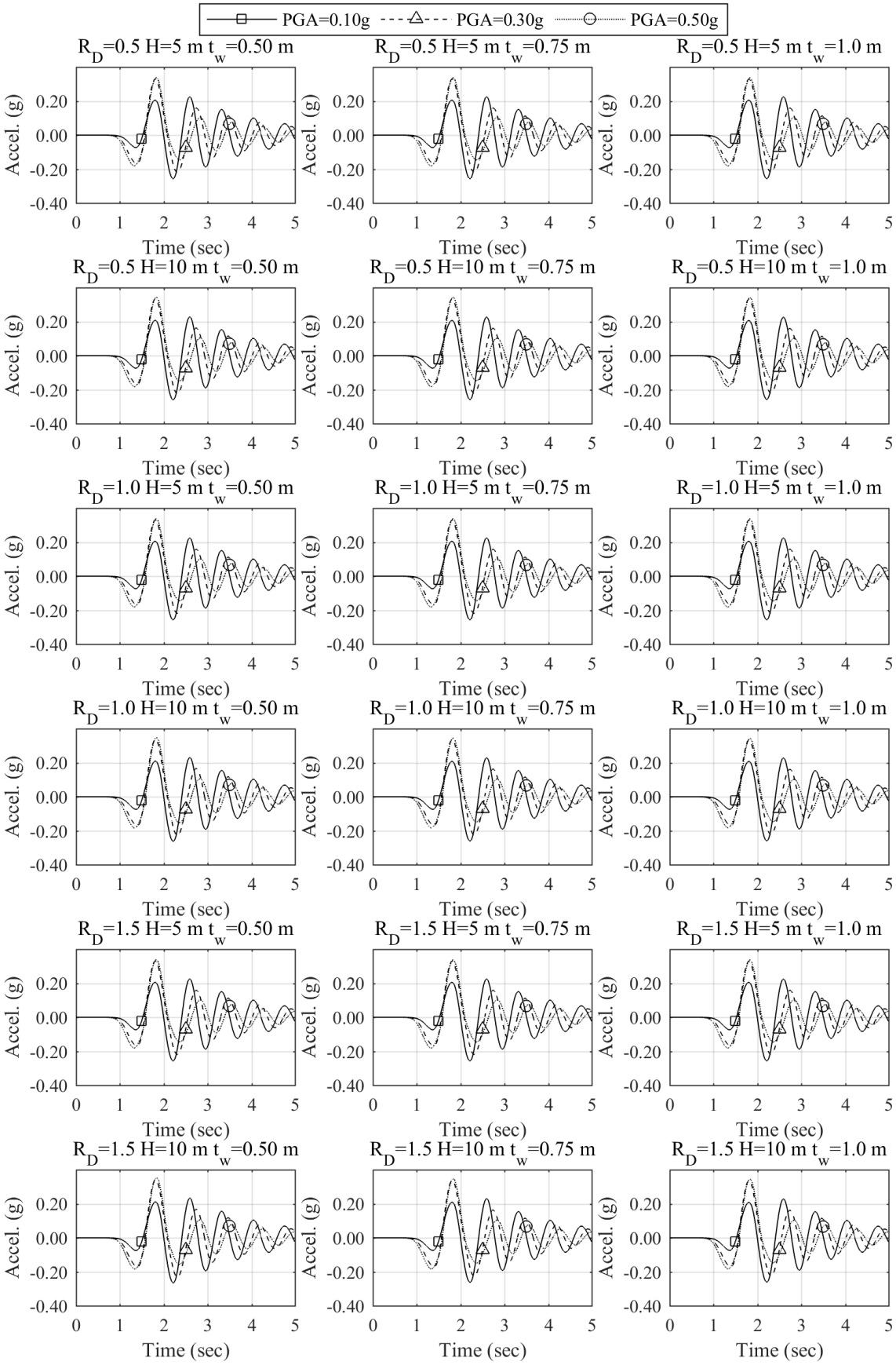

Figure A.18 Surface structure accelerations for Soil Site 4

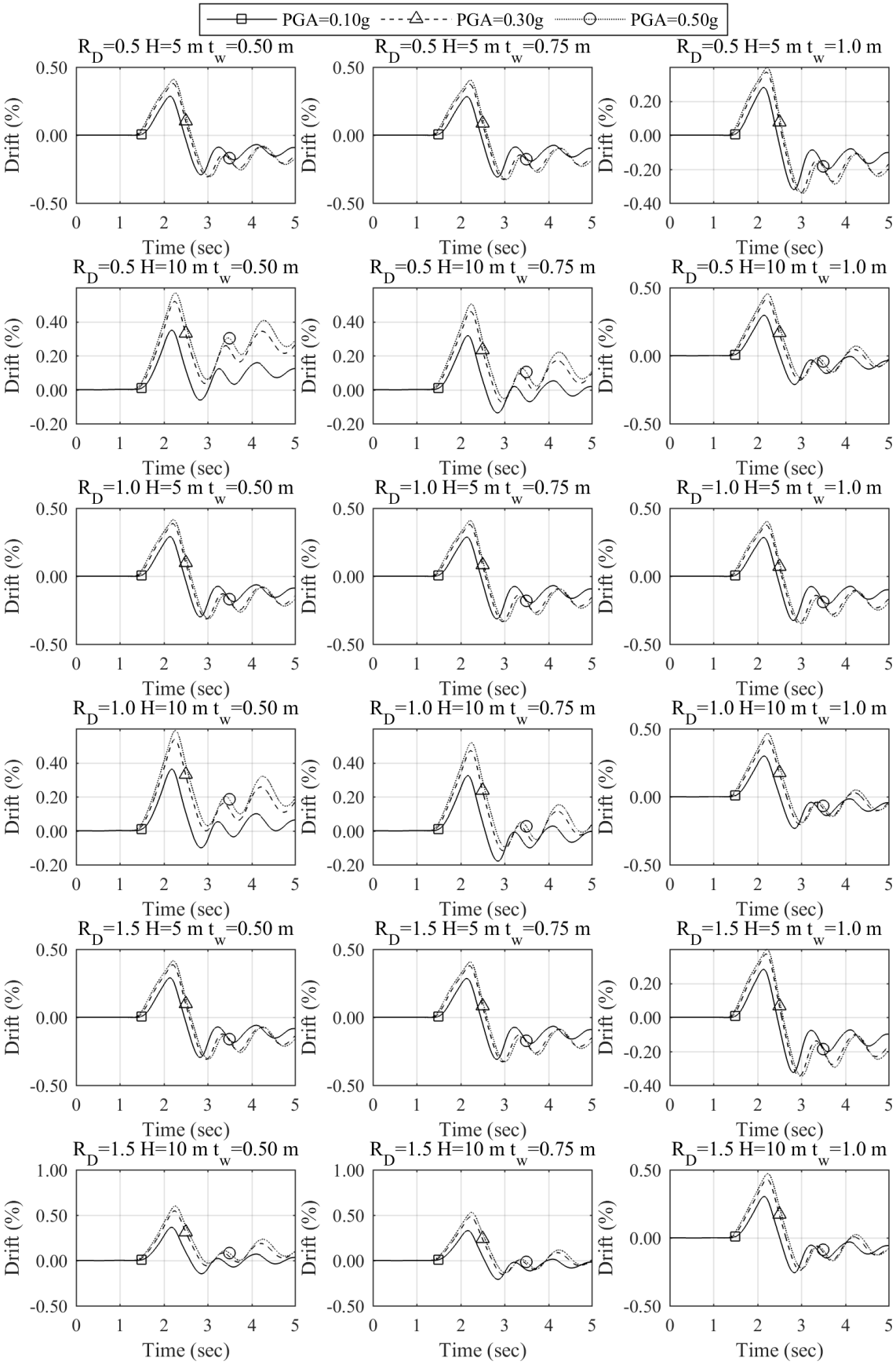

Figure A.19 Surface structure drifts for Soil Site 1

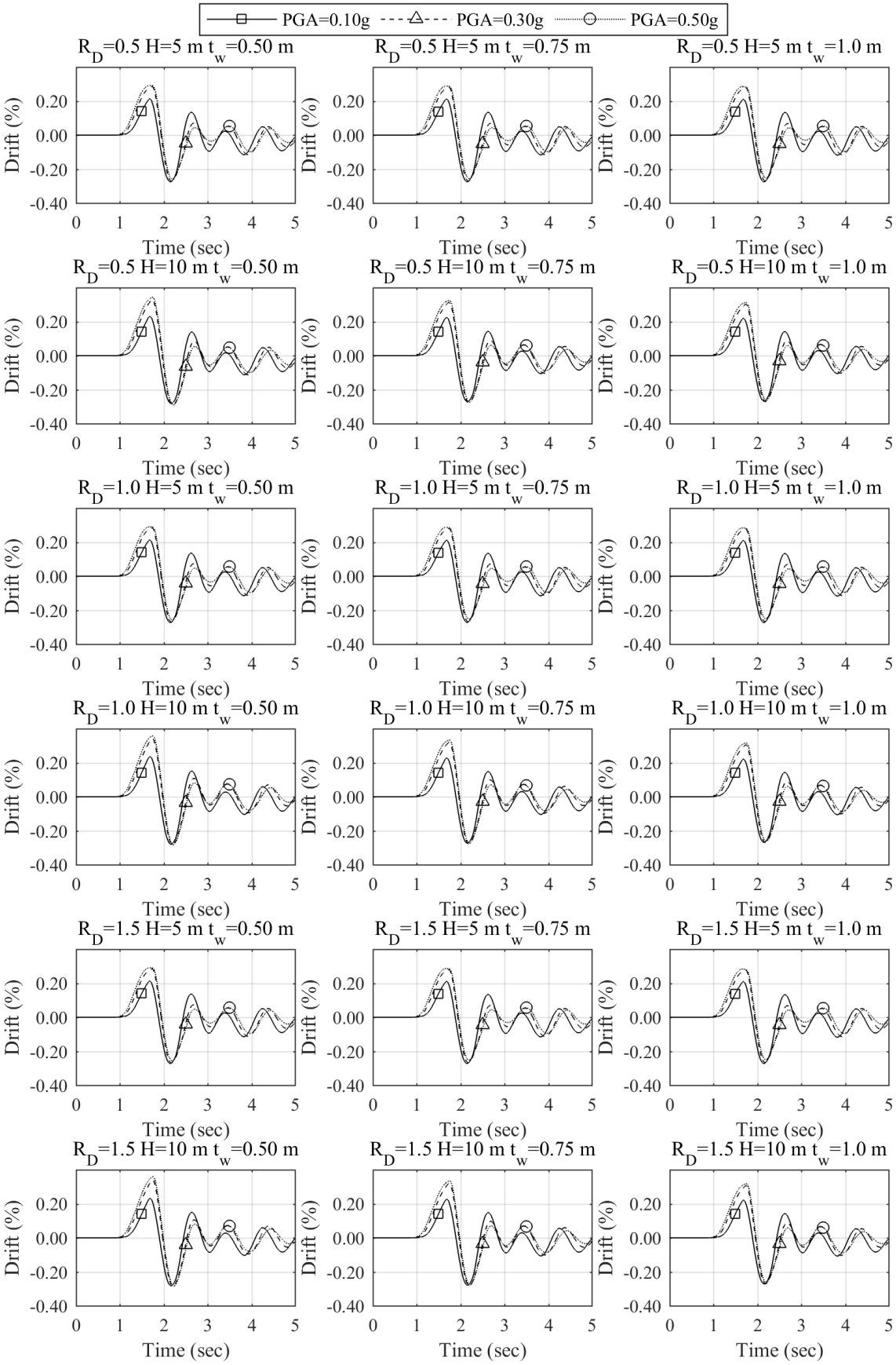

Figure A.20 Surface structure drifts for Soil Site 2

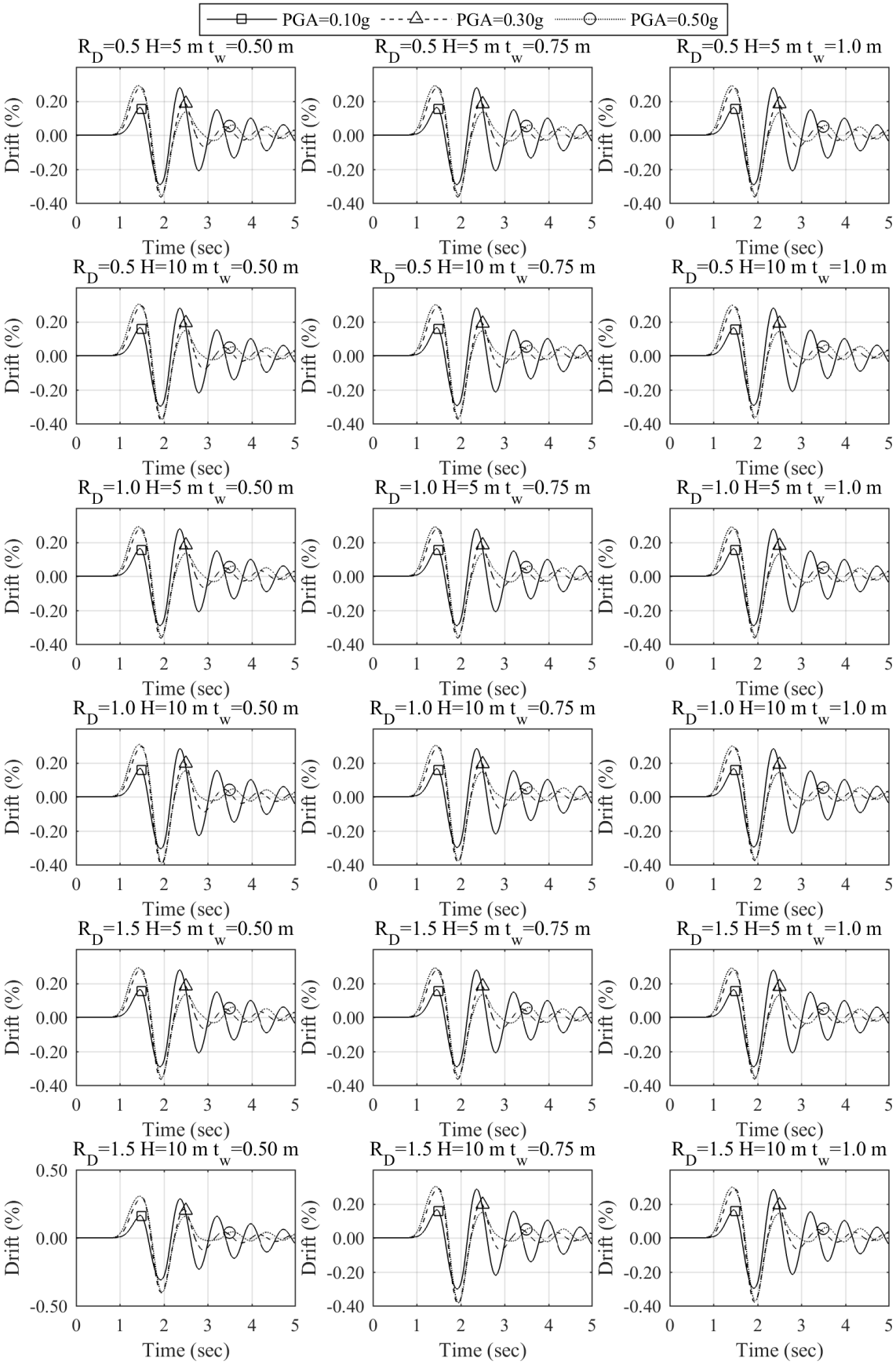

Figure A.21 Surface structure drifts for Soil Site 3

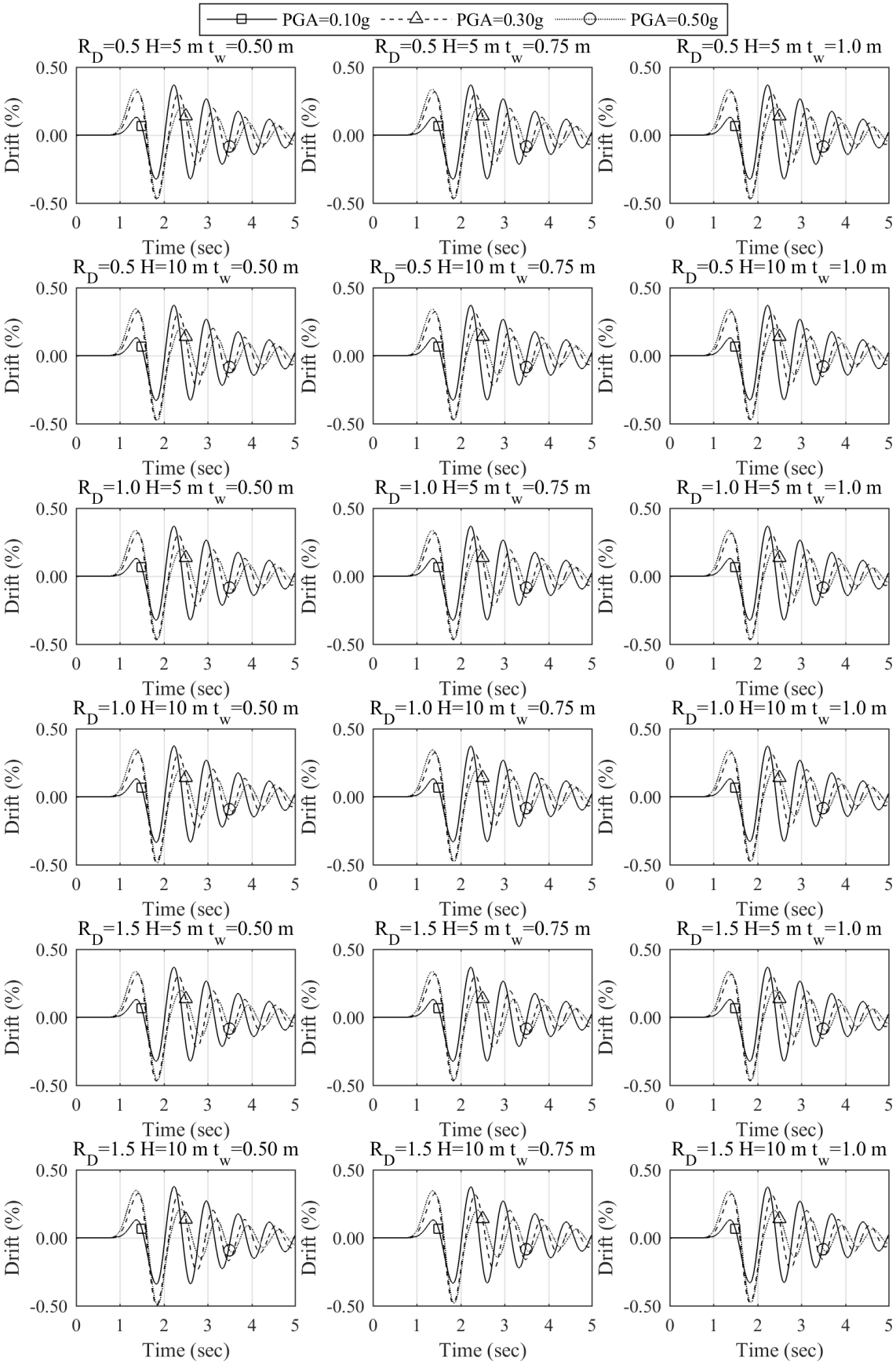

Figure A.22 Surface structure drifts for Soil Site 4

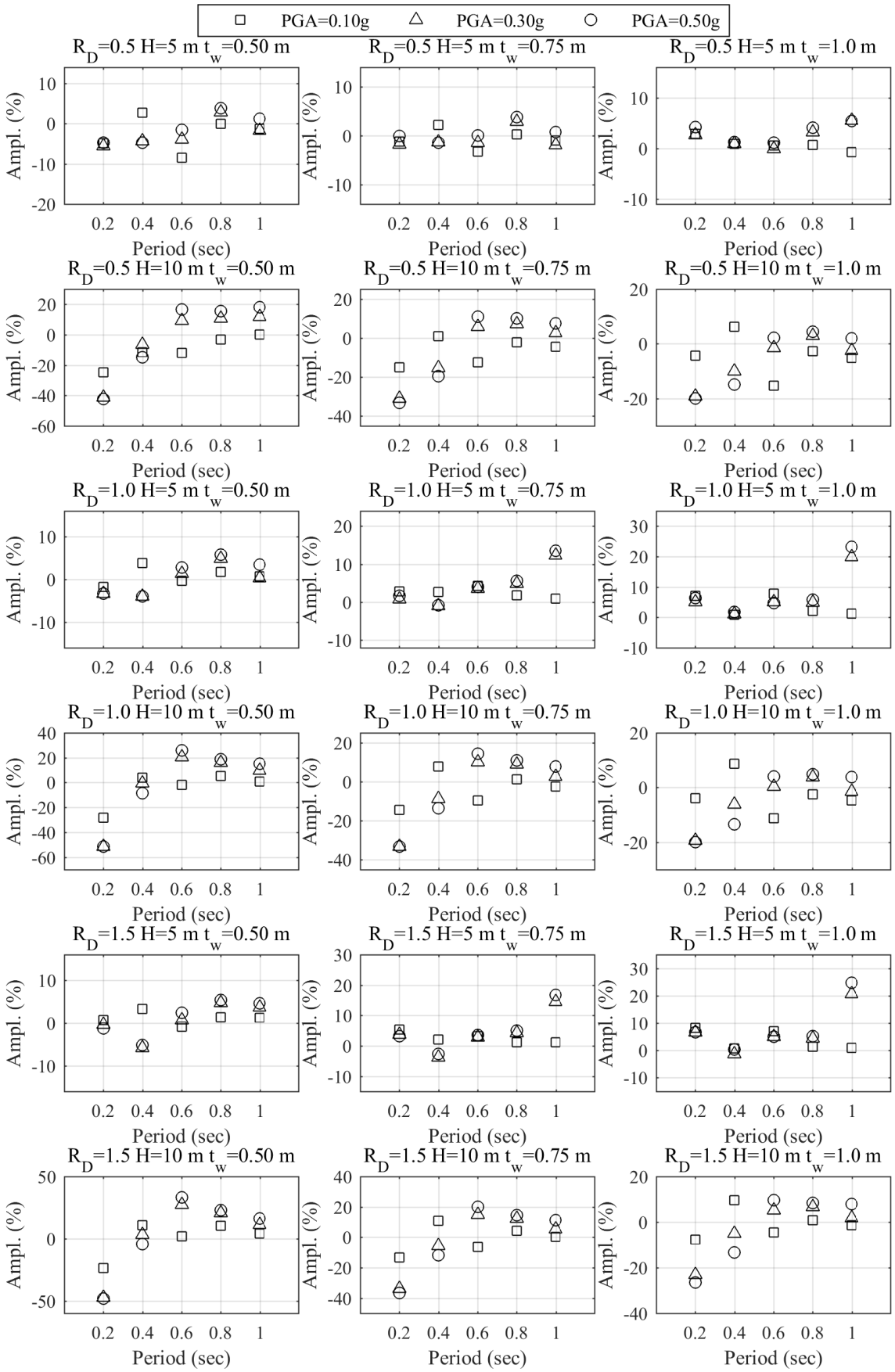

Figure A.23 Peak acceleration amplifications for $R_L = 2$ and Soil Site 1

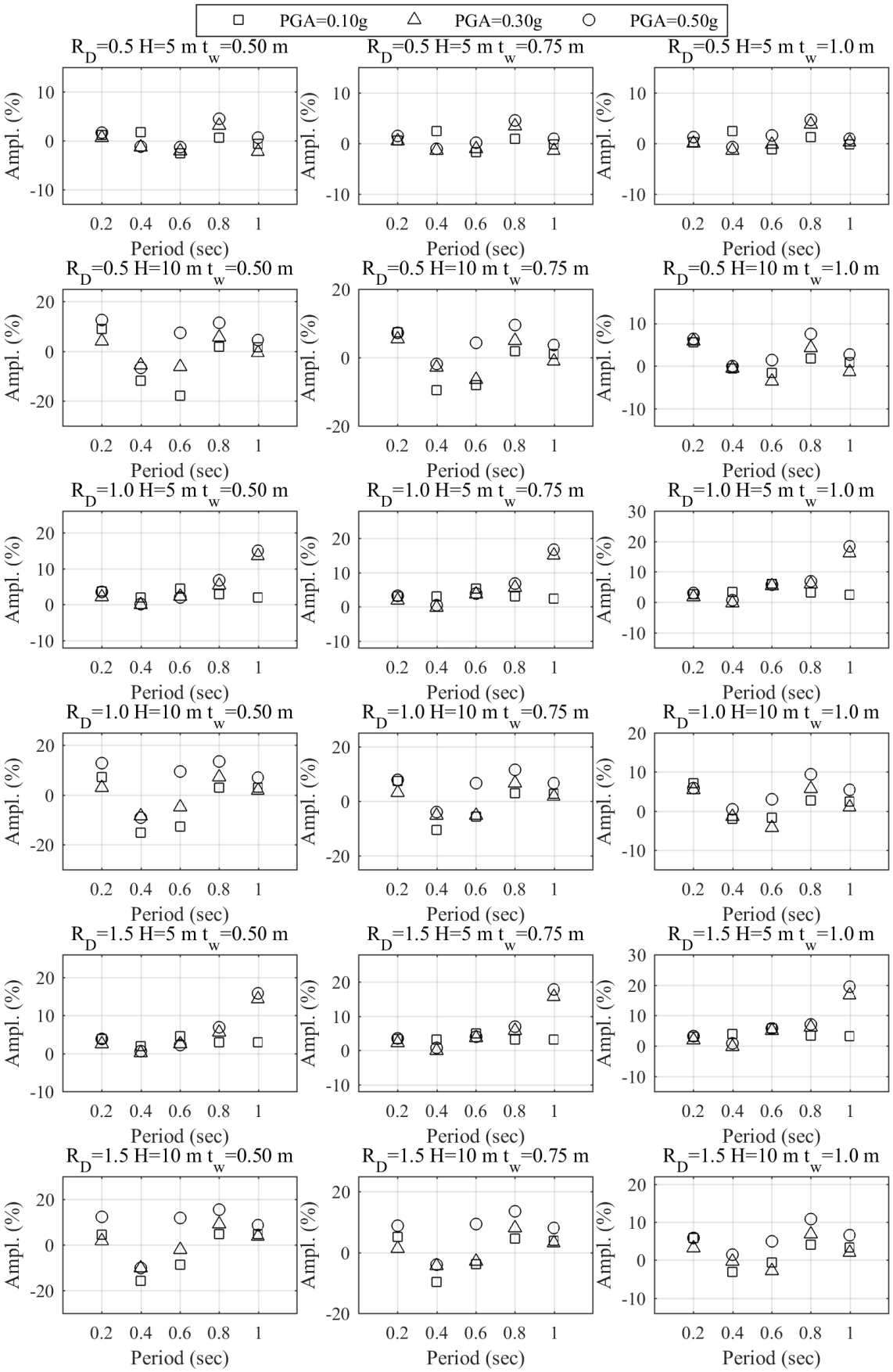

Figure A.24 Peak acceleration amplifications for $R_L = 4$ and Soil Site 1

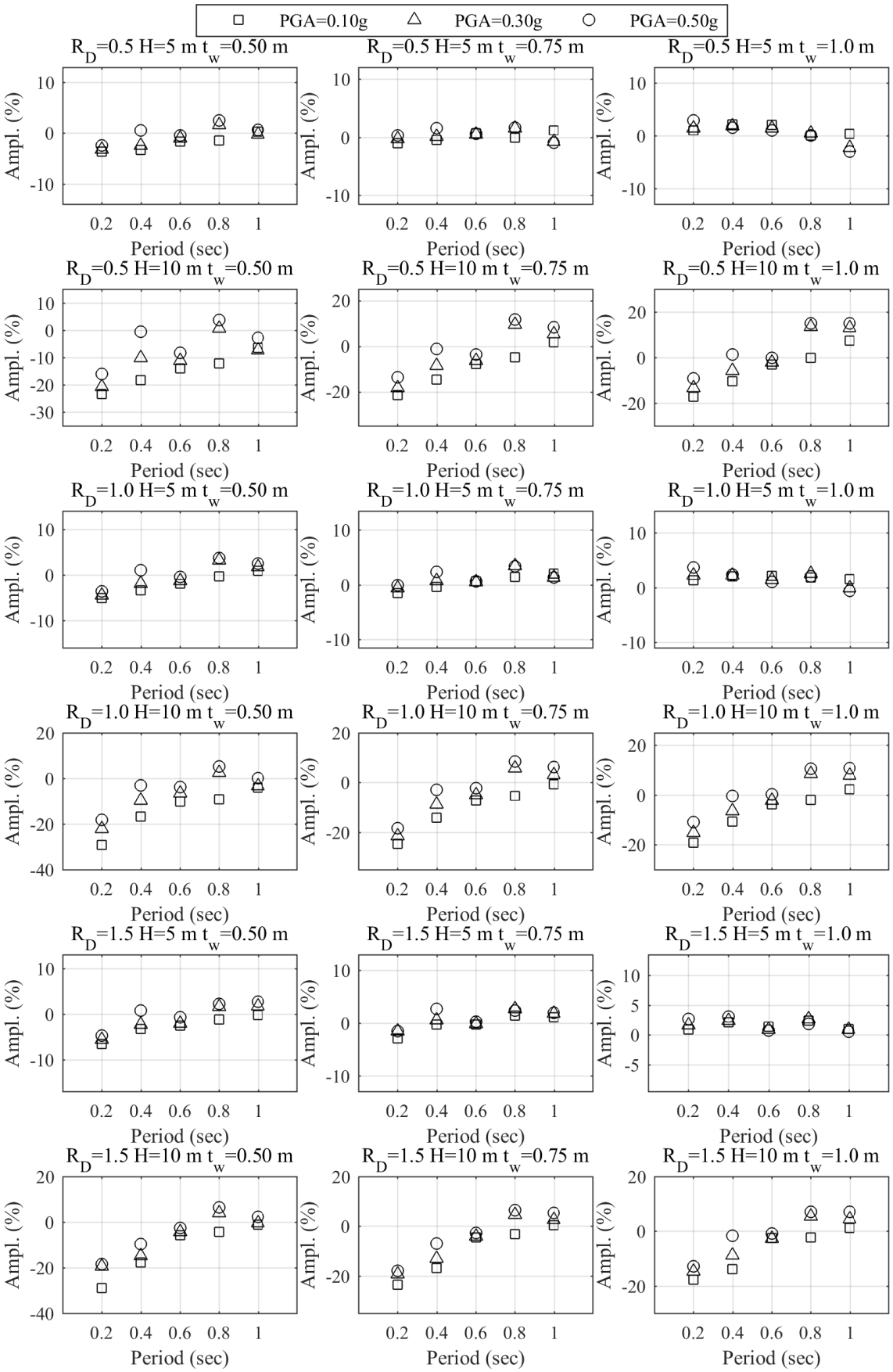

Figure A.25 Peak acceleration amplifications for $R_L = 0$ and Soil Site 2

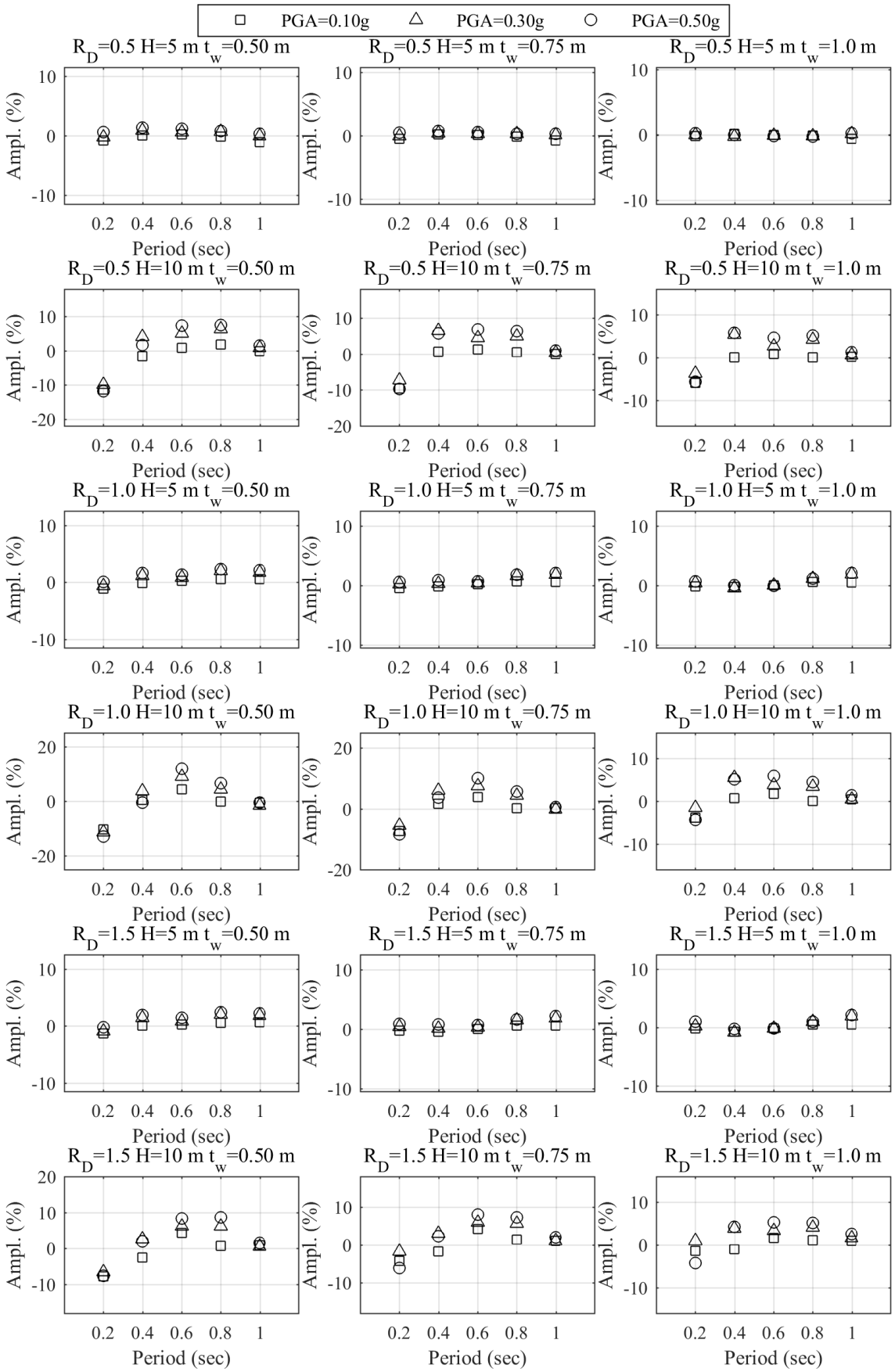

Figure A.26 Peak acceleration amplifications for $R_L = 2$ and Soil Site 2

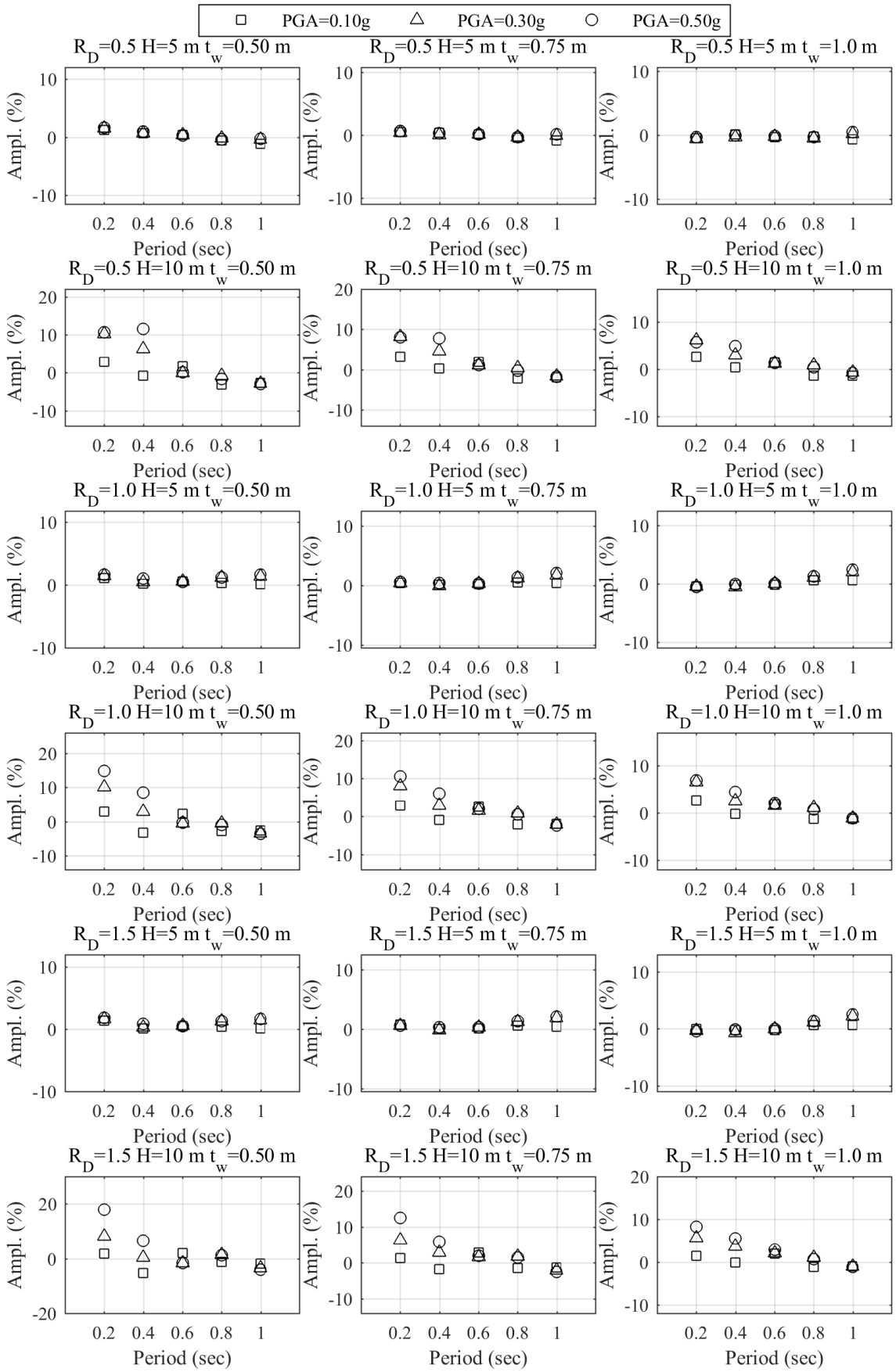

Figure A.27 Peak acceleration amplifications for $R_L = 4$ and Soil Site 2

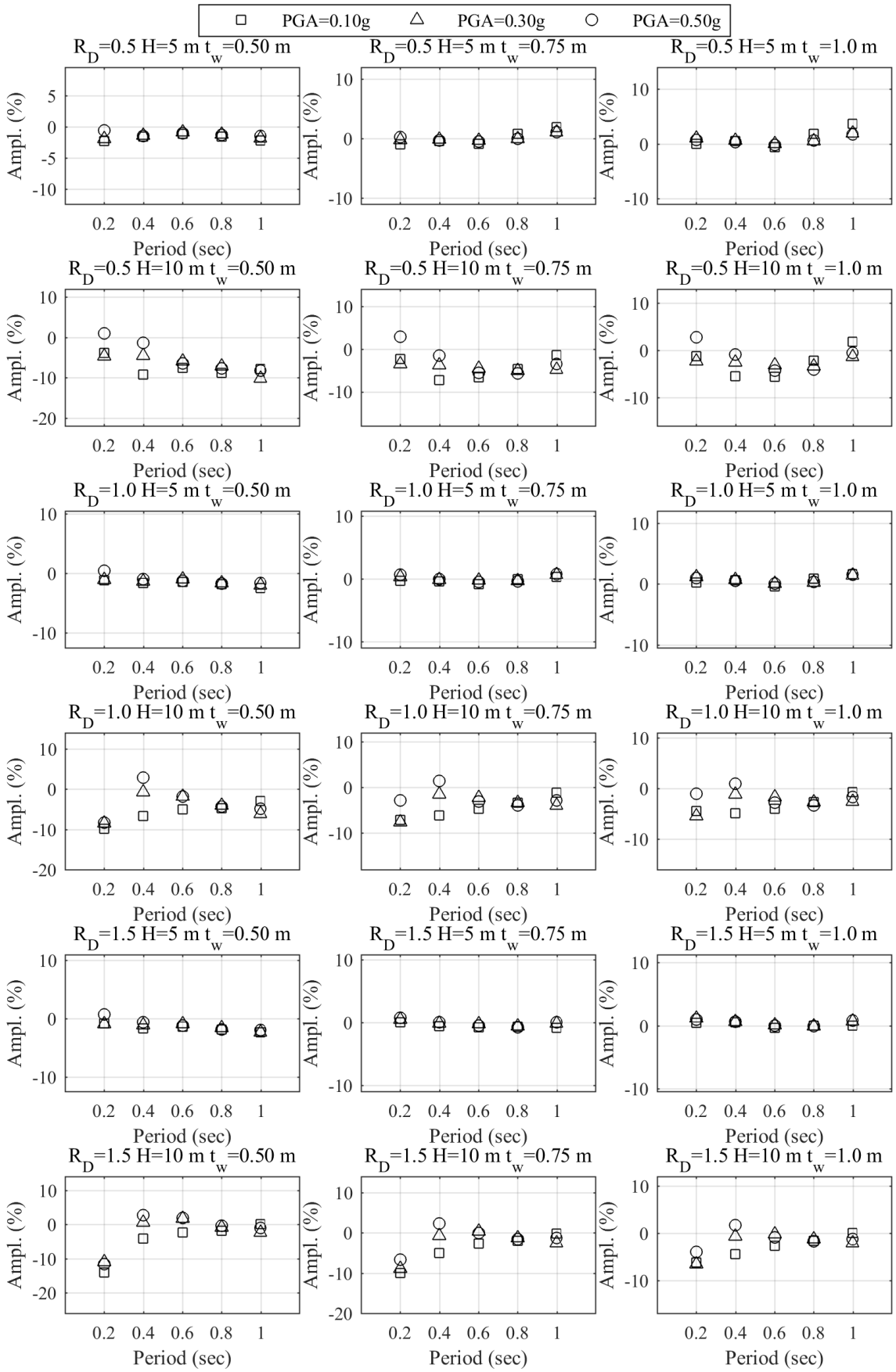

Figure A.28 Peak acceleration amplifications for $R_L = 0$ and Soil Site 3

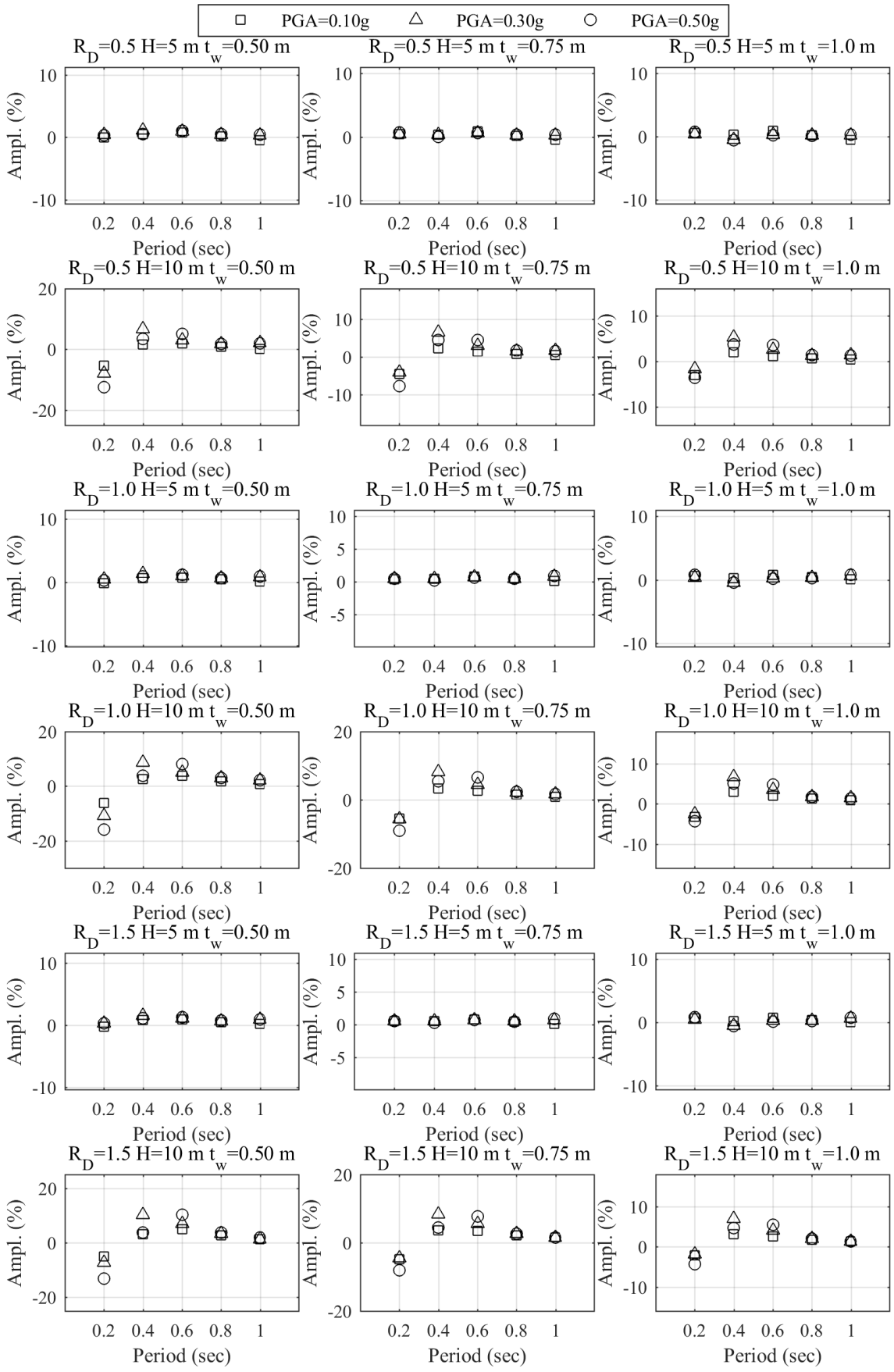

Figure A.29 Peak acceleration amplifications for $R_L = 2$ and Soil Site 3

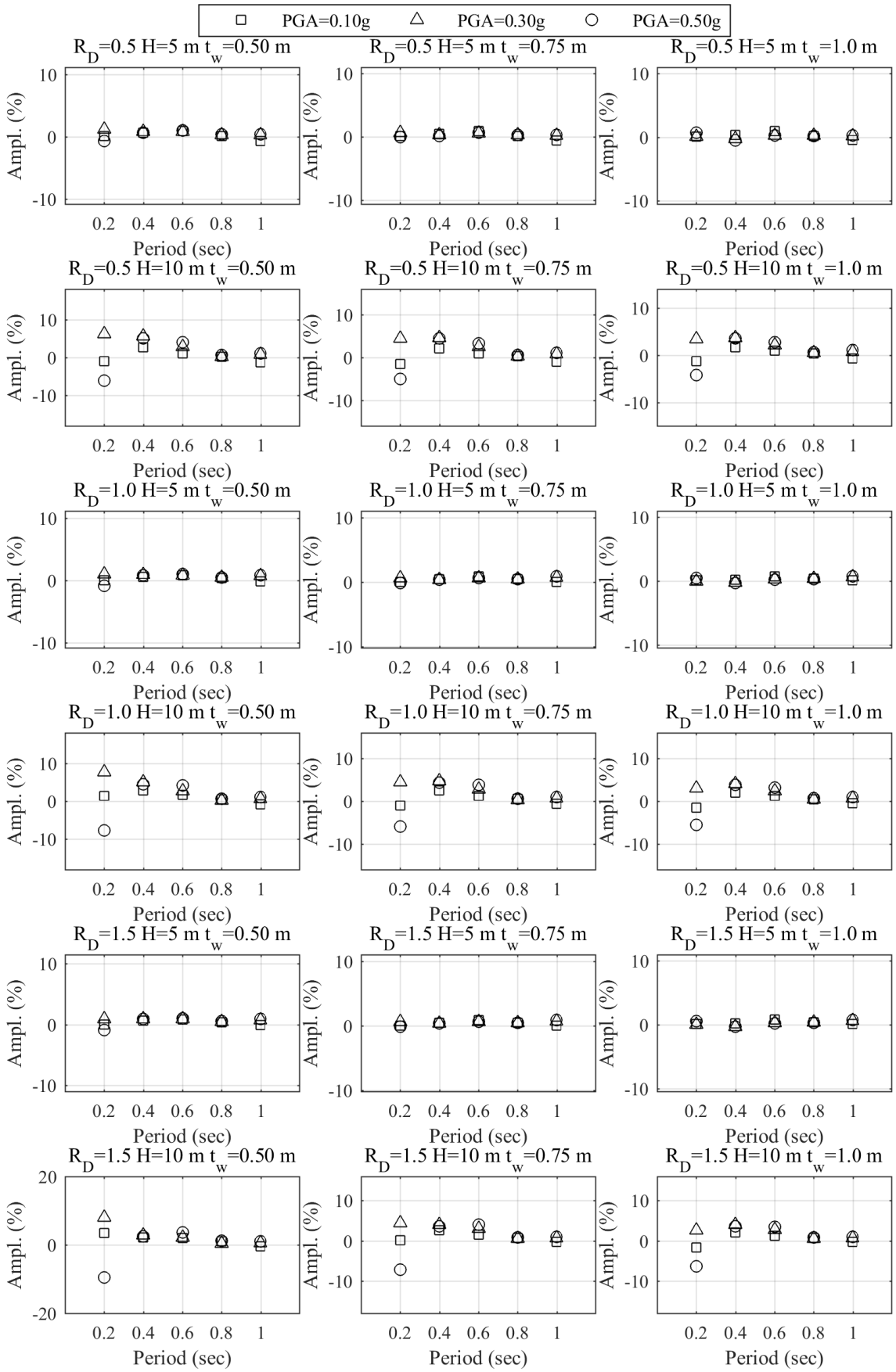

Figure A.30 Peak acceleration amplifications for $R_L = 4$ and Soil Site 3

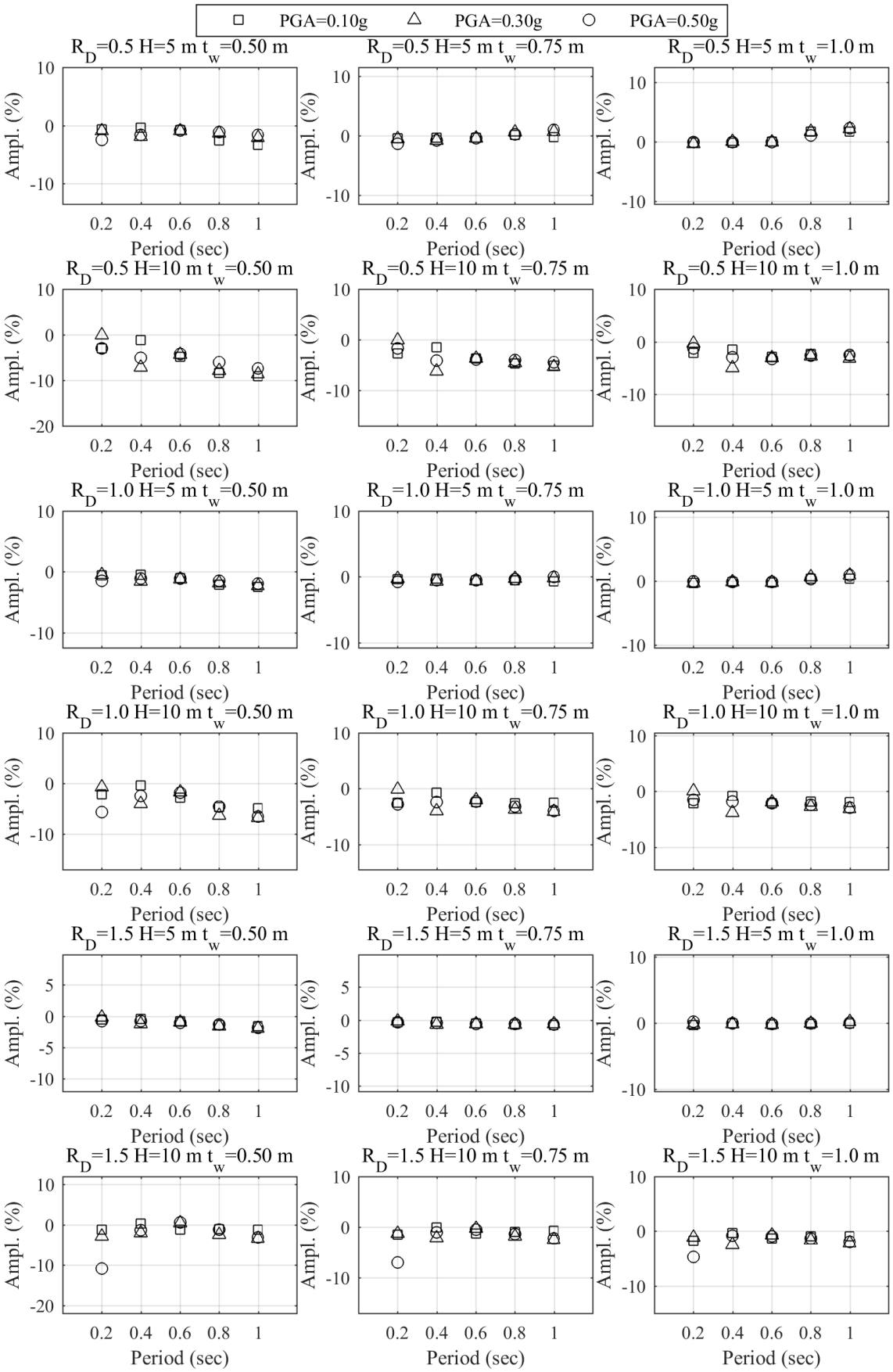

Figure A.31 Peak acceleration amplifications for $R_L = 0$ and Soil Site 4

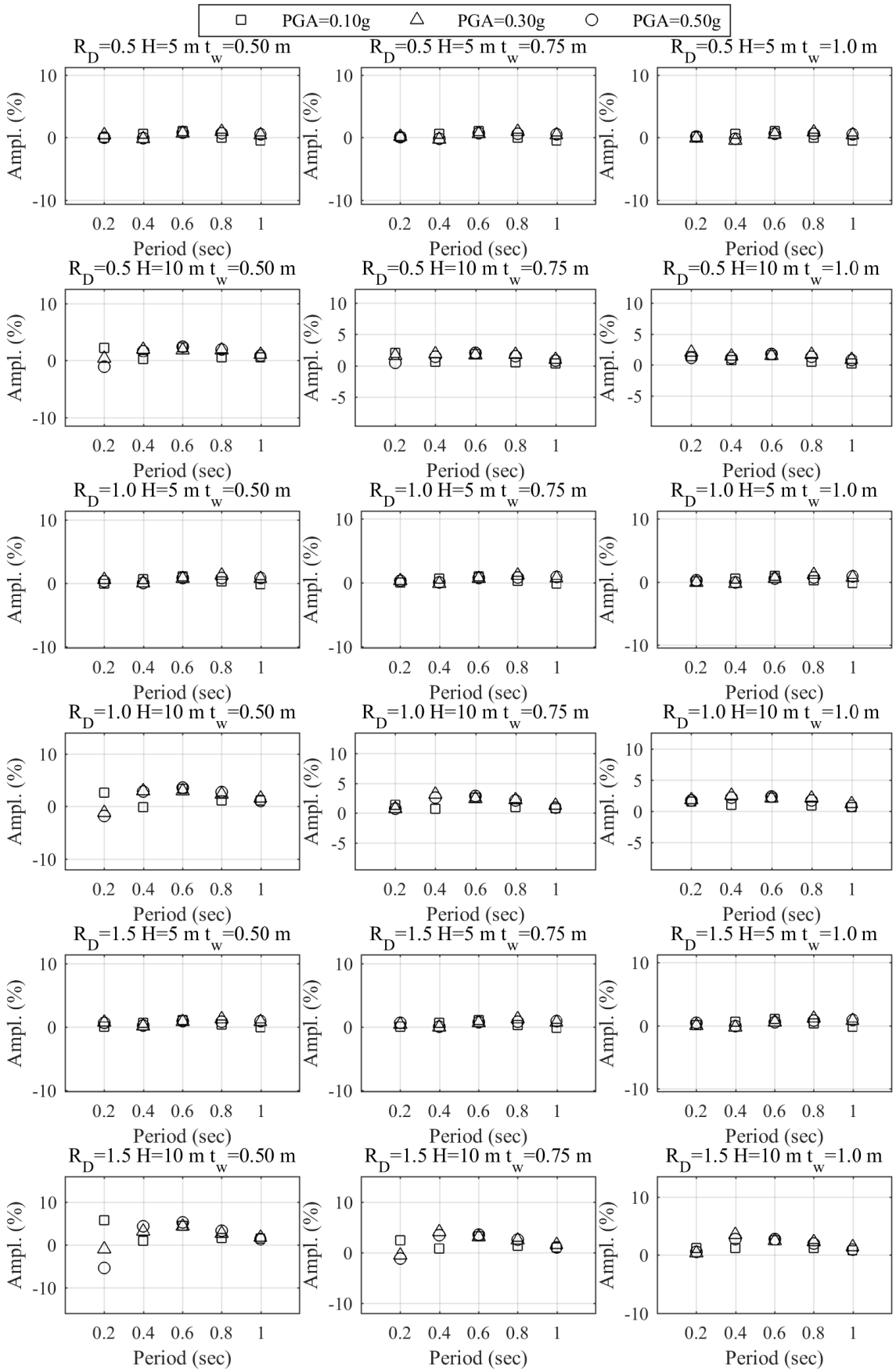

Figure A.32 Peak acceleration amplifications for $R_L = 2$ and Soil Site 4

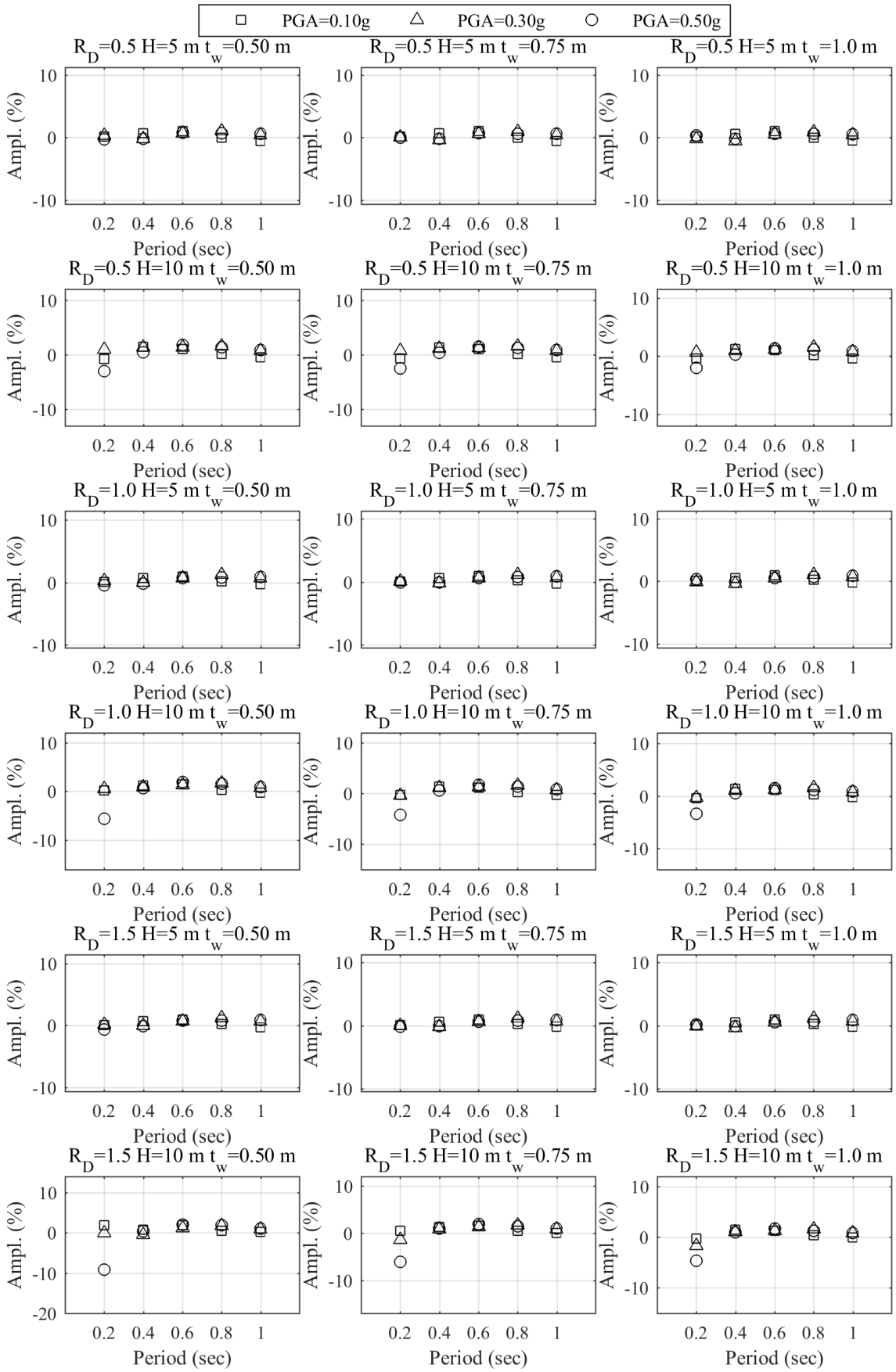

Figure A.33 Peak acceleration amplifications for $R_L = 4$ and Soil Site 4

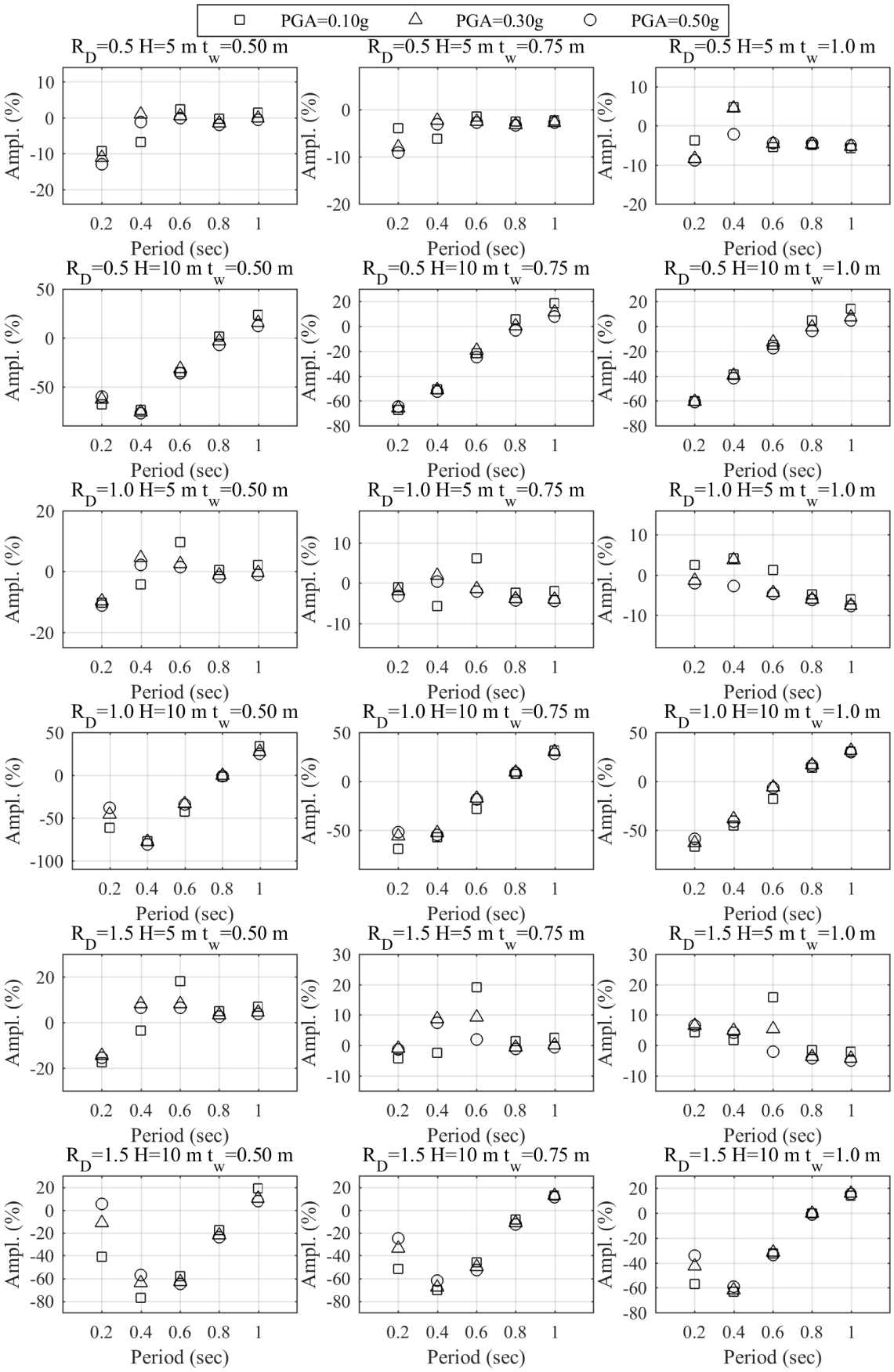

Figure A.34 Peak drift amplifications for $R_L = 0$ and Soil Site 1

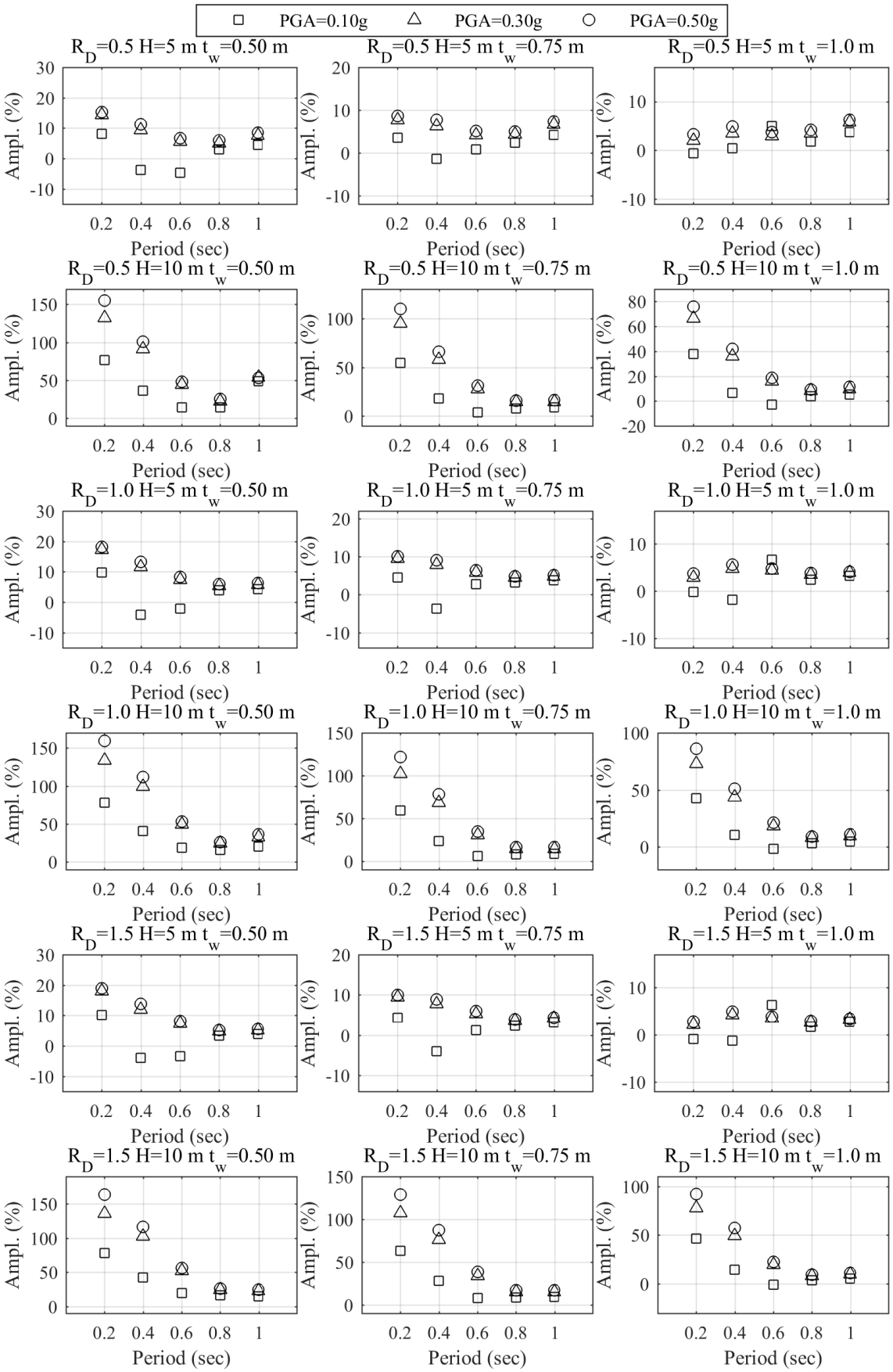

Figure A.35 Peak drift amplifications for $R_L = 2$ and Soil Site 1

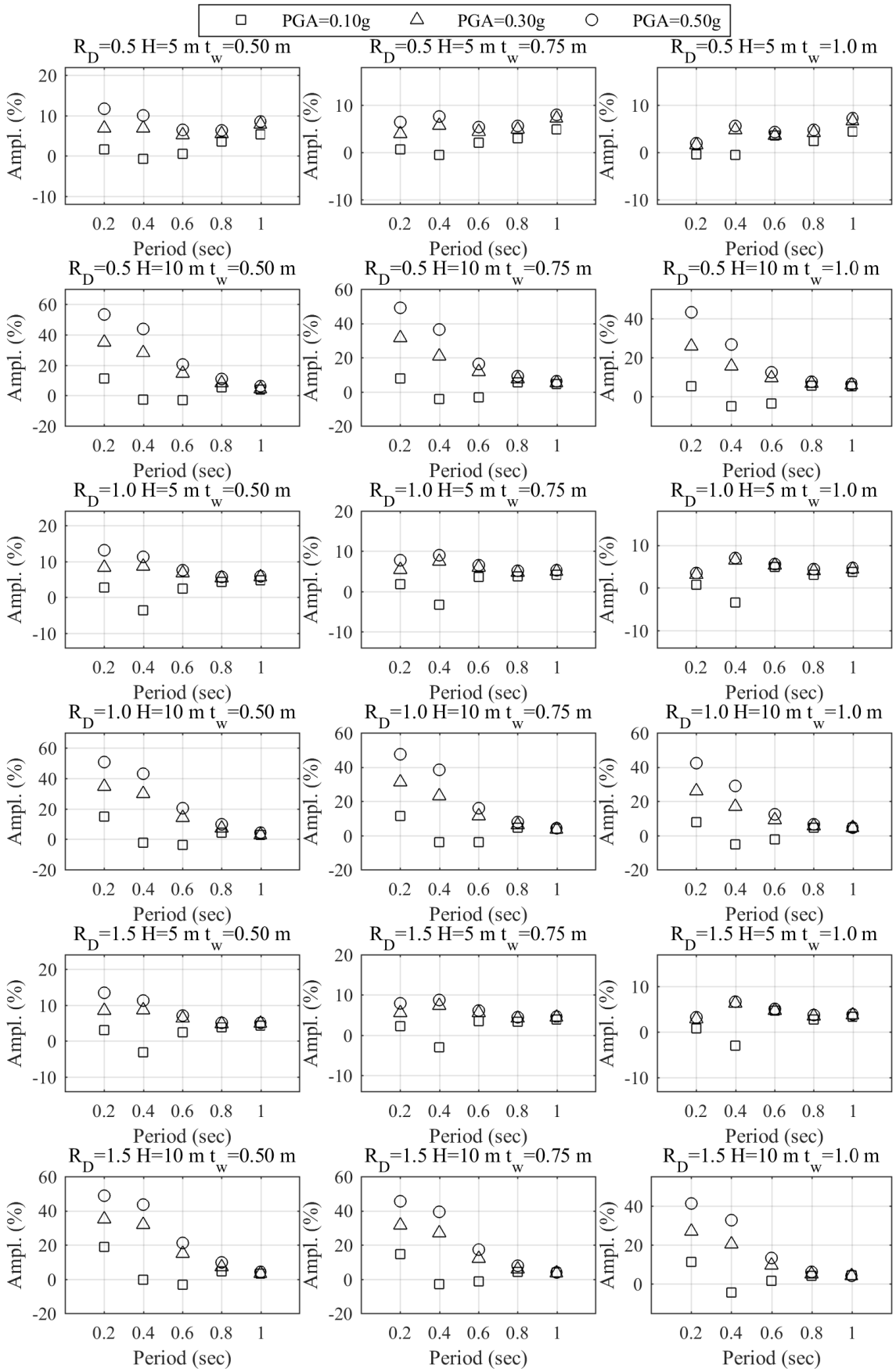

Figure A.36 Peak drift amplifications for $R_L = 4$ and Soil Site 1

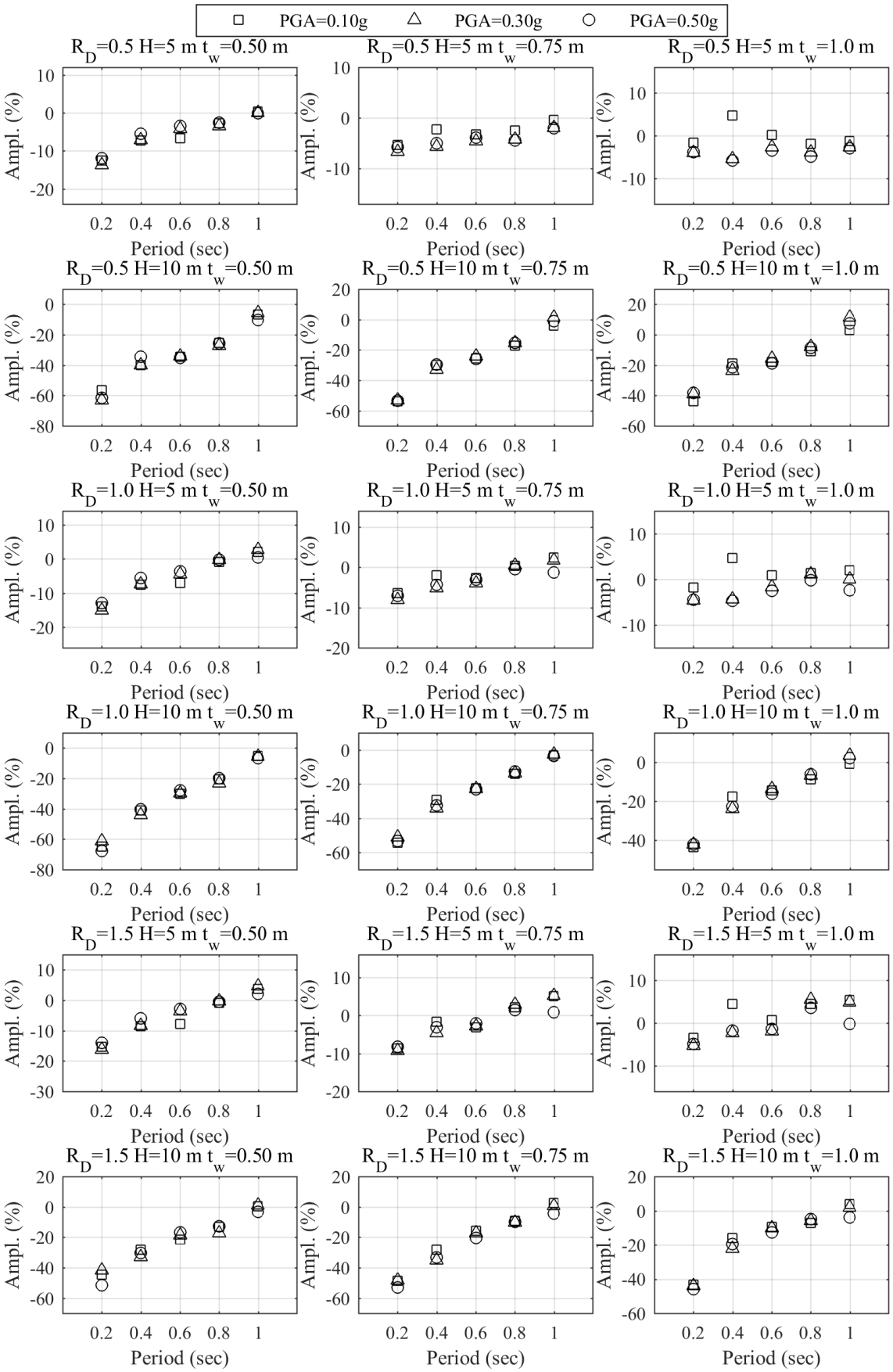

Figure A.37 Peak drift amplifications for $R_L = 0$ and Soil Site 2

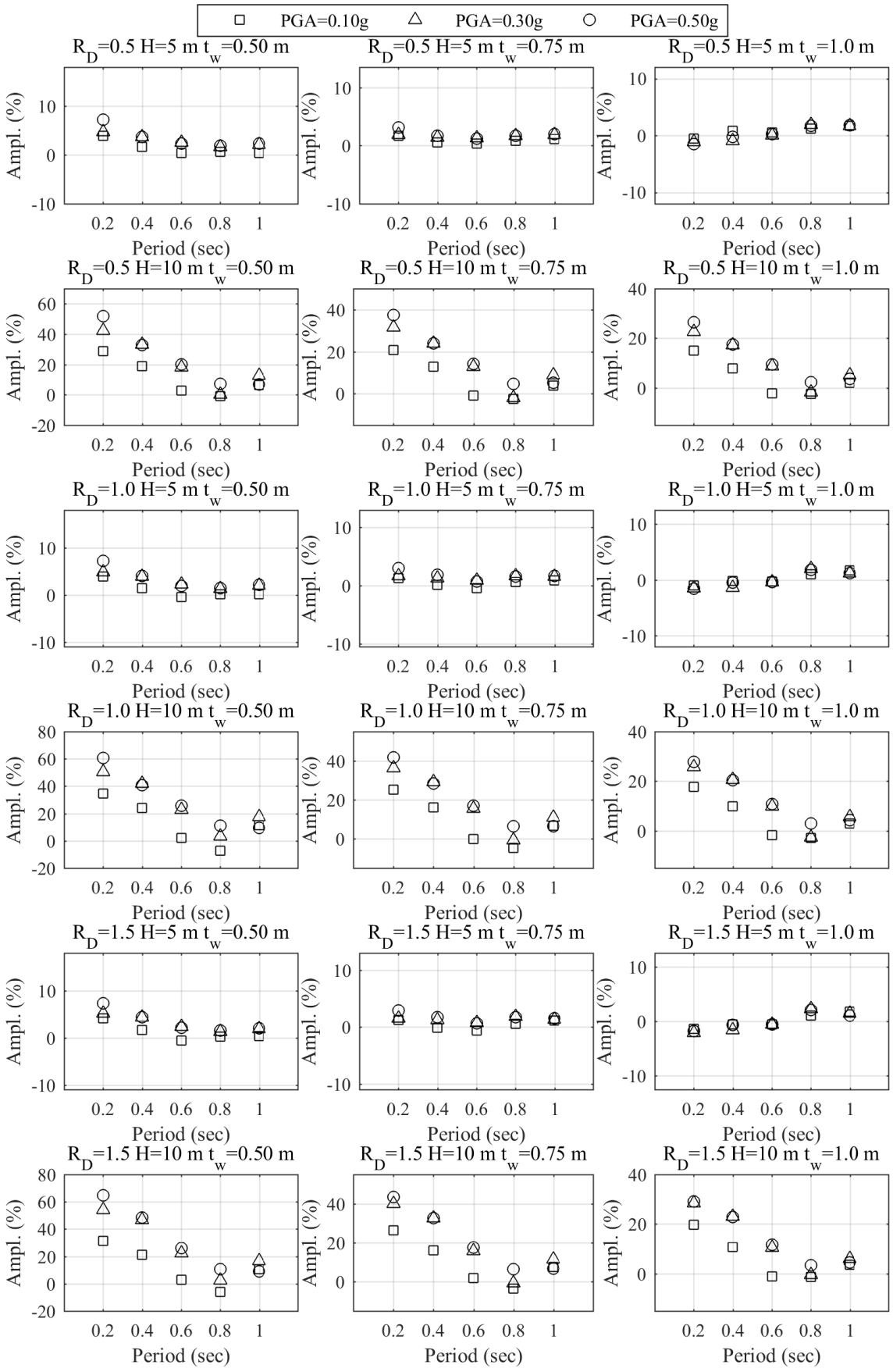

Figure A.38 Peak drift amplifications for $R_L = 2$ and Soil Site 2

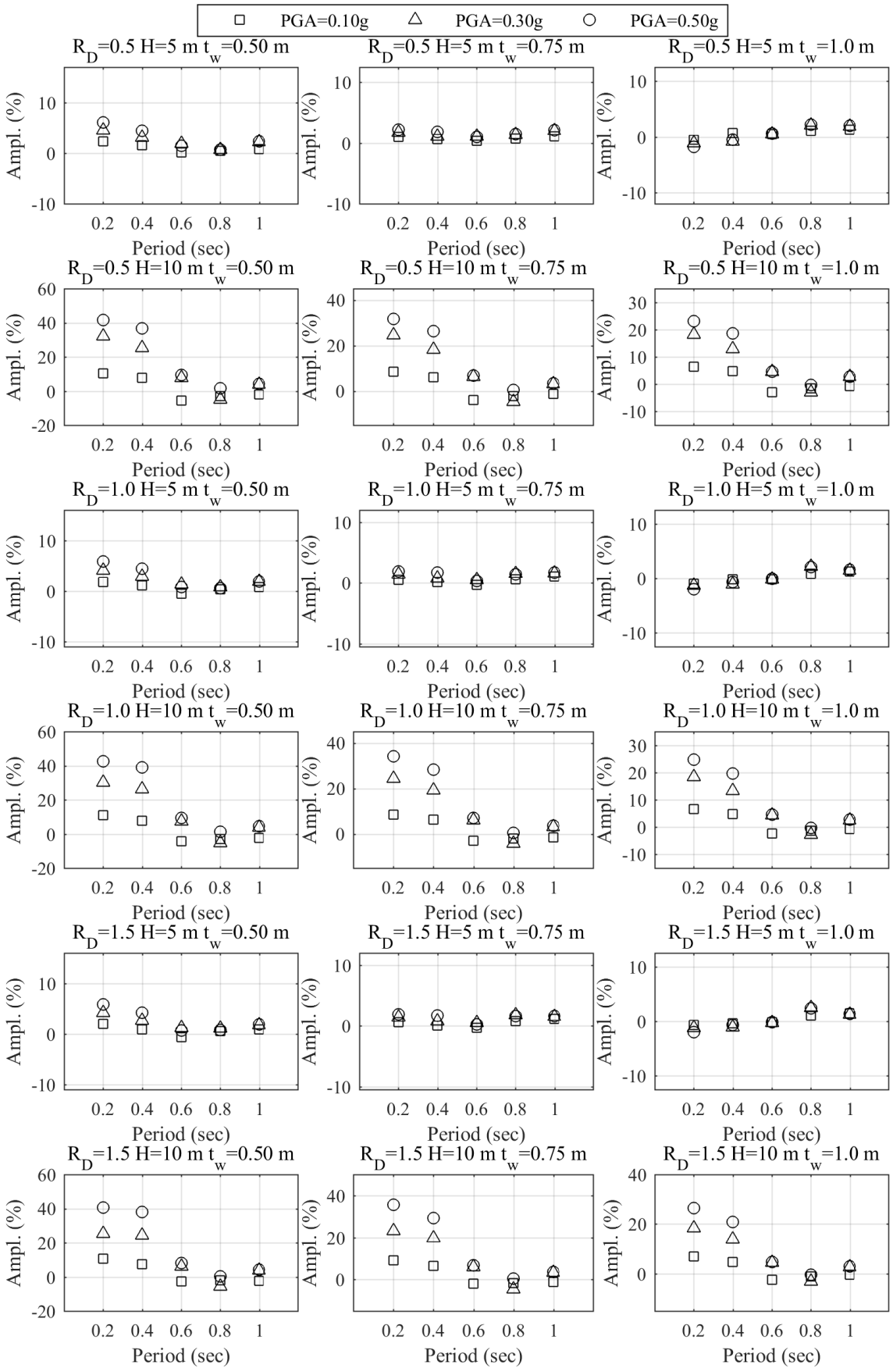

Figure A.39 Peak drift amplifications for $R_L = 4$ and Soil Site 2

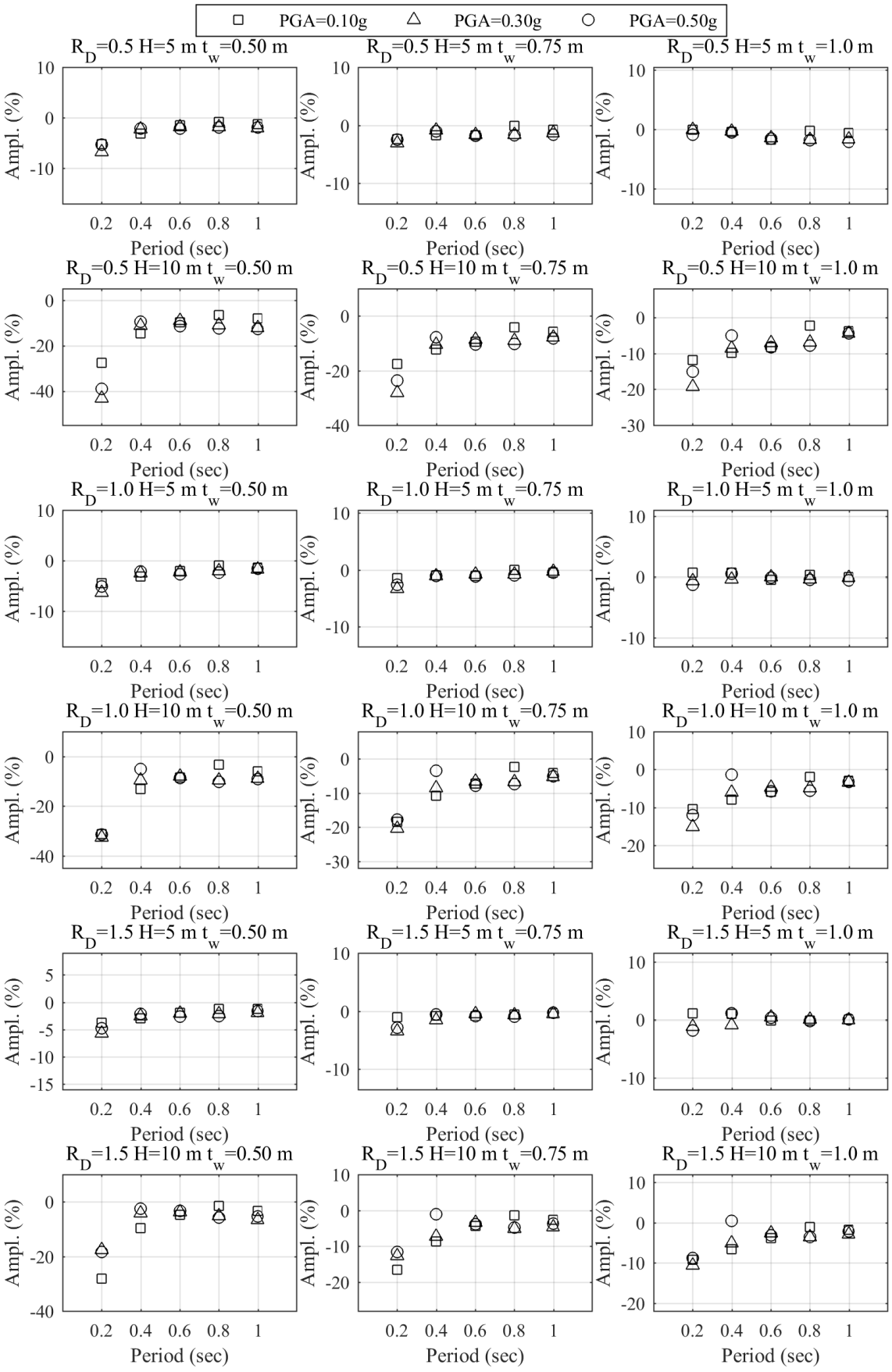

Figure A.40 Peak drift amplifications for $R_L = 0$ and Soil Site 3

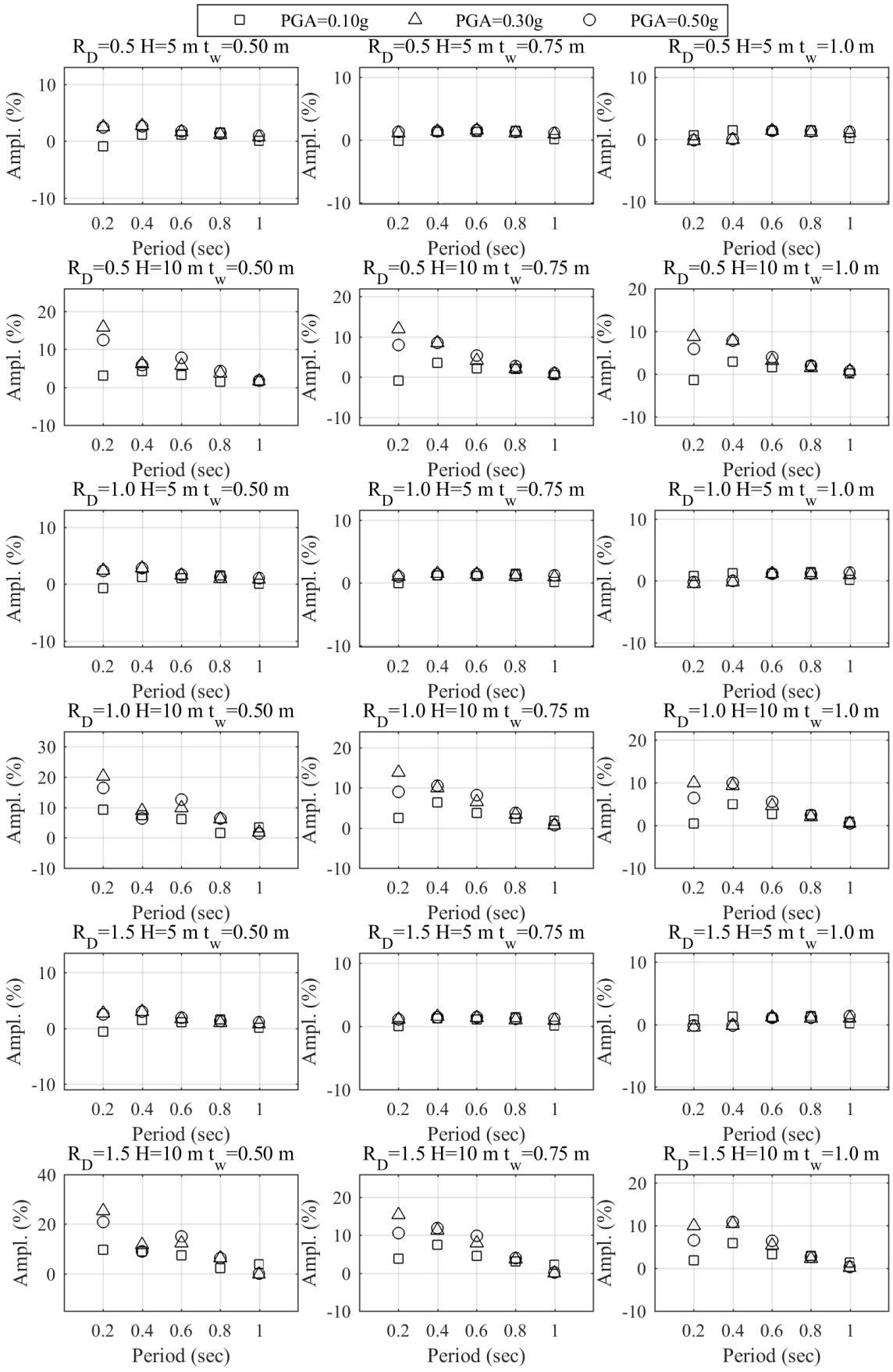

Figure A.41 Peak drift amplifications for $R_L = 2$ and Soil Site 3

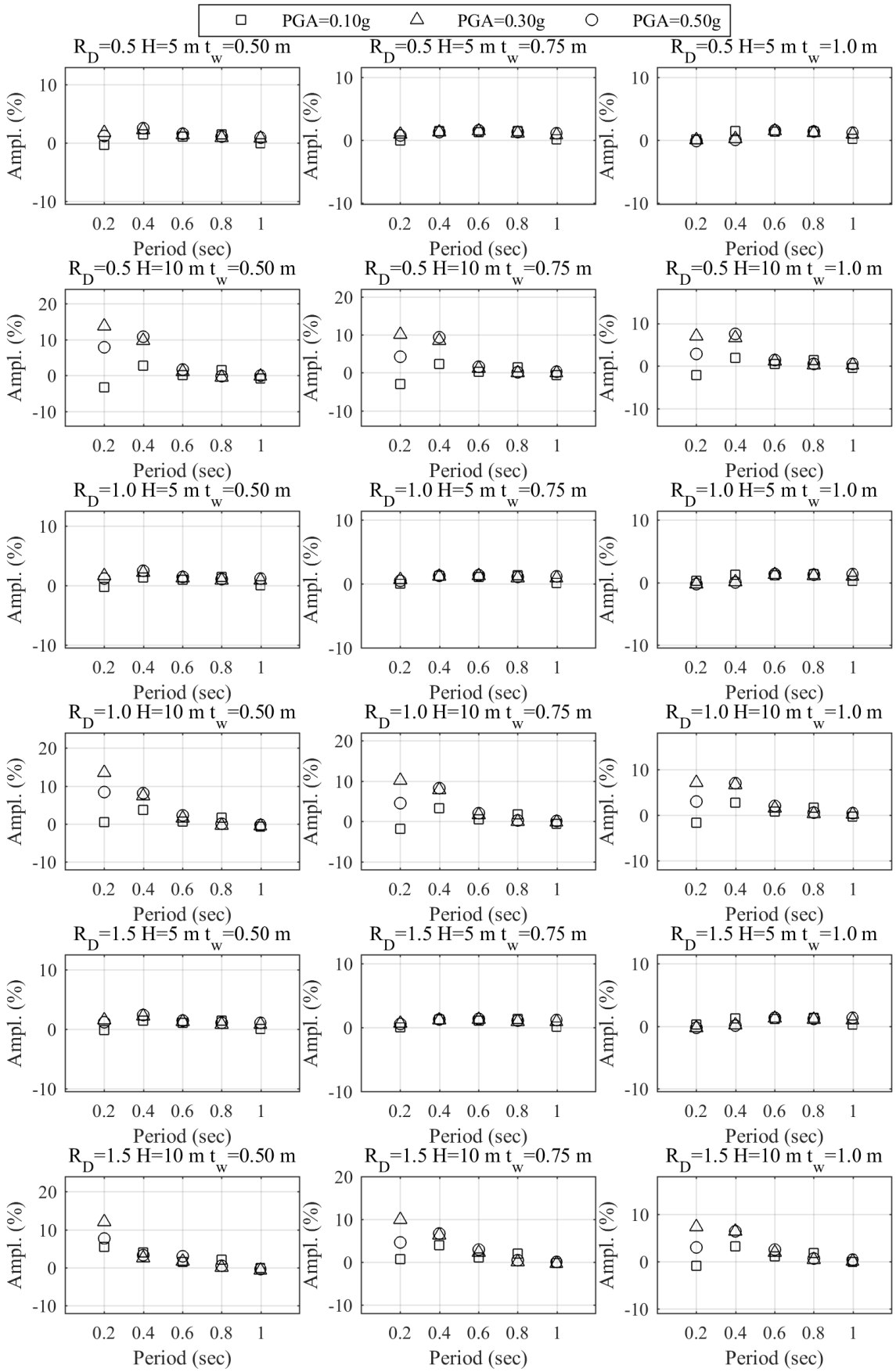

Figure A.42 Peak drift amplifications for $R_L = 4$ and Soil Site 3

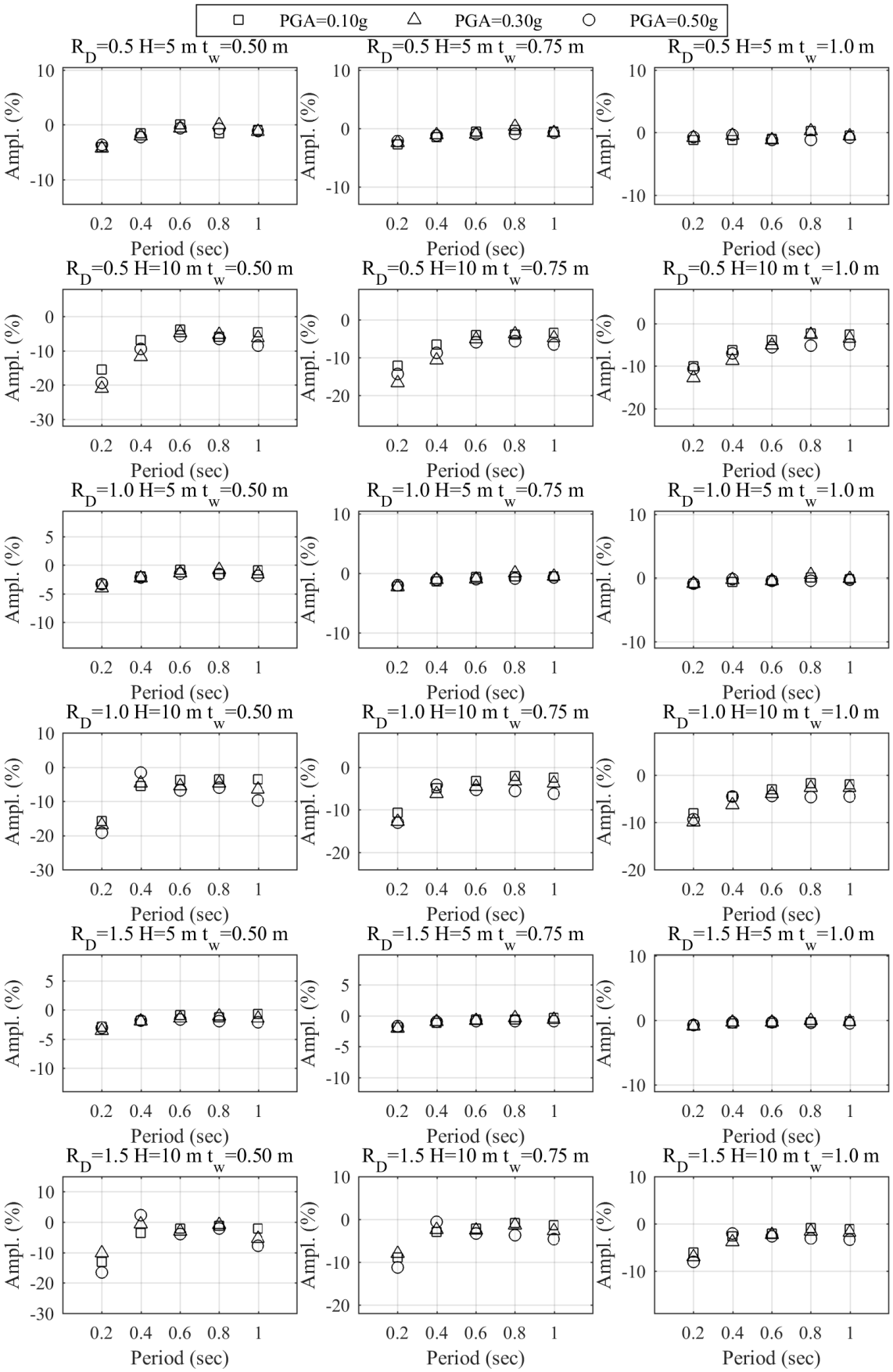

Figure A.43 Peak drift amplifications for $R_L = 0$ and Soil Site 4

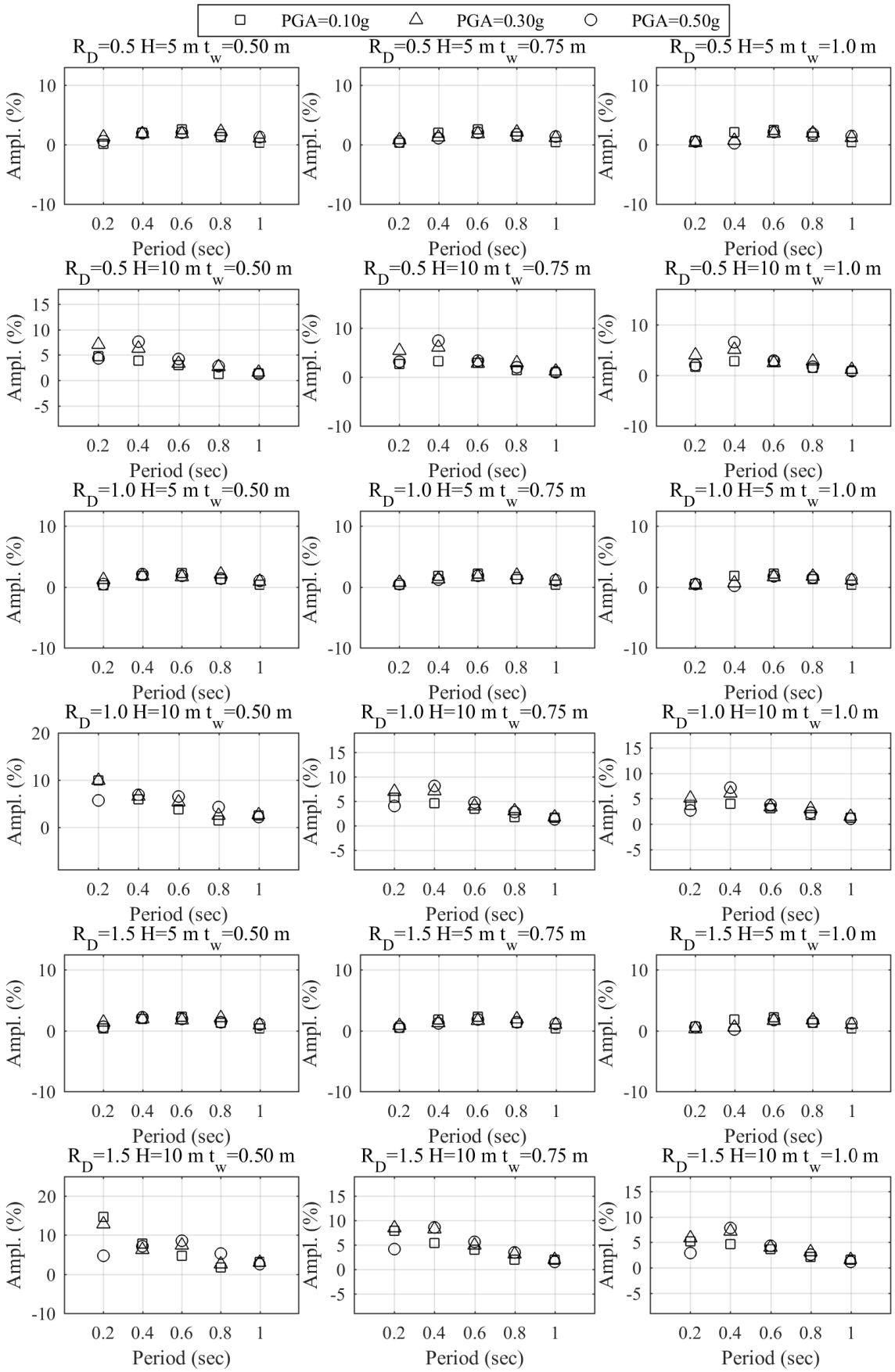

Figure A.44 Peak drift amplifications for $R_L = 2$ and Soil Site 4

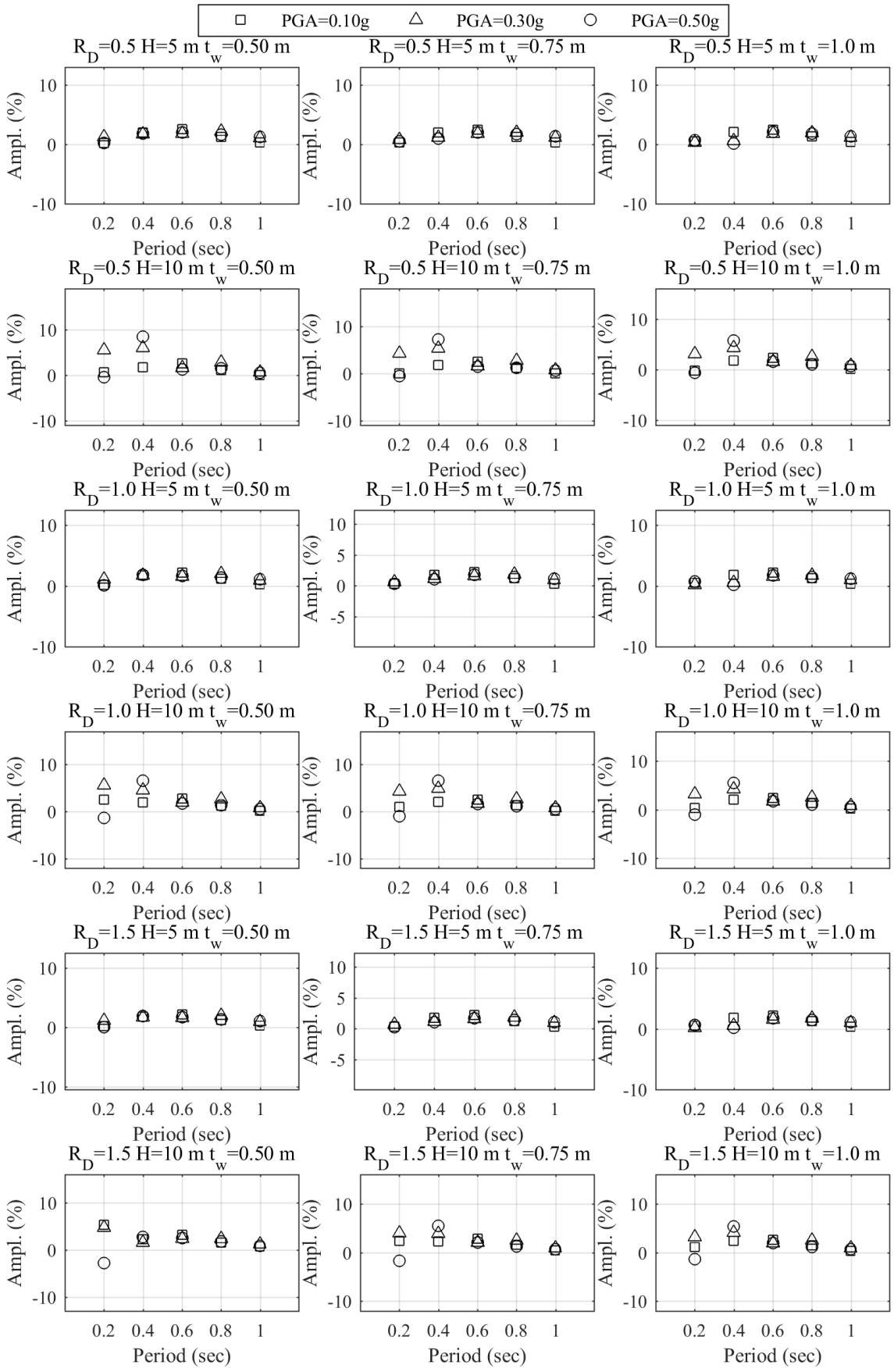

Figure A.45 Peak drift amplifications for $R_L = 4$ and Soil Site 4

Publications From the Thesis

Contact Information: rafet@yildiz.edu.tr

Papers

1. R. Sisman and Y. Ayvaz, "Dynamic interaction effects of buried structures on seismic response of surface structures", *Earthquakes and Structures*, vol. 19, no.1, pp. 1-16, 2020.

Conference Papers

1. R. Sisman and Y. Ayvaz, "A parametric study on the amplification effect of buried box culverts on seismic site response under linear elastic soil conditions", in *Proceedings Book of 13th International Congress on Advances in Civil Engineering*, İzmir, Turkey, pp. 159, 2018.

2. R. Sisman and Y. Ayvaz, "Effect of mass ratio on racking ratios of underground structures under seismic loading", in *Proceedings Book of International Civil Engineering and Architecture Conference*, vol.1, Trabzon, Turkey, pp.1748-1755, 2019.

3. R. Sisman and Y. Ayvaz, "Comparative modelling of soil – underground structure – surface structure interactions", in *Proceedings Book of International Civil Engineering and Architecture Conference*, vol.1, Trabzon, Turkey, pp.1756-1762, 2019.